AD-A166 942 CHARACTERIZATION OF GRAPHITIZATION IN COAL TAR AND PETROLEUM PITCHES(U) AIR FORCE INST OF TECH WRIGHT-PATTERSON AFB OH J C KARIKA AUG 85 1/2

UNCLASSIFIED F/G 11/4 NL

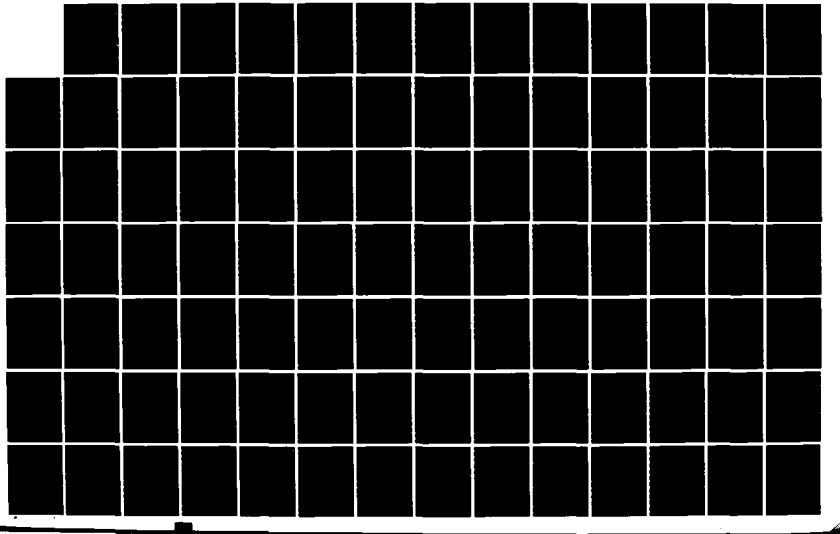

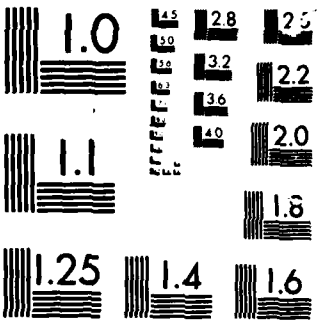

MICROCOPY CHART

SECURITY CLASSIFICATION OF THIS PAGE *(When Data Entered)*

REPORT DOCUMENTATION PAGE		READ INSTRUCTIONS BEFORE COMPLETING FORM
1. REPORT NUMBER AFIT/CI/NR 86-42T	2. GOVT ACCESSION NO.	3. RECIPIENT'S CATALOG NUMBER
4. TITLE *(and Subtitle)* Characterization of Graphitization in Coal Tar and Petroleum Pitches		5. TYPE OF REPORT & PERIOD COVERED THESIS/DISSERTATION
		6. PERFORMING ORG. REPORT NUMBER
7. AUTHOR(s) Janet Claire Karika		8. CONTRACT OR GRANT NUMBER(s)
9. PERFORMING ORGANIZATION NAME AND ADDRESS AFIT STUDENT AT: Arizona State University		10. PROGRAM ELEMENT, PROJECT, TASK AREA & WORK UNIT NUMBERS
11. CONTROLLING OFFICE NAME AND ADDRESS AFIT/NR WPAFB OH 45433-6583		12. REPORT DATE 1985
		13. NUMBER OF PAGES 144
14. MONITORING AGENCY NAME & ADDRESS*(If different from Controlling Office)*		15. SECURITY CLASS. *(of this report)* UNCLASS
		15a. DECLASSIFICATION/DOWNGRADING SCHEDULE

16. DISTRIBUTION STATEMENT *(of this Report)*

APPROVED FOR PUBLIC RELEASE; DISTRIBUTION UNLIMITED

17. DISTRIBUTION STATEMENT *(of the abstract entered in Block 20, If different from Report)*

18. SUPPLEMENTARY NOTES

APPROVED FOR PUBLIC RELEASE: IAW AFR 190-1

LYNN E. WOLAVER 11 April 86
Dean for Research and
Professional Development
AFIT/NR, WPAFB OH 45433-6583

19. KEY WORDS *(Continue on reverse side if necessary and identify by block number)*

20. ABSTRACT *(Continue on reverse side if necessary and identify by block number)*

DD FORM 1 JAN 73 1473 EDITION OF 1 NOV 65 IS OBSOLETE

SECURITY CLASSIFICATION OF THIS PAGE *(When Data Entered)*

CHARACTERIZATION OF GRAPHITIZATION IN COAL TAR AND PETROLEUM PITCHES

by

Janet Claire Karika

A Thesis Presented in Partial Fulfillment
of the Requirements for the Degree
Master of Science

ARIZONA STATE UNIVERSITY

August 1985

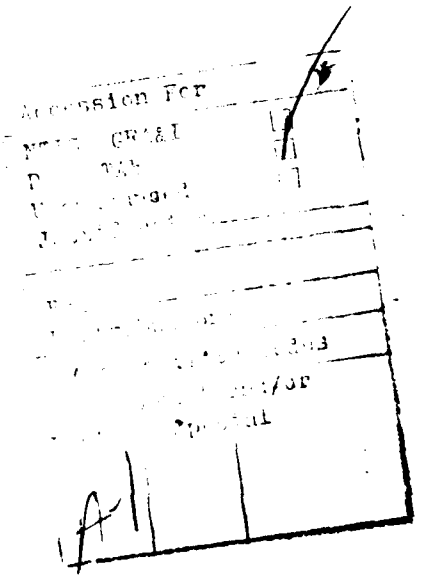

CHARACTERIZATION OF GRAPHITIZATION IN COAL TAR

AND PETROLEUM PITCHES

by

Janet Claire Karika

has been approved

June 1985

APPROVED:

Stephen Krause, Chairperson

Supervisory Committee

ACCEPTED:

Department Chairperson

Charles M. Wolf

Dean, Graduate College

ABSTRACT

This study investigated the effects of heat-treatment temperature and residence time on graphitization of coal-tar pitch and petroleum pitch used in carbon/carbon composites. Samples were heat-treated at various temperatures (550°C-2550°C) and two different residence times of 15 minutes and 30 minutes. They were examined using x-ray diffraction (XRD), scanning electron microscopy (SEM), laser Raman microprobe analysis (LRMA), and electron energy loss spectroscopy (EELS). In addition, a unidirectional carbon/carbon composite was examined using LRMA.

A graphitization index was established using XRD, and degree of graphitization was determined using LRMA. All four techniques showed changes in the pitch materials as a result of processing parameters. With increasing heat-treatment temperature (HTT) XRD showed a decrease in d-spacing indicative of tighter planar packing, a narrowing of peak breadth indicative of an increase in crystallite size, and an increase in peak intensity. This corresponds to an increase in degree of graphitization with increasing HTT. SEM showed establishment of

morphologies representative of two- and then three-dimensional ordering in the pitch samples with increasing HTT indicating the progression of graphitization. LRMA showed an increase in the 1575/cm^{-1} peak intensity and a narrowing of the peak while the 1355/cm^{-1} peak decreased with increasing temperature and residence time, indicating increasing degree of graphitization. EELS showed a change in spectra from one characteristic of amorphous carbon to one characteristic of graphitized carbon as heat-treatment increased. In the unidirectional composite, LRMA showed different spectra for the graphite fiber and the pitch matrix, indicating its potential usefulness as a non-destructive analysis method for characterization of carbon/carbon composites. XRD and LRMA were determined to be excellent complementary analysis techniques for the graphitization process. Together they provided an accurate method for characterizing the progress of graphitization.

DEDICATION

To my husband, Tom, whose love and support have seen me through.

ACKNOWLEDGEMENTS

This thesis could not have existed without the support and guidance of my friends and associates. Through them I have realized a goal that I would otherwise never have attained, and I am deeply indebted to them all.

I would first like to acknowledge the United States Air Force Institute of Technology Civilian Institution (AFIT/CI) thesis program for providing me with the opportunity to pursue this degree. In particular, Captain Alfred Guardino, my section chief at Arizona State University (ASU), always provided a sympathetic ear. He is an outstanding example of what leadership is all about.

The Aerospace Corporation in Los Angeles, California provided the samples used for this research, as well as invaluable guidance and support. Dr. Robert Meyer, Head of the Carbon and Polymers Department, has constantly encouraged me to stay involved with this field and provided the original idea for this thesis. Sandra Gyetvay, Member of the Technical Staff, gave a great deal of her time advising me on the writing of this thesis and providing me with information and references whenever I got stuck. Her enthusiasm and support were crucial to the successful completion of this thesis. I could not

have done it without her.

Research was conducted at ASU through the assistance of the Mechanical and Aerospace Engineering (MAE) Department. The department was particularily sensitive to the special requirements of the AFIT program and helped tailor my thesis to fit within these guidelines. Dr. Harold Nelson, Vice-Chairman for Graduate Affairs for the department, spent a great deal of time providing me with guidance and encouragement through all my classes and thesis preparation. For this and for accepting me into the MAE graduate program in the first place I am truly grateful. To the secretaries of the MAE department I give my thanks for their moral support and sense of humor that always helped me put things back in perspective.

My advisor was Dr. Stephen Krause, Head of the Materials and Manufacturing Group for the department. Dr. Krause spent many long hours trying to make a writer out of me and his talent and patience are deeply appreciated. His guidance in the preparation of my presentations not only helped me in my oral defense but will be put to good use in my Air Force career. He has taught me much about the scientific process, and this knowledge will serve me well in the Aerospace programs

that I will work on.

Many thanks go to Dr. Lester Hendrickson for technical support in the work on x-ray diffraction, Dr. Paul McMillan for the laser Raman microprobe work, and Oscar Vaz for the work with the scanning electron microscope. They have spent a great deal of time and effort to ensure that this thesis is based on solid research that has been presented in the best possible way. Thanks also go to Tim Haddock for the electron energy loss spectroscopy data. They have all spent long hours helping me with the data for this thesis and making room in their schedules for me. I have really enjoyed working with them and hope to again in the near future.

Finally Ms. Mary Redondo, my typist and hero, has put up with numerous revisions and last minute notices for corrections, and through it all has maintained a sense of humor. I thank her for always having a smile for me and staying up late typing so I could finish on time.

TABLE OF CONTENTS

LIST OF TABLES

LIST OF FIGURES

CHAPTER I

Introduction

Carbon/carbon composites are being increasingly used in the aeronautical and aerospace industries because of their excellent thermal and mechanical properties. Various types of pitch are used as material to fill space between woven carbon fibers in order to produce the light-weight carbon/carbon (C/C) composites. The process of filling space involves sequences of infiltration and graphitization of pitch. The pitch materials used as the matrix may originate from two different sources, coal tar and petroleum.

The pitch materials used in the composites are process-sensitive and variations in heating rates, residence times, and heat-treatment temperature (HTT) during graphitization will affect the structure of the pitch and the composite and hence the material properties and performance. This composite of carbon fiber and pitch is manufactured using a process known as pitch impregnation, where liquid pitch is forced through woven cloth fiber by pressure. The pitch in the resulting composite is graphitized and the composite is then machined.

While graphitization and mechanical properties of carbon fibers have been studied extensively, a more limited number of studies have been carried out on structure and properties of pitches. Structural studies on pitches have generally used only a single technique to examine the graphitization process. Various theories have been proposed on the mechanism of the graphitization process based mostly on the results of a single technique. To integrate the knowledge on the qualitative process from individual characterization techniques, a combination of techniques is needed. This research integrates the results of four different microstructural characterization techniques; x-ray diffraction (XRD), scanning electron microscopy (SEM), laser Raman microprobe analysis (LRMA), and electron energy loss spectroscopy (EELS). By correlating results from XRD, SEM, LRMA, and EELS on a variety of pitch samples, it becomes possible to elucidate additional details on the graphitization process. It also may be possible to establish a methodology for determining "per cent graphitization of the pitch."

Additionally, this methodology has been applied to examine a C/C composite sample in order to determine the feasibility of measuring per cent graphitization of pitch within a composite. With this knowledge it may be possible to improve the processing variables of residence time and

temperature to achieve a higher degree of graphitization of pitch in C/C composites.

The purpose of this research was to study and characterize the pitch graphitization process. In particular, the effect of the heat-treatment cycle was studied to determine the effects of pitch-to-graphite conversion. In this study we have investigated coal-tar pitch and petroleum pitch used to produce C/C composites. Finally, the feasibility of using the LRMA technique to characterize graphitization in C/C composites was examined.

CHAPTER II

Background

Currently, there is great interest in determining the mechanism of the pitch graphitization process. The main stages of graphitization are pyrolyzation (350-550°C), carbonization (750-1300°C), and graphitization (1800-3000°C). In the 550-750°C range, impurities (mainly nitrogen, sulfur, and hydrogen) are burned off. Shrinkage of the pitch matrix occurs in the 1300-1800°C range. Temperatures are approximate as different pitches reach these stages at slightly different temperatures. The basic process is shown in Figure 1. Aromatic hydrocarbons are seen to form pitch upon heating below 350°C. The resulting pitch is transformed into coke by increased heating up to approximately 550°C. During further heating up to 1300°C the coke is transformed into almost pure carbon. Finally, the material is graphitized when it is heated up to 3000°C. Industrial pitch originates from two main sources, coal-tar and petroleum (1).

The coal used to produce coal-tar pitch is a bituminous coal, commonly called "soft coal," and contains 70 to 80 percent carbon. The remaining 20 to 30 percent

is hydrogen and organic compounds. Aromatic hydrocarbons, which form the pitch, can be obtained from refining this coal. First, the coal is heated in an inert atmosphere to drive off a gas called "coke-oven gas," composed mainly of hydrogen and methane. Some organic material still remains in the coal after the coke-oven gas is driven off. Further increases in temperature drive this organic material off, and it is collected as a thick black liquid called coal-tar pitch. A ton of bituminous coal will yield about 60 pounds of coal-tar pitch. The degree of aromaticity of the pitch varies depending upon the origin of the bituminous coal (2). McNeil (3) found an aromaticity for coal-tar pitch of above 90 percent.

Petroleum pitch from petroleum oil contains hundreds of different hydrocarbons. These can be separated into different hydrocarbon groups by a refining process known as fractional distillation. Petroleum usually contains aromatic hydrocarbons along with other types of hydrocarbons. The fraction of aromatic hydrocarbon contained in petroleum varies widely depending on the oilfield from which the petroleum originated. Asimov (2) found that samples of petroleum from Borneo contain as much as 40 percent aromatic hydrocarbon. It is the aromatic hydrocarbons that form the petroleum pitch

that are of interest in this study. The molecules in petroleum are predominantly nonaromatic. As a result, petroleum must go through extensive distillation and cracking processes to refine it for use in the petroleum industry. This remainder that is left is composed, for the most part, of carbon atoms in the form of aromatic hydrocarbons. This is petroleum pitch (2).

Pitch

Pitch is a disordered material. It polymerizes only slightly further to produce a more highly-ordered polymer called coke. Prior to producing coke, there is the formation of a carbonaceous mesophase composed of spherules made up of lamellar molecules that grow and coalesce. The whole process is called pyrolyzation. The coal-tar pitches derived from the carbonization of coal are solutions of a wide range of primarily aromatic compounds carrying up to 15 wt% of particles insoluble in quinoline. The petroleum-based materials are usually less aromatic, run very low in insoluble particles, and contain the reduced crudes, thermal tars, decant oils, and other refinery streams that are carbonized to semi-coke under several atmospheres pressure in large drums of the delayed coking units (4). Table I gives pitch properties for coal-tar and petroleum, as reported by the manufacturers, showing their softening

point, per cent of benzene insolubles and quinoline insolubles, coking value, ash content, specific gravity, and sulfur content (5). Table II gives the chemical analyses for coal-tar and petroleum pitch listing carbon, hydrogen, oxygen, nitrogen, and sulfur content (6,7).

Pitch consists of a complex mixture of hundreds of aromatic hydrocarbons of three to eight condensed rings which have an average molecular weight of 300-400 g/mole. The melting point for this mixture is on the order of 90-115°C. These molecules are all planar, non-polar, fused-ring aromatic hydrocarbons with different degrees of aliphatic substitution, depending upon their source and heat treatment. Since different pitches graphitize in different ways, we will be concentrating on coal-tar and petroleum pitch sources (1).

Pyrolysis

Pyrolyzation, or pitch-to-coke transformation, takes place very rapidly during the graphitization process. In terms of temperature this comprises only a few per cent at most of the total extent of the graphitizing heat treatment, when a heat-treatment temperature (HTT) range up to 3000°C is considered. Mesophase transformation takes place between 350°C and 550°C. The formation of a carbonaceous mesophase during pyrolyzation is critical to

the formation of graphitizing versus nongraphitizing material. Large planar molecules formed by the reactions of thermal cracking and aromatic polymerization orient themselves in parallel layers. These result in an optically anisotropic liquid crystal known as the carbonaceous mesophase. This mesophase occurs initially in spherule form. The molecules are believed to be sufficiently large and flat to favour the formation of the mesophase when they reach a molecular weight of approximately 2000 g/mole (20-40 fused rings) (1). In fact, the distinctive feature of the lamelliform morphology of graphite materials is the extensive number of aromatic layer-molecules, which serve as the fundamental microstructural element. These elements are unlike crystal grains of most ceramic and metallic materials (8). Lamellae are stacks of nearly parallel layer planes, sometimes referred to as basal planes.

Brooks and Taylor (8) first reported mesophase spherule formation in pitch by heating pitch above 400°C, either at constant temperature or with gradually increasing temperature. They observed small spherules, initially of sub-micron size, appearing and gradually increasing in size to hundreds of microns in size with increasing time and temperature. Spheres were shown to be anisotropic using polarized light microscopy on a

polished mesophase pitch sample. Poles were seen, representing the intersection of the axis of symmetry of the sphere with the plane of the section (8). This optical anisotropy is characteristic of graphitizable carbons. This anisotropy is indicative of long-range crystallographic order extending from 0.5 μm (500 nm) to 500 μm, as opposed to nongraphitizing isotropic carbons with small-scale crystallographic order ranging from 1-5 nm. Crystallographic order is defined by Marsh and Walker (9) as denoting the distance of parallelism of grouped or stacked constituent molecules.

In determining the lamellar structure of the mesophase spherules to be lamellar, Brooks and Taylor (8) observed that the mesophase spherules exhibited characteristic electron diffraction patterns in ultrathin sections at the earliest detectable stage of spherule growth. The patterns varied with spherule orientation to the beam. Variations were found in characteristic electron diffraction patterns for lamellae parallel to the beam and lamellae oblique to the beam. Such variations in diffraction patterns were clearly not those of crystalline materials, yet a considerable degree of order was indicated. The kind of order giving rise to these patterns was deduced by Brooks and Taylor to

be lamellar.

At the temperature of formation, the mesophase spherules are liquid droplets, immiscible with respect to the surrounding isotropic pitch. They are slightly more dense and more viscous than the isotropic phase and, if left undisturbed in the preparation vessel, will slowly settle out (1). The high viscosity of the mesophase permits microstructures formed in the plastic mesophase to be cooled to room temperature with little apparent disruption, making observation and analysis of the mesophase much easier. Brooks and Taylor (8) heated ultrathin sections of pitch containing spherules in the electron microscope to the temperature at which the spherules had formed and found that the diffraction patterns were indistinguishable from those obtained at room temperature, showing that strain induced by cooling from the temperature of formation to room temperature was not significant.

Hüttinger (10) followed the pyrolysis reactions and mesophase transformation in coal-tar and petroleum pitches pyrolyzed at a heating rate of 1°C/min by making measurements of benzene- and pyridine-solubility. The results of Hüttinger's study are shown in Figure 2 as a plot of insoluble content (wt%) versus pyrolysis. Around 400°C benzene- and pyridine-insolubility content

can be seen to increase rapidly, reaching an asymptotic value approaching 100 wt% by 500°C. Ihnatowicz et al. (11) studied the effects of heating rate on insolubility and found an upward shift of the order of 40°C for an increase in heating rate from 0.5 to 3.0°C/min, indicating the sensitivity of insolubility curves to heating rate.

Honda et al. (12) investigated the effects of residence time on the pyrolyzation of coal-tar pitch using polarized-light microscopy, x-ray diffraction, and density measurements. The formation of mesophase spherules in coal-tar pitch at 410°C was observed at residence times of 2, 4, 8 and 13 hours. Their studies showed that interlamellar spacing of coal-tar pitch decreased with increased residence time. Stacking height of lamellae, weight loss, density, and quinoline insolubles all were found to increase with increasing residence time.

As the mesophase spherules grow to large sizes, they begin colliding with each other and coalesce to form even larger spheres and ultimately large anisotropic regions. The outline of the spheres before they have begun to interfere with one another's growth is mostly circular. The spherical appearance is lost; however, as the volume proportion of spheres to pitch becomes large, say, more than 1:1.

Concentrations of mesophase spheres are usually localized before becoming more generally widespread. Consequently, various stages in the development of the mesophase may be visible simultaneously in a single sample. All spheres tend to have parallel planar molecules that stack up, approaching the sphere surface at a 90° angle. This allows the molecules to form a continuous link when the spheres interact, facilitating initial coalescence. The external margins of the two-sphere composite retain a lamellar orientation perpendicular to the surface. In Figure 3, two spheres are shown with their lamellar orientation indicated. They contact each other, partially rearrange their lamellar structure, and then completely rearrange their structure to form a larger sphere with the same basic initial lamellar structure. Figure 4 shows actual coalescence taking place in a sequence of polarized light photomicrographs of two mesophase spherules.

Since coalescence occurs in three dimensions, a structure is formed in which mesophase, as seen in any plane, comprises areas in which the orientation is fairly uniform. These areas are connected to one another by zones of mesophase in which the lamellae curve around sharply to conform to the orientation of the next fairly uniform area (8).

It should be noted that when pitch is used as a matrix for a carbon fiber composite and the resulting carbon/carbon composite graphitized, the alignment of the mesophase lamellae is no longer random but interacts with the fiber surface.

Cranmer et al. (5) investigated the effects of the fiber matrix on the formation of the mesophase. They conclude that a lesser degree of formation of mesophase occurs in areas where pitch flow is restricted, as in the interior of fibers and between fiber bundles. A region rich in mesophase material around carbon fibers is often separated from the fibers by an interphase layer of isotropic material. The external surfaces of carbon fibers do not act as preferred nucleation sites for the formation of mesophase.

Evangelides (13) has suggested that pressure causes the orientation of the matrix relative to the fibers, based on his studies and studies with Zimmer and Jortner (14). At low pressures, the lamellae orient parallel to the fiber axis except at large distances from the fiber. At large distances orientation tends to be more random. Under high pressure processing, Jortner (14) observed graphite lamellae oriented perpendicular to the fiber axis. A sheath of parallel graphite lamellae was observed to form about the fibers,

but at a small distance from the fibers the orientation abruptly changed to transverse.

The effect of pressure on mesophase formation was noted by Hüttinger and Rosenblatt (10). Coal-tar pitch mesophase was examined at 550°C at 2 bar and 50 bar and petroleum pitch was examined at 450°C at 2 bar and 150 bar. They found that increased pressure leads to an increase in coke yield and a lower temperature required for pitch-to-coke transformation. It was concluded that increased pressure improved preorder and graphitizability of the pitches, coarsens microstructure, and causes enlarged areas of optical anisotropy exhibiting no preferred orientation.

Brooks and Taylor (8) also noted that the surfaces of glass vessels in which insoluble-free pitches had been carbonized were a preferred site for mesophase oriented parallel to the surface. Their general conclusions on nucleation were that any solid surface appeared to be a preferred site for mesophase growth and that the nucleating effect of solids increased with specific surface area. They also stated that insoluble particles are excluded during the sphere's growth, and both stirring and the presence of fine solid particles appear to accelerate slightly the formation of mesophase.

The process of mesophase formation proceeds while

the mesophase molecules undergo continuing reactions of aromatic polymerization. Although the formation of the mesophase should reduce molecular mobility, aromatic polymerization may be expected to continue between the molecules within each mesophase layer, thus building the extent and perfection of the pre-graphitic layers. Additionally, gases are evolved, primarily hydrogen and methane, which nucleate as bubbles and percolate through the increasingly viscous mass. When the mass eventually hardens, relative to the stresses of bubble percolation, the mesophase fossil may be defined as semi-coke.

Interesting flow patterns and stacking defects are produced by bubble percolation. Figure 5a is a polarized light photomicrograph of mesophase deformation just after bubble percolation has begun. A sketch of this structural deformation is shown in Figure 5b and indicates the development of a high degree of preferred orientation, even at this initial stage. The fibrous array of polarized-light extinction contours is seen to correspond to tight folds in the mesophase layers. The nucleation, growth, and percolation of gas bubbles produces extensive plastic deformation, both orienting and reducing the microstructure to a finer texture. Figure 6 shows refinement of a coal-tar mesophase pitch microstructure as a result of bubble percolation during pyrolysis (4).

The density of the mesophase can be used to measure the packing efficiency of the lamellar mesophase in comparison with the inefficient packing in the untransformed pitch. The density at the point of mesophase-hardening fixes the starting point for the shrinkage effects which take place in subsequent heat treatments. White (4) reports density values for various coal-tar pitches around 1.46 g/cm^3. In cases in which the untransformed matrix density is also measured there is a lower density by $\Delta\rho$ approximately equal to 0.17 g/cm^3, i.e., by 12%, which provides the driving force for the segregating action commonly observed during pyrolysis. For a mesophase precipitating from a typical petroleum pitch, the density reported by White was 1.33 g/cm^3.

As pyrolysis proceeds, the mesophase becomes increasingly viscous and thus less capable of plastically deforming during bubble permeation. Eventually, the mesophase solidifies to a semi-coke, thus freezing in the disclinations, folds, bends, and splays which constitute the basic lamelli form morphology. This morphology persists throughout the subsequent heat treatment stages. An illustration of this morphology is shown in Figure 7. Apparent viscosity as a function of temperature was examined by Singer (1) for different levels of pyrolyzed pitches. Viscosity was found to decrease as

the pitches were heated up to about 400°C, the temperature at which Brooks and Taylor (8) first noted the appearance of small mesophase spherules. The viscosity then increased rapidly as the mesophase pyrolyzed to form coke. The viscosity increased as polymerization increased and decreased as polymerization decreased.

The mechanisms of the pyrolysis reactions generally involve the formation of aromatic free radicals, many of which are quite stable. White (4) found that for coal-tar pitch the concentration of free radicals in the pyrolyzing mass rises quite rapidly when mesophase formation initiates, around 350°C. Electron spin resonance continues to increase after the mesophase transformation is complete at 550°C, indicating continued thermal cracking and dehydrogenation reactions continue acting on the mesophase molecules. The maximum free-spin concentration near 560°C and the sharp drop of the concentration to negligible values by 650°C may reflect the completion of reactions that produce mesophase hardening and the formation of lamallae (4).

Coke

Coke is the product of the pyrolyzation process and consists of much higher-molecular weight polymers, or hydrocarbons, above a molecular weight of approximately

3000 g/mole. Coke is a totally infusible solid, in contrast to pitch. It is essentially completely anisotropic (1). Coal derived pitch coke usually has lower graphitizability compared to petroleum coke due to a subdivided mesophase structure caused by a larger concentration of insolubles (15).

Carbonization

Carbonization is the process of forming a material with increasing carbon content from organic material, i.e., pitch that has been pyrolyzed to form coke. The process terminates with an almost pure carbon residue at temperatures up to about 1300°C. The final carbonization temperature controls the degree of carbonization and the remaining content of foreign elements, e.g., at 900°C the carbon content of the residue exceeds 90 wt% whereas at 1300°C, 99 wt% carbon is obtained (16).

The first morphological effect of heat treatment in the carbonization cycle is the appearance of shrinkage cracking at temperatures as low as 600°C. Cracks running parallel to the mesophase layers open up as the result of a greater shrinkage perpendicular to the layers. The initial cracks are short and are confined to folded regions, but by 700°C they multiply and lengthen rapidly. Figure 8 illustrates the long-range fissuring produced

by linkage of shrinkage cracks in an extracted coal-tar pitch heat treated to 800°C. Figure 8a shows this in a polarized light photomicrograph while Figure 8b shows this schematically (4). Hüttinger (10) noted that the extent of shrinkage cracking decreases as the graphitizability of the coke decreases; in the extreme case of nongraphitizable carbons no shrinkage cracks are developed.

On heat treating through the range 600°C-1100°C, the ongoing polymerization reactions are evidenced by weight losses. The initial weight loss consists largely of methane (CH_4) from the cracking of the methyl substituents; Pietzka et al. (17) found that CH_4 evolution from a coal-tar pitch binder reached a maximum of 600°C and became undetectable by 800°C. From then on the major weight loss was by hydrogen (H_2) evolution, which began at approximately 600°C, maximized at approximately 730°C, and continued at decreasing rates to calcining temperatures at approximately 1400°C. Calcining temperature is defined as the point at which the last traces of hydrogen are driven off.

Graphitization

Further increases in temperature above approximately 1100°C cause the almost pure carbon, the product of

carbonization, to continue to increase both to in-plane and layer stacking perfection. The three-dimensionally ordered graphite structure with ABABAB stacking progressively develops above 1800°C and the material is now called graphite (1).

Graphite is defined as the allotropic form of the element carbon consisting of layers of hexagonally arranged carbon atoms in a planar condensed ring system. The layers are stacked parallel to each other. There are two allotropic forms of graphite with different stacking arrangements, hexagonal and rhombohedral (16). Hexagonal graphite is the thermodynamically stable form of graphite. Its equilibrium structure was confirmed by Bernal (18) in 1924 to consist of plane layers of carbon atoms covalently bonded in a regular open-centered hexagonal array, stacked in a ABABAB sequence with weak van der Waals bonding between the layers. At room temperature, the interatomic distance is about 1.42 Å and the unit cell dimension a = 2.4615Å within the layers. The interlayer spacing, $\bar{d}$, equals c/2 which equals 3.354Å, where c is the unit cell height. The equilibrium structure of graphite is shown in Figure 1. It is this hexagonal form, obtained by the graphitization process, that we will be discussing in this study.

There are many hypotheses as to the actual

mechanisms involved in the graphitization process. Fischbach (19) describes the graphitization process in terms of the progressive improvement of an initial highly defective structure which exists in the carbon. Warren (20) was one of the first to recognize the significance of the changes in diffraction parameters during graphitization and formulated the turbostratic model which is still the most prevalent basis for describing the structure of disordered carbons. This model assumes that disordered carbons consist of near-perfect, graphitic layer plane segments arranged in parallel stacks, but with no correlation between adjacent layers. Layers within a stack may be displaced from the equilibrium ABABAB relationship with their neighbors either by small translations parallel to the plane or rotations about the c-axis (normal to the plane).

As more detailed studies have been carried out on an increasing variety of carbons using improved equipment and techniques, it has become apparent that there are many features of the structure of disordered carbons, and of the changes in structure and properties which accompany graphitization, which are difficult to reconcile with the simple turbostratic model. Interest has focused increasingly on the distortion aspects of the structure. Defective layer planes as well as stacking disorder must

be studied to understand disordered carbons (19).

The process of graphitization has been shown as the development of a relatively perfect, crystallographically ordered structure from an initial highly imperfect, disordered structure. The detailed nature of this process is still being debated, but the process itself can be followed using a number of different parameters and techniques.

There are a number of parameters which could be measured to follow the graphitization process. This is due to the anisotropic nature of graphitizable carbons, making most parameters strongly dependent on structure. Parameters used should be easy to measure and have adequate precision, as experimental data cover a wide range of heat-treatment temperatures (HTT). The parameters should be sensitive and directly related to crystallographic structure, and insensitive to microstructural variables such as porosity and morphological features such as preferred orientation texture. The mean interlayer spacing ($\bar{d}$) is the most common parameter used for this purpose. The mean interlayer spacing decreases with the development of a graphitic ordered structure. The symbol $\bar{d}$ is defined as being equal to c/2, half the unit cell height, and is shown in the diagram of hexagonal graphite in Figure 1. The value of $\bar{d}$ decreases from

$\geq$ 3.44Å in a disordered carbon to 3.354Å for near-perfect graphite at room temperature. This is a change of more than 2% in a parameter than can be measured to a precision of 0.1% in partially graphitized carbons, using standard Debye-Sherrer or x-ray diffraction techniques. Ruland (21) defines an index for degree of graphitization ($\bar{g}$) as $\bar{g} = (3.440\text{Å} - \bar{d}_{002})/(3.440\text{Å} - 3.354\text{Å})$. This can be used to follow the change in $\bar{d}_{002}$ as graphitization proceeds, but the value of 3.440Å assumed for disordered layer spacing for pregraphitic carbons heat treated to 1000°C limits its usefulness as an actual measure of degree of graphitization. We will term $\bar{g}$ the XRD graphitization index.

In many studies on the graphitization process apparent crystallite layer diameter (L_a) or apparent crystallite height (L_c) is used to correlate changes in structural or physical properties to increases in order or development of crystalline structure. L_a and L_c are difficult to measure with precision, because they are determined from diffraction peak profile analysis. The difficulty with these measurements arises when attempts are made to separate true particle size broadening from the distortion broadening also present. L_a is essentially a measure of the average size of planar, defect-free layer regions. Graphite layers typically have holes, cracks or bends in them, and so

will give small L_a values when measured by x-ray or electron diffraction peak profile analysis, though the lateral dimensions of the imperfect layer structures may be large. Fischbach (19), on the other hand, suggests L_a values are best interpreted as indications of relative layer flatness and perfection rather than as real crystallite layer diameters. L_a can be a significant measurement for distinguishing order between graphitizing and nongraphitizing carbons when data are properly analyzed and limitations of the analysis are taken into account. Similarly, L_c can be a useful parameter for distinguishing order for partially graphitized materials whose (00ℓ) peaks are measurable. In very disordered carbons only the (002) and perhaps the (004) peaks are measurable; however, and to only a minimum degree of precision. This limits the usefulness of L_c. The turbostratic structure proposed by Warren (20) and described earlier is thought to be a large contributor to an asymmetric (002) peak. Figure 9 shows changes in L_c as a function of HTT. L_c can be seen to decrease slightly from 400°C to approximately 1000°C, then increase through the rest of the heat-treatment cycle up to 3000°C.

Analytical Techniques

Many techniques have been employed to study the changes in material properties and morphology of carbons

from pitches as graphitization proceeds. The changes are then related back to the graphitization process.

X-ray diffraction has been used extensively in studies analyzing the process of graphitization. The x-ray diffraction patterns of disordered carbons, regardless of the source or type of carbon, have certain characteristic features in common. They consist of two types of peaks: (00ℓ) peaks resulting from stacks of parallel layer planes; and two-dimensional (hk0) peaks resulting from the regular structure within the individual layer plane segments. Peaks of the type (hkℓ) are absent, indicating that there is little or no stacking order in the arrangement of parallel layers.

The higher order (00ℓ) reflections and the (hkℓ) reflections are not sufficiently developed in disordered and partially ordered carbons to allow precise measurement of $\bar{d}$. This is of only minor consequence for two reasons. The standard extrapolation techniques are in general designed for metals and alloys with high absorption coefficients, whereas absorption in carbon is low. Disordered and partially graphitized carbon samples display a broad distribution of interlayer spacing values rather than a unique value (19). According to Ruland (21), the root mean square (rms) displacement in the c-axis direction can be as large as 0.05Å even in moderately graphitized

carbons with $\bar{d}$ approximately equal to 3.38Å. Under these circumstances, a simple average of $\bar{d}$ serves just as well (17). Satisfactory $\bar{d}$ values can be obtained from measurements on a single (00ℓ) peak. The (002) peak is the most intense line in the diffraction pattern and has frequently been used to determine $\bar{d}$. However, it occurs at a relatively low Bragg angle (for the commonly used Cu and Cr radiation) where the dispersion is low, and it occurs on top of an angle-dependent background which is often large. Both of these factors make it difficult to obtain results from the (002) peak, though it is the only (00ℓ) peak which is measurable in very disordered carbons.

As graphitization proceeds, an initial diffraction pattern that was weak and diffuse changes upon an increase in heat-treatment temperature. The reflections are seen to sharpen, the (00ℓ) peak maxima moves to higher angles, and the (hkℓ) reflections develop. This evolution of the diffraction pattern indicates, respectively, that average interlayer spacing decreases; lattice distortion decreases and/or mean crystallite size increases, both parallel and perpendicular to the layer; and ordered layer stacking sequences develop. The (004) peak is now measurable throughout the rest of the graphitization process and gives more reliable results for determination of $\bar{d}$ than the (002) peak (19). Polarized light microscopy and

scanning electron microscopy are the most common techniques for analysis of the morphological changes that occur during graphitization.

The initial morphology of the graphitized carbon initiates by chemical reactions which polymerize aromatic molecules in the same layer, building strong lamellae. Shrinkage-cracks open to afford some relaxation of the spatial constraints. The stage is then set for thermally activated lamellar displacements to occur which will promote formation of three-dimensional crystalline geometry which will replace the more disordered curved layers of carbon lamallae. This relaxation of spatial constraints is suggested by the x-ray diffraction measurements in Figure 9, as described earlier. In the figure a period of inactivity immediately after mesophase hardening is shown, possibly indicating a relaxation of geometrical constraints prior to the initiation of crystallite size growth around 1000°C. After temperature increases beyond 1000°C, crystallite size is seen to increase at a steady rate up through 3000°C, which is the maximum temperature considered in the heat-treatment process.

White (4) identified the first point at which graphitization is evident as the phenomenon of fold sharpening. As the heat treatment is increased to reach calcining temperatures near 1400°C, i.e., driving off the

last traces of hydrogen, shrinkage cracking tends to occur at regular intervals along folded regions. The resulting segments, relieved of lateral constraints, tend to alter their shape by decreasing their radii of curvature at some point near the center of the fold. In many cases the curvature lies beyond optical resolution limits and the fold takes on the appearance of a twin boundary. These phenomena are illustrated in Figure 10, where fold-sharpening is seen as a twin boundary in the micrograph of coal-tar pitch derived coke heated to 1400°C.

The shrinkage cracks are found in a variety of sizes and spacings. Running parallel to the layers, the cracks absorb a major portion of the high thermal expansion in the direction of the c-axis within the coke particle. The shrinkage cracks also provide mechanisms to decrease the elastic modulus and the cleavage strength of a coke particle. Furthermore the progress of a fracture across the convoluted folded structure will prove to be difficult, and many blind fractures will open before the main fracture path is developed. This effect will provide an energy absorbing mechanism and contribute to the fracture toughness of the coke particle. The net result of the preferred orientation of layers and the shrinkage is that good thermal stress resistance is produced in graphitized pitches (4).

Mesophase densification as a function of heat-treatment

temperature for three types of coke was described by White (4). Changes in density as a function of HTT are shown in Figure 11. He compared real density of acenaphthylene, extracted coal-tar pitch, and petroleum cokes by immersing samples in liquid so that the coke particles would be wetted. Good agreement is found for aromatic mesophase from acenaphthylene coke and extracted coal-tar pitch coke. The data for petroleum coke follow a curve of similar shape but at slightly lower level of density. Density is seen to increase from 550°C to 1400°C. The maximum rate of densification at approximately 800°C correlates with hydrogen evolution. A reasonable level of dimensional stability is attained by 1400°C, the calcining temperature.

Laser Raman microprobe analysis (LRMA) is emerging as one of the most promising techniques for analysis of composite materials. It has proved particularily useful in the area of C/C composites due to its ability to non-destructively characterize in situ a C/C composite surface rapidly, with a resolution as small as 1 μm. LRMA has been demonstrated to be able to detect the stages of graphitization for a variety of carbons. Nemanich and Solin (22) studied the dependence of first- and second-order graphite Raman spectra on crystallite dimensions, L_a and L_c. First- and second-order Raman spectra refer to transitions between the atomic vibrational levels. First-order spectra

represent a transition from vibrational level zero to one. Second-order spectra represent a transition from vibrational level zero to two or higher. In the study of Nemanich and Solin (22), single crystal graphite, highly oriented pyrolylic graphite (HOPG), glassy (nongraphitizing, i.e., amorphous) carbon, pressed carbon rods, and carbon powders were analyzed. Features in the second-order spectrum broaden noticably and additional broad features appear in both the first- and second-order spectra as crystallite size decreases. This is shown in Figure 12, for first- and second-order Raman spectra. Nemanich and Solin related the strong peak at 1581 cm^{-1} to the high-frequency E_{2g} first-order mode. The continuum scattering from 2200 to 3250 cm^{-1} represents second-order features. The second-order spectrum exhibits three distinct groups of bands. These bands are dominated by strong features near 2710 cm^{-1} and by two weaker features at 2450 and 3250 cm^{-1}. These represent additional vibrational levels; however, they are not used in this analysis of graphitization so we will not consider them further.

Tuinstra and Koenig (23) extended this work by comparing spectra of single crystal graphite to other less graphitic materials in order to get a precise determination of crystallite size. In Figure 13, the Raman spectrum for single crystal graphite is compared with Figure 14 which

shows Raman spectra for stress-annealed pyrolytic graphite, commercial graphite, and activated charcoal. Single crystal graphite shows only a peak at 1575 cm^{-1}. In comparison, Raman spectra for the less graphitic materials show increasing intensity of the peak at 1355 cm^{-1} in conjunction with decreasing intensity of the 1575 cm^{-1} peak. This is indicative of decreasing crystallite size. Peaks are broader when crystallite size is smaller. The single crystal graphite peak at 1575 cm^{-1} is seen to be quite narrow with a high intensity. In contrast, the Raman spectrum for activated charcoal had smaller peaks of almost equal intensity for both the 1355 and the 1575 cm^{-1} peaks. These peaks are quite broad in comparison to the single crystal graphite 1575 cm^{-1} peak. This indicates crystallite size is considerably smaller in the activated charcoal.

Lespade et al. (24) took these studies yet one step further and developed a method for determining the path of graphitization for any graphitic material. Pitch cokes, anthracene cokes, saccharose cokes (sugar), fibers from polyacryonitrite (PAN), and pyrocarbons deposited from methane were examined. The samples were graphitized at temperatures up to 3000°C. Mean diamagnetic susceptibility, $\bar{\chi}$, and the average interlayer spacing, $\bar{d}_{002}$, were measured to characterize the degree of graphitization within each material. Both are properties that are dependent on

graphitic order. Raman spectra for all materials were then taken. Four graphitization indices were selected: $\nu_{E_{2g}}$, the frequency; $\Delta\nu(E_{2g})$, the line width of the E_{2g} line; R, the ratio of the intensities of the 1350 cm^{-1} and E_{2g} lines; and $\Delta\nu(2700)$, the line width of the main line in the second-order spectrum. Good correlation was found for all types of carbons between these indices and $\bar{\chi}$ and $\bar{d}_{002}$.

The relationship of d-spacing to peak intensity ratio is shown in Figure 15 as a function of $\bar{d}_{002}$ versus R. R is seen to decrease with decreasing d-spacing, within a moderate range of scatter. The relationship of d-spacing to $\nu_{E_{2g}}$ is shown in Figure 16 as a function of $\bar{d}_{002}$ versus E_{2g} peak position. The E_{2g} peak position is seen to decrease with decreasing d-spacing, within a moderate range of scatter. The complete graphitization path for these carbons is shown in Figure 17 as a function of $\nu(E_{2g})$ versus $\Delta\nu(2700)$. Lespade et al. (24) related the path of graphitization to structural changes occuring during graphitization. $\Delta\nu(E_{2g})$ is seen to decrease with $\Delta\nu(2700)$ as the graphitic layers grow in two dimensions. As three-dimensional ordering commences, $\Delta\nu(E_{2g})$ is seen to decrease slightly with a slight increasing of $\Delta\nu(2700)$.

In addition, Lespade et al. (24) studied the spectra of carbon/carbon composites using various fibers and matrices. The Raman spectra of the fiber substrates

and matrices were obtained separately. Typical spectra of a composite of PAN fiber and a pitch matrix are shown in Figure 18. Characteristic differences in the evolutions of each type of substrate and matrix are clearly seen. No evidence was seen of the matrix or substrate influencing the evolution of the other.

There is a possibility that the progress of graphitization in a pitch derived carbon could be followed by use of electron energy loss spectroscopy (EELS). In a comparison of the EELS spectrum of diamond, graphite, and amorphous carbon Egerton and Whelan (25) noted significant differences. The diamond spectra exhibited marked differences in position and structure when compared to the spectra of graphite and amorphous carbon. The spectrum of amorphous carbon and graphite showed a similarity in position, but the structure of the amorphous carbon was less distinct when compared to graphite. Egerton and Whelan attributed this to the loss of fine structure in density of crystalline states in comparison with spectra for an amorphous sample. Two of the spectra are shown in Figure 19. The diamond spectrum is seen to have three main peaks, at 3.8, 10, and 17.5 eV. Graphite is seen to exhibit two peaks in the EELS spectrum, at 3.75 and 12.0 eV.

Experimental Procedures

White (4) noted that experimental procedures for sample processing are quite relevant to any studies done, as the material is sensitive to the mechanisms acting to form the microstructure before the mesophase hardens. Due to the tendency of the mesophase to segregate in the liquid matrix and to the sensitivity of the plastic microstructures to stress, liquid-sampling techniques are not suitable to obtain specimens representative of the microstructure forming at various stages of pyrolysis. However, differential or incremental pyrolysis methods have been found useful to obtain sequential specimens for every stage of interest in microstructure formation. A convenient experimental method is to employ a large, uniformly heated metal block with penetrations to accommodate a number of tubes containing the specimens to be subjected to identical programs of heat treatment. Tubes are withdrawn with minimum disturbance at desired intervals. Drastic cooling procedures are not required to quench the microstructures. A complete vertical cross-section of each pyrolysis residue should be prepared to ensure full characterization of segregated microstructures.

Heat treatment should be carried out in a nonoxidizing atmosphere, usually in a vacuum or with an inert gas.

Inert gas is preferred because there is less chance of evaporation/deposition effects and it is experimentally easier. In a study by Thakur and Brown (26), the inert atmosphere used during material processing was found to affect the surface characteristics and pore structures of coal initially pyrolyzed to 586°C in a helium atmosphere and then heated to 886°C under three different nonreactive atmospheres; helium, argon, and nitrogen. Smoothness of the surface, absorption capacities, and reactivitiy during processing all decreased with respect to a particular order of inert atmospheres: He > Ar > N_2.

While the stages in the graphitization process have been well established, a reliable and reproducible method for quantatively measuring the state of graphitization has not. XRD, SEM, LRMA, and EELS all are promising tools for characterization of the graphitization process; however, they need to be utilized in a complementary way to verify any quantative analysis that is to be made.

CHAPTER III

Experimental Procedures

Sample Preparation

Nine samples of mesophase pitch and one C/C composite sample were obtained from Aerospace Corporation, Los Angeles, California. Their specific time and temperature profiles are listed in Table III for each pitch source. The coal-tar pitch samples used are Allied Chemical Corporation 15V mesophase pitch. The petroleum pitch is Ashland Petroleum A240 pitch. Properties for the two pitches are listed in Table I which shows the softening point, percent of benezene and quinoline insolubles, coking value, ash content, specific gravity, and sulfur content (5). Chemical analyses for the two pitches are listed in Table II which shows carbon, hydrogen, oxygen, nitrogen, and sulfur content. The C/C composite sample is a unidirectional composite, with a coal-tar pitch matrix and Thornel P-55 fiber.

The pitch samples were all pyrolyzed at the same time in a copper core furnace constructed at Aerospace Corporation. The samples are processed by weighing out ground pitch into aluminum cylinders (140 mm x 19 mm diameter). A cap with a 1 mm hole in the center is

placed over each cylinder. The samples are loaded into glass tubes (340 mm long x 25 mm diameter) that serve as retorts, and heated to 550°C at a rate of 20°C per hour. The atmosphere in each tube was nitrogen from a liquid nitrogen tank. The tubes are inserted into bores in a very large copper block. Each glass tube has an atmosphere inlet with its own flow meter and an outlet tube that is vented to outside the furnace. The controller thermocouple is located at the center of the large copper block. The heat treatment schedule is entered into a Data Trak programmer which controls the rate. All cool down rates were gradual.

The calcining furnace used for the carbonization of the samples is an alumina tube furnace. The samples were heat treated with an increasing temperature rate of 50°C per hour up to 1000°C in a flowing nitrogen atmosphere. The maximum temperature of 1000°C was held for 15 minutes. Temperature was monitored with a type K thermocouple inside the furnace hot zone. It should be noted that the 1000°C HTT sample appeared anomalous when examined using XRD, SEM, and LRMA. This could be due to a labelling or processing error and does not effect the processing of the other samples.

The samples were graphitized with an increasing temperature rate of 400°C per hour in an argon atmosphere. The furnace used is a graphite element furnace. Temperature

readings are made by sighting through a port on the sample with an optical pyrometer, used once the sample has reached approximately 800°C. Graphitization temperatures ranged from 2100°C to 2550°C, with residence times of 15 or 30 minutes for the final HTT.

The inert gases used for heat treatment were chosen for our sample preparation to reproduce the processing parameters used by manufacturers of carbon/carbon composites (26).

Due to the effect of pressure on mesophase formation (20) the samples were processed using the same pressures as the manufacturers of carbon/carbon composites. When a sample was prepared, care was taken to sample a cross-section of the specimen to reduce the effects of the sample processing selected (8).

X-ray Diffraction

Samples were crushed using an agate morter and pestle to a particle size ranging from approximately 100 to 400 μm. Each sample powder was then glued to a glass slide approximately 1 mm thick with Duco cement. A glass slide with only Duco cement was first run on the diffractometer to assure that the cement would not have any effect on the subsequent scans with pitch samples.

A General Electric X-ray Diffractometer, Model No. 11GN1, was used for the scans. Copper K_{α} radiation was

selected as the appropriate radiation source. A Nickel target filter was used to reduce the effect of K_β peaks.

Scanning Electron Microscopy

Samples were crushed using an agate mortar and pestle to a particle size of 100-400 μm. Each sample powder was then attached to a piece of aluminum foil with Aduadag Colloidal Graphite paint. Four samples at a time were placed on a brass tab, again using carbon paint as an adhesive. Each quadrant of the tab was marked according to which sample was in it. Two samples were made of each pitch to insure representative morphologies.

A JEOL 840 Scanning Electron Microscope was used to analyze the samples. A standard accelerating voltage of 15 keV was used with a working distance of 6 mm or 7 mm, unless otherwise specified. The probe current ranged from 6×10^{-10}A to 1×10^{-10}A.

Laser Raman Microprobe Analysis

Laser Raman microprobe analysis was used to examine nine pitch samples and a unidirectional C/C composite. The pitch samples were prepared by crushing them and placing them on a glass slide with no adhesive. The unidirectional C/C composite sample was placed on a glass slide with a small amount of amorphous adhesive to prevent it from shifting. Spectra were obtained using an

Instruments S.A. U-1000 micro-Raman system which projected laser light through an Olympus 50x objective, providing a one micron spot size at the sample. Instrumental slit width was 1000 micrometers, near 9 cm^{-1}; step size was 1 cm^{-1}. Collection times ranged from 1 to 10 seconds per point, the 10 second collection time being needed for the unstable pyrolyzed pitch samples. This translates to spectrum run times of 30 minutes to 2.5 hours per spectrum. The laser used for sample excitation was a Coherent Innova 90-4 argon ion laser using the 5145Å line (green line). Power at the sample ranged from 3 to about 50 mW.

Electron Energy Loss Spectroscopy

Samples were crushed using an agate mortar and pestle to approximately 50-100 μm in size. Care was taken to crush them in such a way that particles would shear so sufficiently thin particles could be obtained. Each sample powder was placed in a vial containing acetone. The dilute solution was then sonicated for 10 minutes to ensure random uniform distribution of particles in solution. A holey carbon grid was dipped in the solution, letting some particles adhere to it, and dried. Each grid was labelled on the grid container to indicate which sample it contained. Spectra were obtained using a Philips 400T transmission electron microscope with a Gaton Model 607 EELS.

CHAPTER IV

Results and Discussion

X-ray Diffraction

X-ray diffraction scans obtained from the chart recorder are located in Appendix A. X-ray diffraction peaks, corresponding d-spacings, and graphitization indices for each of the nine pitch samples are presented in Table IV. 2θ values for the (002) and (004) peaks are listed in this table for each x-ray diffraction scan. The relationship of d-spacing to heat-treatment temperature is shown in Figure 20 as a plot of $\bar{d}$ for the (002) and (004) peaks versus heat-treatment temperature. The relationship of graphitization index to heat-treatment temperature is shown in Figure 21 as a plot of $\bar{g}$ versus heat-treatment temperature. The d-spacing corresponding to each 2θ value was calculated using the formula $\bar{d} = \frac{\lambda}{2\sin}$ where $\lambda = 1.5418\text{Å}$ for Copper K_α radiation (27). Values were obtained from the Joint Committee on Powder Diffraction Standards (JCPDS) diffraction data cards for use as references (28,29). Values for estimated intensities were obtained from Set 23, Card 64 for Ceylon single crystal graphite using Copper K_α radiation with a Nickel filter (28). Calculated values for x-ray diffraction

lattice parameters were obtained from Set 25, Card 284 and showed values of a_o = 2.456 and c_o = 6.696 (29). The graphitization indices ($\bar{g}$) were calculated using $\bar{d}_{002}$ values and Ruland's formula (21): $\bar{g} = \frac{(3.440\text{Å} - \bar{d}_{002})}{(3.440\text{Å} - 3.354\text{Å})}$ where 3.440Å = disordered layer spacing and 3.354Å = single crystal graphite ordered layer spacing.

Initially the 2θ value for the (002) peak in the coal-tar pitch sample decreases from the 500°C HTT value of 26.00° to the 585°C HTT value of 25.80°. This corresponds to an increase in d-spacing from 3.4270Å (500°C HTT) to 3.4531Å (585°C HTT). The 2θ value then increases with increasing HTT, from the 585°C value to the 2550°C value of 26.25°. *This corresponds to a decrease in* d-spacing from 3.4531Å (585°C HTT) to 3.3949Å (2550°C HTT). The 1000°C HTT sample is an exception, it has the lowest 2θ value obtained, 25.30°. The 2300°C HTT sample has a 2θ value of 26.25°, slightly higher than the 2400°C sample, and so is also slightly exceptional. The 2θ value for the coal-tar pitch sample heat treated to 2400°C and held for 30 minutes, as opposed to the standard 15 minutes, is the same as the 2400°C-15 minute sample (26.20°). This corresponds to a d-spacing of 3.4013Å. The 2θ value for the petroleum pitch sample heat-treated to 2400°C and held for 30 minutes is the highest 2θ

value obtained for the (002) peak, 26.60°, corresponding to a d-spacing of 3.3510Å.

Graphitization indices are seen to follow the same trends as the 2θ values for the (002) peak. An initial decrease is seen from 0.151 (500°C HTT) to -0.152 (585°C), followed by an increase from -0.152 to 0.524 (2550°C HTT). The 1000°C HTT and 2300°C HTT samples are again exceptions to this trend. The 2400°C HTT-30 minute sample had the same graphitization index as the 2400°C HTT-15 minute sample, 0.450. The petroleum pitch sample had the highest graphitization index, 1.035.

The 2θ value for the (004) peak in the coal-tar pitch sample increases from the 2100°C HTT value of 53.75° to the 2550°C HTT value of 54.35°, corresponding to a decrease in d-spacing from 1.7054Å to 1.6879Å. The 2θ value for the 2400°C-30 minute coal-tar pitch sample is the same, 54.20°, corresponding to a d-spacing of 1.6923, as the 2400°C-15 minute sample; indicating residence time had no effect on the d-spacing of 2400°C coal-tar pitch. The 2400°C-30 minute petroleum sample is the highest 2θ value obtained for the (004) peak, 54.70°, corresponding to a d-spacing of 1.6780Å.

White (4) states that d-spacing values for carbons decrease from $\geq$ 3.44Å in a disordered carbon to 3.354Å for single crystal graphite. This corresponds well with

the results shown in Table IV and Figure 20 for the (002) peak. The actual values should only serve as indications of the graphitization process as angular offset was not corrected for by using an internal standard. The petroleum pitch sample (2500°C-30 min) is seen to be the most graphitic in Figure 29. This would be expected as petroleum pitch graphitizes easier than coal-tar pitch, according to Kochling et al. (15). There appears to be no change in the peaks for 2400°C-15 minute coal-tar pitch or 2400°C-30 minute coal-tar pitch for 2θ values d-spacings or for $\bar{g}$, indicating that graphitic ordering has stabilized. Some change is still noted for the 2500°C HTT peaks; however, indicating some slight ordering taking place in the 2550°C sample.

The initial decrease in graphitization index from 0.151 to -0.152 for the 500°C HTT sample and 585°C HTT sample, respectively, corresponds to an increase in 2θ values of 0.50°C. These values are well within the range of error due to the extreme broadening effects in the range of lower angles. Also, the XRD pattern for a glass slide with only Duco cement on it produced a large background effect in the lower angle range, contributing to the error. In addition, no internal standard was used, so the values are well within the range of experimental error for 2θ peak values. Therefore, these values should

not be considered as an indication of a reversal in the graphitization process.

X-ray diffraction peak intensities are shown in Table V. The relationship between peak intensities and HTT is shown in Figure 22 for the nine pitch samples. Estimated intensities are obtained from JCPDS diffraction card 23-64 (28). Calculated values are obtained from JCPDS diffraction card 25-284 (29). In general, the (002) peak intensity, measured in chart units, increases from the 500°C HTT value of 8.0 to the 2550°C HTT value of 60.1 for the coal-tar pitch samples. Two exceptions should be noted. The intensity of the 2300°C HTT peak has the highest intensity obtained, 80.75, and the 2100°C HTT peak intensity is slightly higher than the 2400°C HTT peak. The 2400°C-30 minute petroleum pitch peak intensity (49.1) falls between the 2400°C-15 minute and 2500°C-15 minute coal-tar pitch samples. Also, the 1000°C sample peak intensity is lower, indicating a less ordered structure, than the 500°C and 585°C HTT samples.

The (004) peak intensities were normalized using the formula:

$$\frac{(002)}{(004)} = \frac{N(002)}{N(004)} \text{ where } N = \text{normalized value.}$$

The (004) peaks were normalized to see the effect heat treatment had on the relationship between the (002) peak

intensity and the (004) peak intensity. In general, the (004) peak intensity, measured in chart units, increases from the 2100°C HTT value (3.1) to the 2550°C HTT value (4.1) for coal-tar pitch. The 2300°C HTT sample (004) peak is 5.1, the highest value seen. Peak intensities for the 2400°C-30 minute coal-tar and petroleum pitch samples are the same (4.0). The normalized peak intensities for the (004) peak increase with increasing heat-treatment temperatures from the 2100°C HTT value of 6.0 to the 2400°C and 2550°C HTT values of 6.8. The 2400°C-30 minute coal-tar pitch intensity (7.1) is higher than the 2400°C- and 2550°C-15 minute samples. The 2400°C-30 minute petroleum pitch sample is the highest value obtained for the (004) peak, 8.1. It appears that the 2100°C and 2300°C HTT samples have higher intensities than would be expected.

The normalized values for the (004) peak intensities give the expected result of increased order with increasing heat-treatment temperature and residence time. The petroleum pitch is seen to be the most graphitic as predicted by Kochling et al. (15). These trends could indicate that the (004) peak is the most reliable measurement for increased graphitic structure due to heat treatment as stated by Fischbach (19). However, it may also be that there is some orientation effects present, possibly due to the particle aspect ratios being larger in

some samples that normalizing cancells out.

X-ray diffraction broadening measurements are shown in Table VI. The table shows half-peak intensity values for the (002) and (004) peaks, the 2θ values measured at the half-peak intensity point, and the broadening value calculated from these values. The formula used to calculate the broadening value is:

$$B\ (\text{rad}) = \frac{\pi(2\theta_1 - 2\theta_2)}{360}$$ where $2\theta_1$, $2\theta_2$ = 2θ values at half-peak intensity (°) (27).

The relationship between (002) and (004) peak broadening and heat-treatment temperature is shown in Figure 23 for the nine pitch samples. Broadening for the (002) peak is seen to increase from the 500°C HTT value of 0.02269 radians to the 1000°C value of 0.03752 radians. Broadening for both the (002) and the (004) peaks is seen to decrease from 1000°C HTT for the (002) peak and 2100°C HTT for the (004) peak, to 2300°C HTT. This is a decrease from 0.03752 radians to 0.00742 radians for the (002) peaks and a decrease from 0.00916 radians to 0.00829 radians for the (004) peaks. There is an increase in broadening from the 2300°C HTT value of 0.00742 radians to the 2400°C HTT value of 0.00873 radians for the (002) peak. The (004) peaks increase in broadening from 0.00829 radians to 0.01091 radians for the same temperature range. The broadening

value for the (002) peak 2400°C-15 minute sample is the same as for the coal-tar and petroleum 2400°C-30 minute samples, 0.00873 radians. The (002) broadening value decreases to 0.00742 radians for the 2550°C HTT sample. The broadening value for the (004) peak decreases to 0.00960 radians for the petroleum and coal-tar pitch 2400°C-30 minute samples, and to 0.00698 radians for the 2550°C HTT sample. In general, broadening decreases with increasing HTT as reported by Fischbach (19). As seen previously in the intensity measurements, the 1000°C HTT sample seems to indicate the lowest state of graphitization. If broadening is thought to be due to crystallite size effects only, and no disorder effects are considered, the Sherrer formula (27) may be used to estimate crystallite size, L_a:

$$L_a = \frac{0.9\lambda}{\beta\cos\theta_B} \text{ where } \theta_B = \text{half the } 2\theta \text{ sample value.}$$

Crystallite size increases from 37.9Å for the most disordered 1000°C HTT sample to 192.1Å for the highly ordered 2550°C HTT sample. These values are only rough orders of magnitude due to the great effect of disordered layer spacing on actual crystallite measurements. They do support the contention that the 1000°C sample does exhibit the least amount of ordering of all nine samples. The initial decrease in (002) peak broadening from the 500°C HTT sample to the

585°C sample is within the area of experimental error due to the difference in 2θ readings of the peak values of 0.20°C.

Scanning Electron Microscopy

The 585°C HTT coal-tar pitch sample is shown in the micrograph in Figure 24. It shows a surface of smooth curves with no distinctive features. Curves of flow patterns from the molten pitch can be seen. This is indicative of a highly disordered carbon structure. This sample is much closer in structure to amorphous carbon than to the highly ordered structure of graphite.

The morphology of the 1000°C HTT coal-tar pitch sample is shown in the micrographs of Figures 25 through 28. Two possible scenarios are suggested by these photomicrographs. In the first case, the spheres seen could be mesophase spheres indicating a much lower graphitization stage, that of pyrolyzation, than would be expected for a pitch sample heat treated to 1000°C with a residence time of 15 minutes. In the second case, these spheres could be globular grains of carbon, which would correspond well with the carbonization stage of graphitization, described earlier. For now, both scenarios will be addressed. Which scenario is more likely will be considered in the Discussion section.

Figure 25 shows mesophase spheres or possibly globular grains of carbon, 5-10 μm in diameter covering the surface. Large areas of untransformed pitch, or coarse grains of

carbon dispersed in globular formed grains, can be seen. A few long-range cracks run through the sample, 10-30 μm in length. Figure 26 is an enlargement of Figure 25 and shows even smaller, sub-micron spherules or quinoline-insoluble particles surrounding the larger coalesced spherules or globular grains of carbon. The spheres and spherules (or possibly globules) have a slightly roughened texture. These figures either represent the stages of coalescence in a localized area of the pitch, as described by Brooks and Taylor (8) and verified in their micrograph shown in Figure 4, or grains of carbon dispersed in globular grains as would be expected at 1000°C HTT. The cracks, or fissures, can be attributed to shrinkage of the pitch matrix as it is heat treated; or to disinclinations within the carbon grains. This long-range fissuring is produced by linking of shrinkage cracks and is very similar to fissures found by White (4) as shown in Figure 16 for 800°C HTT coal-tar pitch.

Figure 27 shows mesophase spherules, 5-10 μm in diameter, covering a valley through an area of untransformed pitch. This could also be interpreted as spheritic or globular matrix grains between coarse matrix grains. A few cracks, 15-50 μm in length, are seen running through the untransformed or coarse area of the matrix, but not

in the mesophase spherule or fine grains areas. Figure 28 is an enlargement of Figure 27 and shows small pits, or possibly particles, 1-3 μm in diameter, surrounding the spherules or fine grains. The spherules or grains have a slightly roughened texture. These figures represent the morphology solidified in the coke when mesophase coalescence takes place in a localized area of the pitch as described by Brooks and Taylor (8), accompanied by bubble percolation described by White (4) and verified in his micrograph and schematic drawing shown in Figures 5a and 5b, respectively. The cracks are shrinkage cracks due to carbonization heat treatment described by White (4).

The 2100°C HTT coal-tar pitch sample is shown in Figures 29 and 30. Figure 29 shows extensive flaking and delamination of the surface in two dimensions. Figure 30 shows short, 5-7 μm in length, cracks running basically parallel to each other. The flaking and delaminations seen run parallel to the lamellar structure of this partially graphitized sample, as described by White (4). The path these delaminations take reveals the tight folds, bends, and disinclinations discussed by White and verified in his micrograph shown in Figure 7. This results from mesophase refinement due to bubble percolation. Cracks are due to continued matrix shrinkage but essentially in two dimensions.

The 2300°C HTT coal-tar pitch sample is shown in Figures 31 and 32. Figure 31 shows extensive cracking on the surface. The cracks are short, 40-50 μm in length, and cover the surface. The surface surrounding the cracks is slightly rough and flat. No flaking or delaminations can be seen. Figure 32 is an enlargement of Figure 31 and shows the cracks to be deep and narrow. Some are curved and some are relatively straight. The cracks are longer than those found in the 2100°C sample, almost by a factor of ten, and run in all directions, indicating progression of matrix cracking. That no extensive delamination or flaking is seen is indicative of random orientations of fine grains. Carbon grains are finer in this sample than in the 2100°C HTT sample. Orientations seem to be more random. Lamellae patterns are present, but on a much finer level than the 2100°C HTT sample.

The 2400°C HTT coal-tar pitch sample that was held at that temperature for 30 minutes, as opposed to the standard 15 minutes, is shown in Figures 33 through 38. Figures 33 and 34 show an extensively linked sample surface with numerous openings in all directions. Cracks are seen, 10-60 μm in length, with separated layers running perpendicular to the length of the crack inside. Figures 35 and 36 are enlargements of Figures 33 and 34, respectively. Separated layers can now be seen clearly to

run across the width of the cracks. Along the length of the cracks, the surface looks as if the separated layers have broken off as the cracks widened.

Figure 37 shows a surface with extensive holes. The surface has a "fish scale" appearance and is flat. This results from lamellae intersecting the surface at an angle. Figure 38 is an enlargement of Figure 37 and shows the holes to be round with a diameter of 2-3 μm. This morphology could be attributed to foam at the top of the sample, formed during pyrolyzation. The extensive linkage of the sample in all directions indicates three-dimensional ordering. The surface cracks showing layers perpendicular to the length of the cracks also show that the two-dimensional lamellar structure originally seen in less graphitized samples has given way to orientation in all three directions. The holes are typical of porosity holes due to the foam formed by earlier gas evolution of methane, hydrogen, and sulfur as described by White (4) and Pietzka (17). The cracks and openings are due to increased shrinkage of the matrix due to higher HTT, described by White (4).

The 2400°C HTT petroleum pitch sample held at that temperature for 30 minutes is shown in Figures 39, 40, and 41. Figure 39 shows the surface to have a fish scale appearance with an extremely rough surface underneath. The "fish scales" are 4-6 square microns. Figure 40 shows

an extensively linked surface, with surface ridges running in all directions. Figure 41 is an enlargement of Figure 40 showing a delamination area running along a wall of the sample surface. This extensive linkage is similar to that of the 2400°C HTT coal-tar pitch sample held for 30 minutes, and is indicative of good lamellar structure. The delamination area is also similar in appearance. These figures indicate a three-dimensional ordering indicative of graphitized pitch derived carbon.

Laser Raman Microprobe Analysis

Raman spectra of individual samples are located in Appendix B. Raman spectrum peak positions for the nine pitch samples are presented in Table VII. The relationship between peak position and heat-treatment temperature is shown in Figure 42 as a plot of peak position versus heat-treatment temperature. Two peak positions were found, at approximately 1355 cm^{-1} and at approximately 1575 cm^{-1}. Actual peak positions for the nine samples oscillated around those two main peaks.

Initially, for the 1355 cm^{-1} peak, the position generally decreases from the 500°C HTT coal-tar pitch sample position of 1367 cm^{-1} to the 2300°C HTT sample value of 1347 cm^{-1}. The position of the 585°C HTT sample is the highest obtained, 1370 cm^{-1}. The position of the 1355 cm^{-1} peak then increases from the 2300°C HTT sample

to the 2400°C HTT sample value of 1356 cm^{-1}. Finally, the position decreases to the 2550°C HTT sample value of 1352 cm^{-1}. The 2400°C HTT-30 minute coal-tar pitch sample had the highest value, with the exception of the 585°C HTT sample, for the 1375 cm^{-1} peak position. The 2400°C-30 minute petroleum pitch sample had the same 1375 cm^{-1} peak position as the 2400°C-15 minute sample.

For the 1575 cm^{-1} peak, peak position initially increases from the 500°C HTT value of 1598 cm^{-1} to the 585°C HTT and 1000°C HTT values of 1602 cm^{-1}. Then the 1575 cm^{-1} peak position decreases from the 1000°C HTT value to the 2100°C HTT value of 1579 cm^{-1}, and increases to the 2300°C HTT value of 1586 cm^{-1}. Finally, the peak position decreases from the 2300°C-15 minute sample to the 2550°C-15 minute sample value of 1579 cm^{-1}. The 2400°C-30 minute sample has a higher peak position than the 2400°C-15 minute sample. The 2400°C-30 minute petroleum pitch sample has the same peak position as the 2400°C-15 minute coal-tar pitch sample.

In general, peak position decreases with increasing heat-treatment temperatures within experimental error. The 585°C HTT sample seems to be anomolous in this regard. This could be due to the large amount of background and broadening effects found in the pregraphitized sample spectra.

Peak intensities, their ratios for each spectrum, and the degree of graphitization for each spectrum are listed in Table VIII. The relationship between the ratio of intensity versus heat-treatment temperature is shown in Figure 43. The ratio is a measure of the disordered 1355 cm^{-1} peak to the ordered 1575 cm^{-1} peak. The relationship between degree of graphitization and heat-treatment temperature is shown in Figure 44. Peak intensities were calculated by estimating a baseline, then measuring with a ruler. The ratio of peak intensities, R, was calculated using the formula:

$$R = \frac{I(1355\ cm^{-1})}{I(1575\ cm^{-1})} \text{ where I = peak intensity.}$$

The degree of graphitization, g, was calculated using the formula:

$$g(\%) = [1-\frac{R}{n}] \times 100, \text{ where n = maximum R value obtained.}$$

Initially 1355 cm^{-1} peak intensity increases from the 500°C HTT value of 90 to the 1000°C HTT value of 100. Peak intensity then decreases from the 1000°C HTT value to the 2300°C HTT value of 41, increases to the 2400°C HTT value of 46, and finally decreases to the 2550°C HTT value of 24. The 2400°C-30 minute coal-tar pitch sample decreases from the 2400°C-15 minute sample value to 34. The 2400°C-30 minute petroleum pitch sample intensity is the lowest seen for the 1355 cm^{-1} peak (12).

The 1575 cm^{-1} peak intensity initially decreases from the 500°C HTT value of 125 to the 1000°C HTT value of 97. The intensity then increases from the 1000°C HTT value to the 2400°C HTT intensity (122) which is just slightly higher than the 585°C HTT value (121). Finally the intensity decreases to the 2550°C HTT value of 135. The 2400°C-30 minute coal-tar pitch sample intensity is slightly lower than the 2400°C-15 minute sample intensity (143). The 2400°C-30 minute petroleum pitch sample intensity (148) is the highest value seen.

The ratio of peak intensities (R) initially decreases from the 500°C HTT value of 0.72 to the 585°C HTT value of 0.69. R then increases from the 585°C HTT value to the 1000°C HTT value of 1.03, and then decreases to the final 2550°C HTT value of 0.18, with the exception of the 2100°C HTT value which is lower (0.30) than the 2400°C-15 minute sample (0.32). The 2400°C-30 minute coal-tar pitch sample value (0.24) is less than the 2400°C-15 minute sample. The 2400°C-30 minute petroleum pitch sample value of 0.08 is the lowest seen. In general, the ratio of peak intensity increases with increasing heat-treatment temperature and residence time. The 1000°C HTT value seems high, indicating a less ordered structure than either the 500°C HTT or the 585°C HTT samples. The 2300°C HTT value seems low, but is within the experimental

error due to background and broadening effects.

Initially, g increased from the 500°C HTT value of 30.2% to the 2100°C HTT sample value of 71.1%. The value g then decreased to 67.4% for the 2300°C HTT sample, and finally increased with increasing heat-treatment temperature and residence time to the 2550°C HTT sample value of 82.8% for coal-tar pitch. The 2400°C-30 minute petroleum pitch sample had the highest degree of graphitization, 92.1%. The 1000°C HTT sample had the highest R value so was used as the base for the g values, and had a g value of 0.00%. The 2100°C HTT sample value seems a bit high, but is within experimental error, $\pm$4%.

The petroleum pitch sample has the highest amount of crystalline order, which is to be expected as Kochling et al. (15) states petroleum pitch graphitizes easier than coal-tar pitch. The Raman spectrum for the 1000°C HTT sample appeared to be the least graphitic of all the sample spectra. The spectrum of the 1000°C HTT sample possessed a high degree of noise, indicative of pregraphitic carbons. The most highly graphitized samples (2100°C HTT through 2550°C HTT) are stable even under high laser power.

The nominal laser power was 1700mW, approximately 100mW at the sample for a 1 micron spot size. The coal-tar pitch samples of 500°C HTT, 585°C HTT, and 1000°C HTT show signs of physical change at even moderate laser power. The

optical diffraction pattern "shimmered and broke," generally an indication of sample heating and/or some phase change. Raman spectra for these samples showed a rising background not present in the higher heat-treated samples. This could be due to flourescence from unreacted hydrocarbons in the pitch samples. This background disappeared upon laser heating, perhaps suggesting burn-off of the hydrocarbons.

In general, the Raman spectrum 1355 cm^{-1} peak intensity decreased with increasing HTT, as the 1575 cm^{-1} peak increased. Peaks broadened with decreasing HTT. This corresponds with the results reported by Tuinstra and Koenig (23). The ratio of peak intensities (R) follows the graphitization process well, especially in the high-temperature region (2100°C HTT-2550°C HTT). The degree of graphitization, g, is a good measure of the extent of graphitization within a sample.

The unidirectional carbon/carbon composite orientation is shown in Figure 45. The composite spectra are shown in Figures 46 and 47 for the graphite fiber and coal-tar pitch matrix, respectively. The spectra of both fiber and matrix were dominated by a spectrum similar to that of the 2400°C HTT-30 minute coal-tar pitch sample. The fiber shows an extra broad band near 1200 cm^{-1}, not part of the graphite spectrum. The matrix does not show this peak but does have an extra feature between the graphite

peaks at about 1450 cm^{-1}. The matrix more closely resembles the 2400°C HTT-30 minute coal-tar pitch sample, as they are the same material and have been processed together.

Electron Energy Loss Spectroscopy

EELS spectrum of the holely carbon grid is shown in Figure 48. It shows a broad peak at 14.0 eV. This spectrum is indicative of amorphous carbon and agrees well with the carbon EELS spectrum in the EELS Atlas of the Elements.

EELS spectrum of the 1000°C HTT coal-tar pitch sample is shown in Figure 49. The spectrum exhibits a main peak at 12.0 eV, and two lesser peaks at 3.75 eV and 22.0 eV. The main peak is narrower and more intense than that for the amorphous carbon EELS spectrum. The peaks occur at the same general energy as those found by Egerton and Whelan (25) for graphite, but at lesser intensities.

EELS spectrum of the 2400°C HTT coal-tar pitch sample is shown in Figure 50. The spectrum exhibits a main peak at 12.0 eV, and two lesser peaks at 3.75 eV and 22.0 eV. The peaks are less broad and more intense than those for the 1000°C HTT sample. The spectrum agrees well with that found by Egerton and Whelan (25) for graphite.

In general, electron energy peaks become less broad and intensity increases indicating the progress of

graphitization. Two additional peaks appear as crystallite structure begins to form, in as low a heat-treatment temperature as 1000°C.

Discussion

In x-ray diffraction, d-spacing was seen to decrease with increasing heat-treatment temperature (HTT) from the 500°C HTT sample value of 4.270Å to the 2550°C HTT sample value of 3.3949Å. The 2400°C HTT petroleum pitch sample had the lowest d-spacing value, 3.3510Å. The (002) peak was seen to increase in intensity with increasing HTT from the 500°C HTT sample value of 8.0 chart units to the 2550°C HTT sample value of 60.1 chart units. The (004) peak was seen to increase in intensity also, from the 2100°C HTT value of 6.0 chart units to the 2550°C HTT sample value of 6.8 chart units. The 2400°C HTT petroleum pitch sample had the highest intensity value, 8.1 chart units. The (002) peak broadening was seen to decrease with increasing HTT from the 500°C HTT sample value of 0.02269 radians to the 2500°C HTT sample value of 0.00742 radians. The XRD graphitization index, $\bar{g}$, was seen to increase with increasing HTT from the 500°C HTT sample value of 0.151 to the 2550°C HTT sample value of 0.524. The 2400°C HTT petroleum pitch sample had the highest $\bar{g}$ value, 1.035.

These trends indicate the progress of graphitization with increasing heat-treatment temperature (19). There was no appreciable difference in the XRD patterns of the 15 minute and the 30 minute 2400°C HTT coal-tar pitch samples, indicating either no change in graphitization or that XRD is not sensitive to the change in residence time. The petroleum pitch sample was found to be the most graphitic. The 1000°C HTT sample XRD pattern indicated a state of heat treatment lower than what would be expected for a sample processed at that temperature. In fact, it seemed to be less ordered than either the 500°C HTT or the 585°C HTT samples, based on their XRD patterns. This supports both the SEM and LRMA results for this sample.

In the 2300°C HTT sample, the XRD (002) and (004) peak intensities and broadening values seemed to indicate a higher state of graphitization than would be expected for a sample processed at that temperature. Intensity alone; however, is not a reliable indicator of graphitization. There are small crystallites present in the sample, but they can be dispersed on a turbostratic disordered matrix. Three-dimensional order is not established yet for this heat-treatment stage, so these measurements are within experimental error. To verify the stage of graphitization within this sample, L_a and L_c determinations based on the (002) and (110) peaks should

be made.

Scanning electron microscopy showed the establishment of a two-dimensional ordering from highly disordered morphology, and finally the establishment of a three-dimensional order in the pitch samples with increasing HTT. This supports the XRD results, indicating the progress of graphitization with increasing HTT. The 1000°C HTT sample could be interpreted to follow the progress of graphitization as expected, or the morphology could have been interpreted to be characteristic of a sample processed at a much lower HTT. This would support both the XRD and LRMA results for this sample.

For the laser Raman microprobe analysis, two peaks were seen for the nine pitch samples, one around 1355 cm^{-1} and one around 1575 cm^{-1}. The 1355 cm^{-1} peak is a disorder peak, and the 1575 cm^{-1} peak is the ordered peak, called the E_{2g} peak. The relative state of graphitization is measured using a ratio of these peak intensities, R. The value R decreased with increasing HTT and residence time from the 500°C HTT sample value of 0.72 to the 2550°C HTT sample value of 0.18. The 2400°C-30 minute petroleum pitch sample had the lowest R value, 0.08. Decreasing R indicates increasing progress of graphitization (22,23,24).

The 1355 cm^{-1} peak position was seen to decrease from the 500°C HTT sample value of 1367 cm^{-1} to the 2550°C HTT value of 1352 cm^{-1}. The 2400°C-30 minute petroleum pitch

sample had the lowest 1375 cm^{-1} peak position, 1356 cm^{-1}. The 1575 cm^{-1} peak position was seen to decrease from the 500°C HTT sample value of 1598 cm^{-1} to the 2500°C HTT sample value of 1579 cm^{-1}.

The degree of graphitization, g, was seen to increase with increasing HTT and residence time from the 500°C HTT sample value of 30.2% to the 2500°C HTT sample value of 82.8%. The 2400°C-30 minute petroleum pitch sample had the highest g value, 92.1%.

These trends indicate the progress of graphitization with increasing heat-treatment temperature and residence time. This supports the XRD and the SEM results for increasing HTT. LRMA can be used to measure the degree of graphitization within a sample, for even 100°C increments of HTT, and can distinguish between 15 minute and 30 minute residence times. The 1000°C HTT sample Raman spectrum indicated a state of heat treatment much lower than what would be expected for a sample processed at that temperature. In fact, it seemed less ordered than the 500°C HTT or the 585°C HTT samples, based on their Raman spectra. This supports both the XRD and the SEM results for the 1000°C HTT sample.

In the LRMA of the unidirectional carbon/carbon (C/C) composite, differences could be seen in the spectra for the fiber and matrix. The spectra was dominated by a spectrum similar to that for coal-tar pitch processed at the same time and temperature, 2400°C-30 minutes, indicating

that the spectra were indicative of graphitized carbon.

Electron energy loss spectroscopy showed a change from amorphous to graphitic carbon by an increase in peak intensity and a sharpening of the peaks. The appearance of a minor peak at 3.75 eV in addition to the standard 12.0 eV peak for carbon as graphitization proceeds could be indicative of the establishment of crystalline structure. The technique is not sensitive to small changes in grpahitization; however, and should only be used to verify trends already established.

The relationship between d-spacing and Raman peak intensity ratio is shown in Figure 51 as a plot of $\bar{d}_{002}$ versus R. R is seen to decrease with decreasing d-spacing. The "path of graphitization" is indicated by an arrow. The least graphitic point shown corresponds to the 1000°C HTT sample. This lends further support to the conclusion that, possibly due to some processing error, it is less graphitic than either the 500°C HTT or 585°C HTT samples. The most graphitic point corresponds to the 2400°C HTT-30 minute petroleum pitch sample. This supports the conclusion that petroleum pitch graphitizes easier than coal-tar pitch, as stated by Kochling et al. (15). The data corresponds quite well with that presented by Lespade et al. (24) for graphitizing and nongraphitizing carbons, shown in Figure 15.

The relationship between Raman peak position and d-spacing is shown in Figure 52 as a plot of $\bar{d}_{002}$ versus peak position for both the $\nu_{E_{2g}}$ peak (1575 cm^{-1}) and the 1355 cm^{-1} peak. Peak position is seen to decrease with decreasing d-spacing. The general trend as graphitization proceeds is indicated by an arrow. The data for the $\nu_{E_{2g}}$ peak corresponds well with that presented by Lespade et al. (24) for graphitizing and nongraphitizing carbons, shown in Figure 16.

XRD and LRMA are excellent complementary analysis techniques for the graphitization process. Together they provide an accurate method for following the progress of graphitization within a sample.

CHAPTER V

Summary and Conclusions

XRD, SEM, LRMA, and EELS can all be used to follow the progress of graphitization of carbon pitches. SEM is a subjective technique which is an important qualitative tool for determining gross morphological changes and for confirmation of the structural changes determined from other characterization techniques. SEM showed establishment of morphologies representative of two- and then three-dimensional ordering in the pitch samples with increasing HTT.

XRD is a semi-quantative technique that can be used to follow the progress of graphitization through a graphitization index, $\bar{g}$, based on d-spacing calculations. XRD could be used as a limited quantative technique, but it is less sensitive than LRMA. The value $\bar{g}$ measures the decrease in d-spacing as graphitization proceeds, but cannot be considered to give absolute values. With increasing HTT, XRD showed a decrease in d-spacing indicative of tighter planar packing, a narrowing of peak breadth indicative of an increase in crystallite size, and an increase in peak intensity. This corresponds to an increase in graphitization with increasing HTT.

LRMA is a more quantative technique for measuring an index for the degree of graphitization, g, which is based on relative intensity ratios of specific spectral peaks. These changes are based on the ratio of the 1355 cm^{-1} disordered peak intensity to the E_{2g} 1575 cm^{-1} ordered peak intensity. It is unique to the range of samples being tested. The small one micron probe size allows characterization of very small volumes of material. This permits characterization of individual components in carbon/carbon composites. LRMA can detect changes in graphitization in pitches for changes in residence times from 15 minutes to 30 minutes, and for 100°C increments. The 1355 cm^{-1} peak intensity decreases with increasing HTT and residence time, coupled with an increase in intensity and a narrowing of the 1575 cm^{-1} peak. This indicates an increasing degree of graphitization. It can also, in situ, detect differences in graphitization between fiber and matrix in a C/C composite. When LRMA and x-ray diffraction d-spacing are plotted against one another, the plot gives a straight line with moderate scatter in the data. The use of the two techniques in conjunction with one another provide unique complementary data about the graphitization process.

EELS is a qualitative tool for measuring the progress of graphitization and may be used to support results of

other more quantitative techniques. EELS showed a change in spectra from one characteristic of amorphous carbon to one characteristic of graphitized carbon as HTT increased.

Overall, the combined use of the four techniques indicated that increased heat-treatment temperature and residence time increase degree of graphitization for a petroleum and coal-tar pitch. Petroleum pitch graphitizes easier than does coal-tar pitch.

Table I

Pitch Properties [From Cranmer et al. (5)]

	Coal-tar Pitch Allied 15V	Petroleum Pitch Ashland A240
Softening point, °C	90-95	115
Benzene insolubles, %	18-29	5
Quinoline insolubles, %	5-10	0.5
Coking value, %	35 min	47
Ash, %	0.25 max	0.7
Specific gravity, g cm^{-3}	1.26-1.32	1.25
Sulphur, %	0.75 max	4.5

*As reported by the manufacturer.

Table II

Pitch Chemical Analyses [From Miyazawa et al. (6) and Sheaffer (7)]

Element	Coal-tar (6)	Petroleum (7)
% Carbon	92.1	92.38
% Hydrogen	4.8	5.45
% Oxygen	1.5	< 0.10
% Nitrogen	1.3	0.12
% Sulfur	0.5	1.83

Table III

List of Samples

Type	Source	Heat-treatment Temperature	Residence Time
Pyrolyzed pitch	Coal-tar	500°C	15 min.
	Coal-tar	585°C	15 min.
Carbonized pitch	Coal-tar	1000°C	15 min.
Graphitized pitch	Coal-tar	2100°C	15 min.
	Coal-tar	2300°C	15 min.
	Coal-tar	2400°C	15 min.
	Coal-tar	2400°C	30 min.
	Petroleum	2400°C	30 min.
	Coal-tar	2550°C	15 min.
Unidirectional composite	Thornel P-55 fiber Coal-tar pitch matrix	2400°C	30 min.

Table IV

X-ray Diffraction Peaks, d-spacings, and Graphitization Indices

Heat-treatment Temperature \ Plane	(002)			(004)	
	2θ(°)	d-spacing (Å)	$\bar{g}$	2θ(°)	d-spacing (Å)
Est. Intensities	26.53	3.3597	0.934	54.70	1.6780
Calc. Values	26.62	3.3485	1.064	54.84	1.6740
500°C-15 min	26.00	3.4270	0.151	-	-
585°C-15 min	25.80	3.4531	-0.152	-	-
1000°C-15 min	25.30	3.5202	-0.932	-	-
2100°C-15 min	26.00	3.4270	0.151	53.75	1.7054
2300°C-15 min	26.25	3.3949	0.524	54.30	1.6894
2400°C-15 min	26.20	3.4013	0.450	54.20	1.6923
2400°C-30 min (CT)	26.20	3.4013	0.450	54.20	1.6923
2400°C-30 min (Pet)	26.60	3.3510	1.035	54.70	1.6780
2550°C-15 min	26.25	3.3949	0.524	54.35	1.6879

Table V

X-ray Diffraction Peak Intensities

Heat-treatment Temperature \ Plane	(002)		(004)	
	Units	Normalized	Units	Normalized
Est. Intensities	N/A	100	N/A	80
Calc. Values	N/A	100	N/A	6
500°C-15 min	8.0	100	-	-
585°C-15 min	9.8	100	-	-
1000°C-15 min	7.8	100	-	-
2100°C-15 min	51.75	100	3.1	6.0
2300°C-15 min	80.75	100	5.1	6.3
2400°C-15 min	47.0	100	3.2	6.8
2400°C-30 min (CT)	56.5	100	4.0	7.1
2400°C-30 min (Pet)	49.1	100	4.0	8.1
2550°C-15 min	60.1	100	4.1	6.8

Table VI

X-ray Diffraction Broadening Measurements

Heat-treatment Temperature \ Plane	(002)				(004)			
	(1/2)I	$2\theta_1$(°)	$2\theta_2$(°)	B (rad)	(1/2)I	$2\theta_1$(°)	$2\theta_2$(°)	B (rad)
500°C-15 min	4.00	27.30	24.70	0.02269	-	-	-	-
585°C-15 min	4.90	27.25	24.50	0.02400	-	-	-	-
1000°C-15 min	3.90	27.50	23.20	0.03752	-	-	-	-
2100°C-15 min	25.88	26.50	25.60	0.00785	1.55	54.30	53.25	0.00916
2300°C-15 min	40.38	26.75	25.90	0.00742	2.55	54.75	53.80	0.00829
2400°C-15 min	23.50	26.75	25.75	0.00873	1.60	54.75	53.50	0.01091
2400°C-30 min (CT)	28.25	26.75	25.75	0.00873	2.00	54.70	53.60	0.00960
2400°C-30 min (Pet)	24.55	27.20	26.20	0.00873	2.00	55.20	54.10	0.00960
2550°C-15 min	30.05	26.75	25.90	0.00742	2.05	54.80	54.00	0.00698

Table VII

Raman Spectrum Peak Positions

Heat-treatment Temperature \ Peak	1355cm^{-1}	E_{2g} 1575cm^{-1}
500°C-15 minutes	1367	1598
585°C-15 minutes	1370	1602
1000°C-15 minutes	1357	1602
2100°C-15 minutes	1353	1579
2300°C-15 minutes	1347	1586
2400°C-15 minutes	1356	1580
2400°C-30 minutes (CT)	1359	1582
2400°C-30 minutes (Pet)	1356	1580
2550°C-15 minutes	1352	1579

Table VIII

Raman Spectra Peak Intensities, Intensity Ratios, and Degrees of Graphitization

Heat-treatment Temperature	$I(1355cm^{-1})$	$I(1575cm^{-1})$	R	g(%)
500°C-15 minutes	90	125	0.72	30.2
585°C-15 minutes	84	121	0.69	32.7
1000°C-15 minutes	100	97	1.03	-
2100°C-15 minutes	42	141	0.30	71.1
2300°C-15 minutes	41	122	0.34	67.4
2400°C-15 minutes	46	144	0.32	69.0
2400°C-30 minutes (CT)	34	143	0.24	76.9
2400°C-30 minutes (Pet)	12	148	0.08	92.1
2550°C-15 minutes	24	135	0.18	82.8

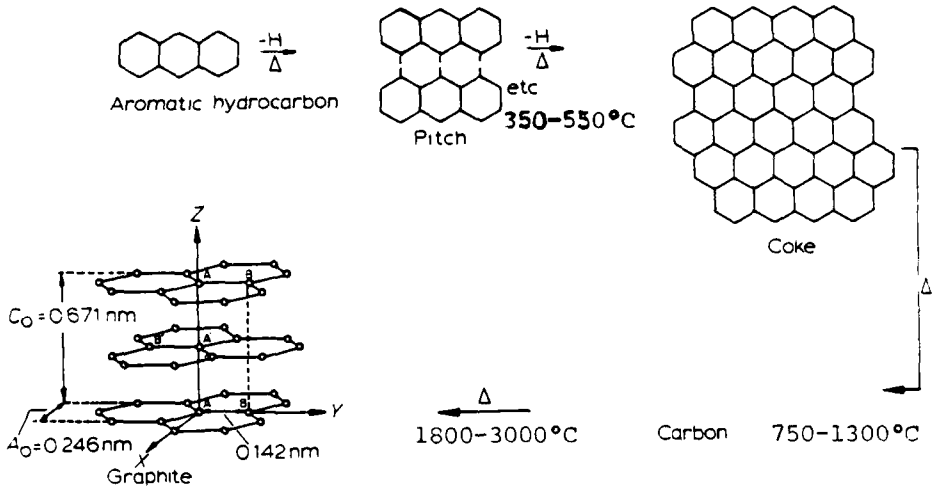

Fig. 1. Schematic diagram of the graphitization process for a graphitizing carbon. [From Singer (1)]

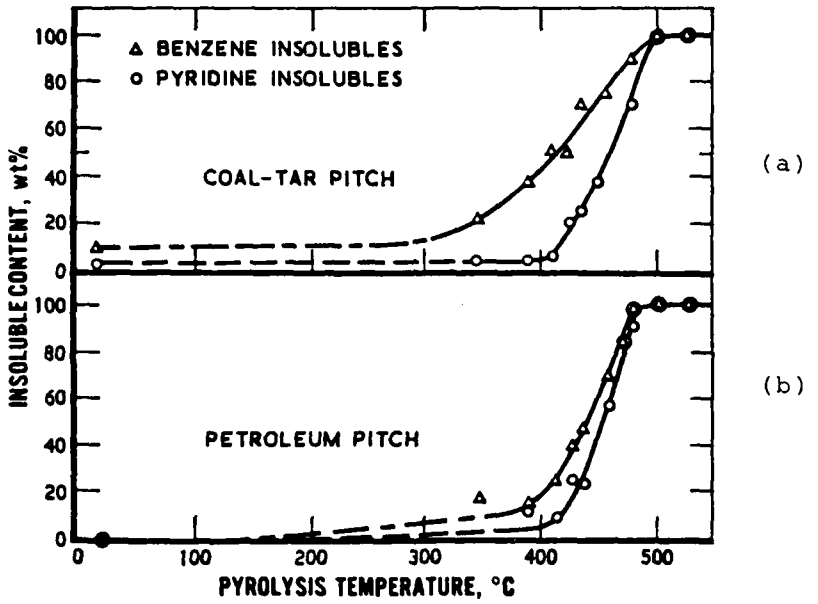

Fig. 2. Mesophase transformation as indicated by pyridine- and benzene-solubility measurements: (a) coal-tar pitch, (b) petroleum pitch. [From Hüttinger and Rosenblatt (10)]

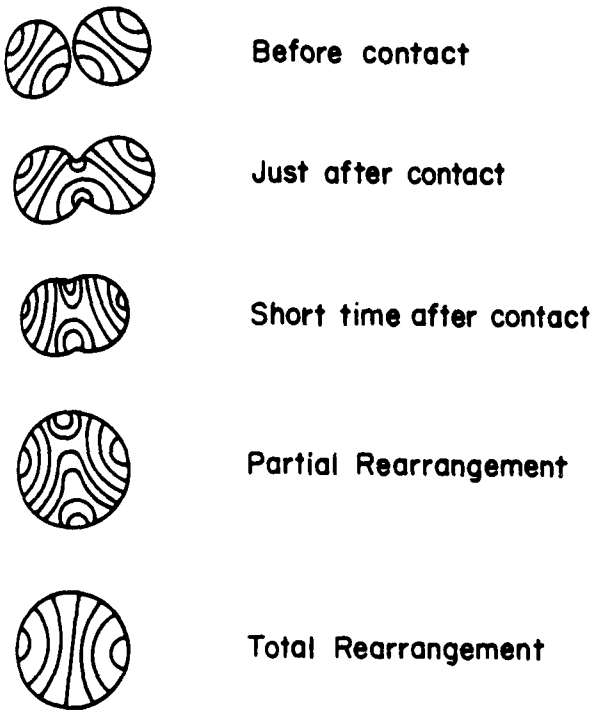

Fig. 3. Schematic diagram of the contact and coalescence of two mesophase spherules. [From Singer (1)]

AD-A166 942 CHARACTERIZATION OF GRAPHITIZATION IN COAL TAR AND PETROLEUM PITCHES(U) AIR FORCE INST OF TECH WRIGHT-PATTERSON AFB OH J C KARIKA AUG 85 2/2

UNCLASSIFIED F/G 11/4 NL

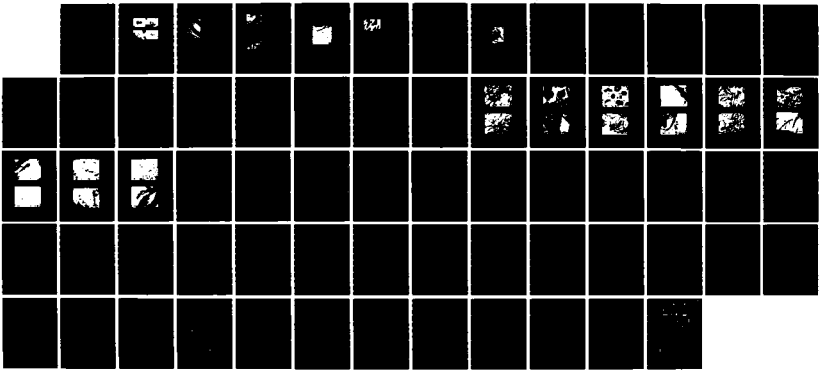

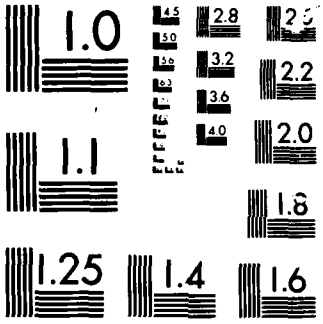

MICROCOPY CHART

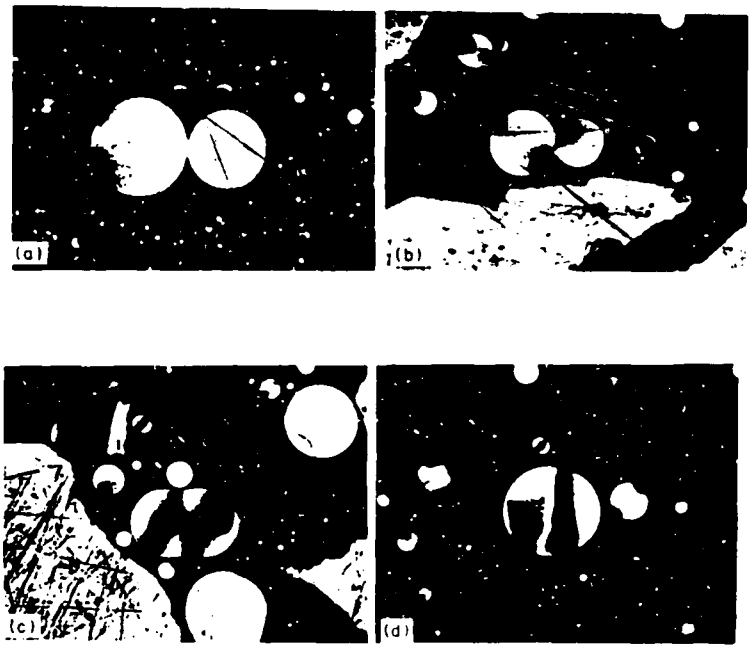

Fig. 4. Polarized light photomicrograph (260x) of the coalescence of two mesophase spherules: (a) initial contact; (b), (c) coalescence; (d) contraction to form a composite sphere. [From Brooks and Taylor (8)]

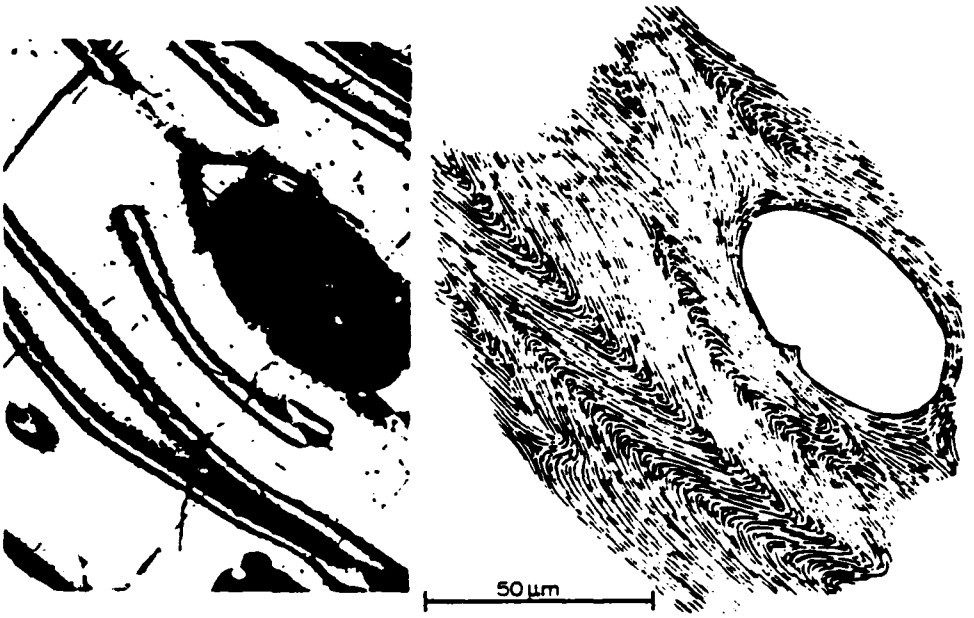

Fig. 5. Mesophase deformation due to initiation of bubble percolation: (a) polarized light photomicrograph, (b) structural sketch. [From Singer (1)]

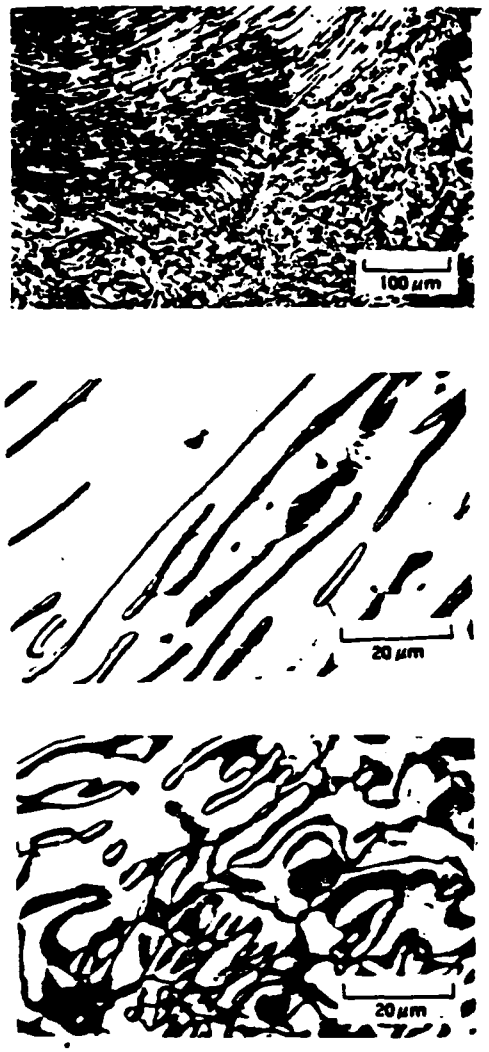

(a)

(b)

(c)

Fig. 6. Mesophase refinement due to bubble percolation in a coal-tar pitch: (a) polarized light photomicrograph of mesophase, (b) higher magnification of fibrous regions, (c) higher magnification of mosaic regions. [From White (4)]

Fig. 7. Replication electron micrograph of folds, bends, and disinclinations in a graphitized petroleum coke, shown by ion etching. [From White (4)]

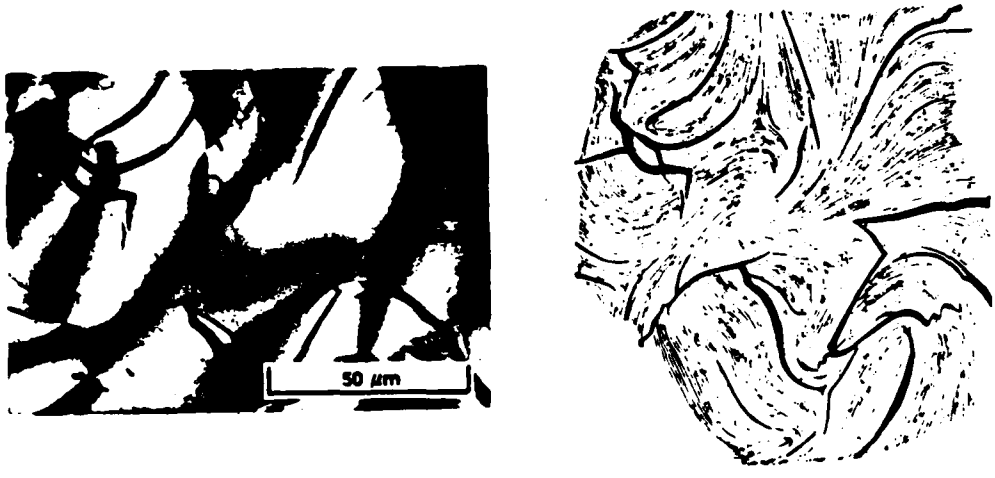

(a) (b)

Fig. 8. Shrinkage-cracking in an extracted coal-tar pitch heat treated to 800°C: (a) polarized light photomicrograph, (b) structural sketch. [From White (4)]

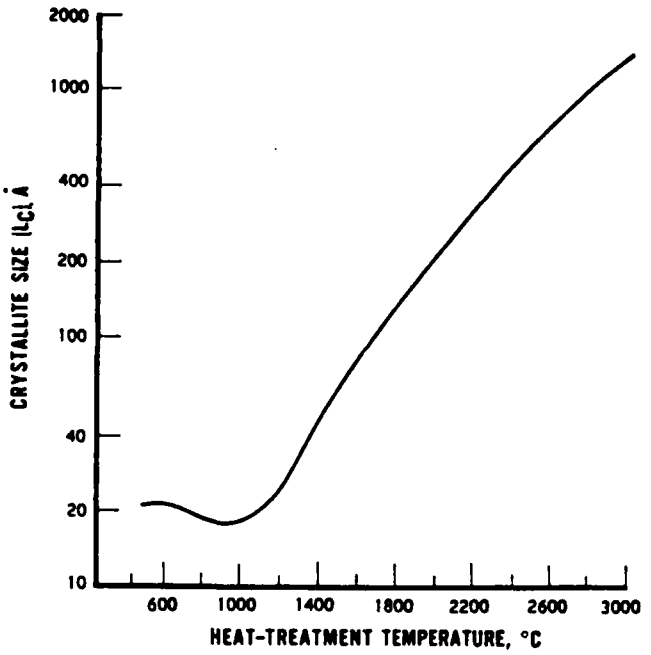

Fig. 9. Crystallite size, L_c, as a function of heat-treatment temperature. [From White (4)]

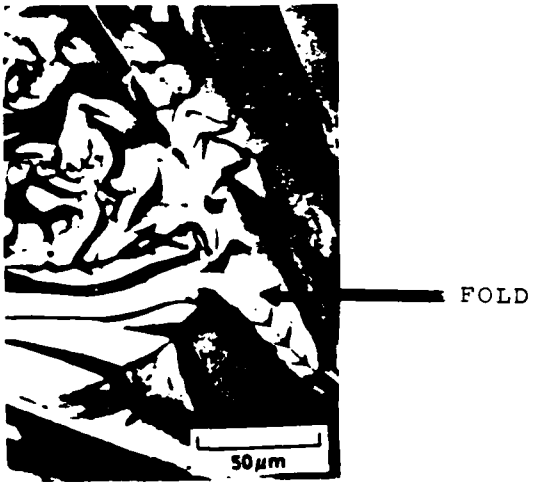

Fig. 10. Polarized light photomicrograph of fold-sharpening in a coal-tar pitch heat-treated to 1400°C. [From White (4)]

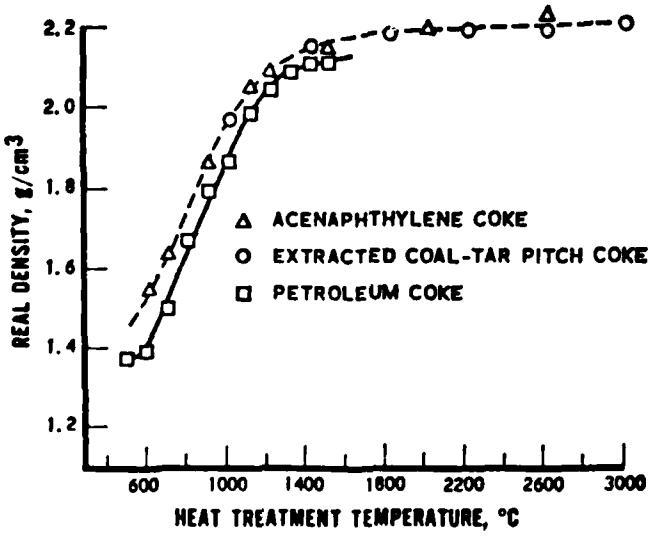

Fig. 11. Mesophase densification as a function of heat-treatment temperature for acenaphthylene coke, extracted coal-tar pitch coke, and petroleum coke. [From White (4)]

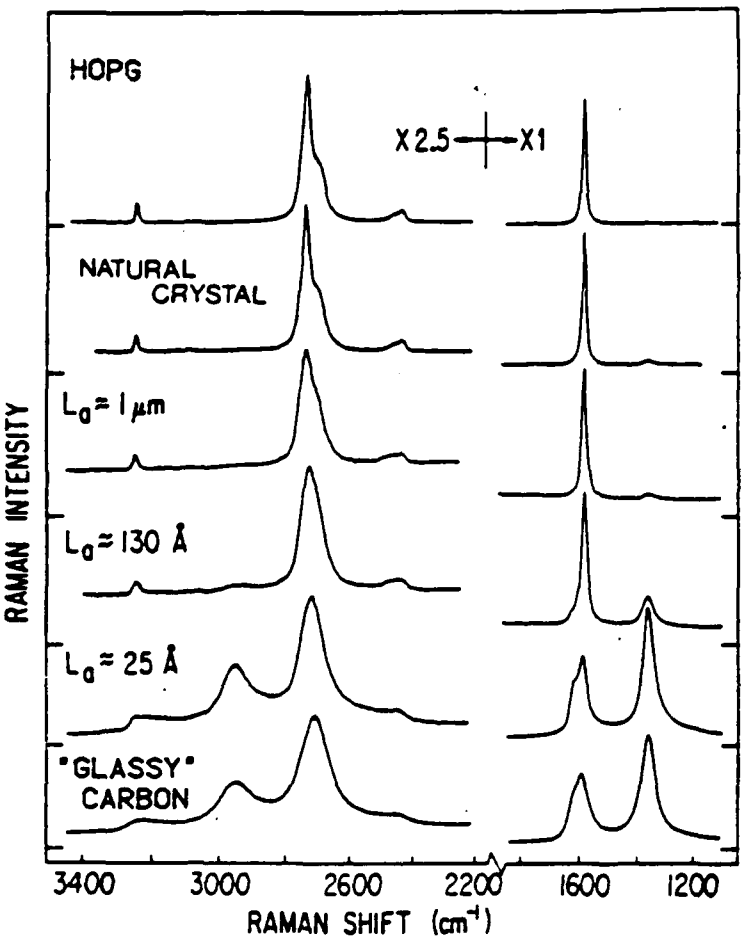

Fig. 12. First- and second-order Raman spectrum of various graphites as a function of L_a. Spectral slit width is approximately $10cm^{-1}$. Wavelength is linear. [From Nemanich and Solin (22)]

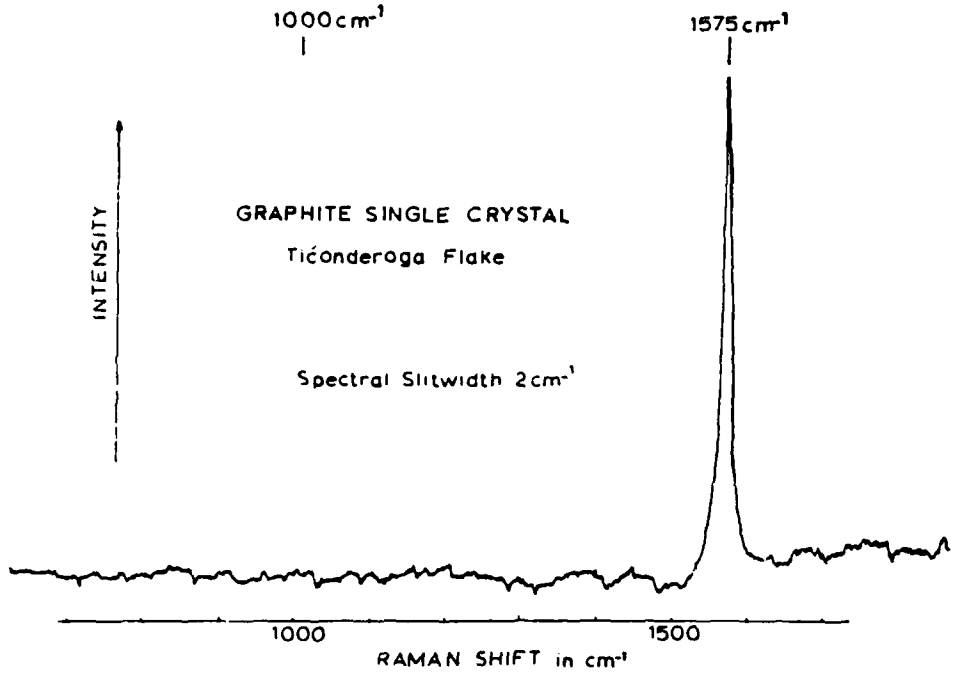

Fig. 13. Raman spectra of single crystal graphite.

[From Tuinstra and Koenig (23)]

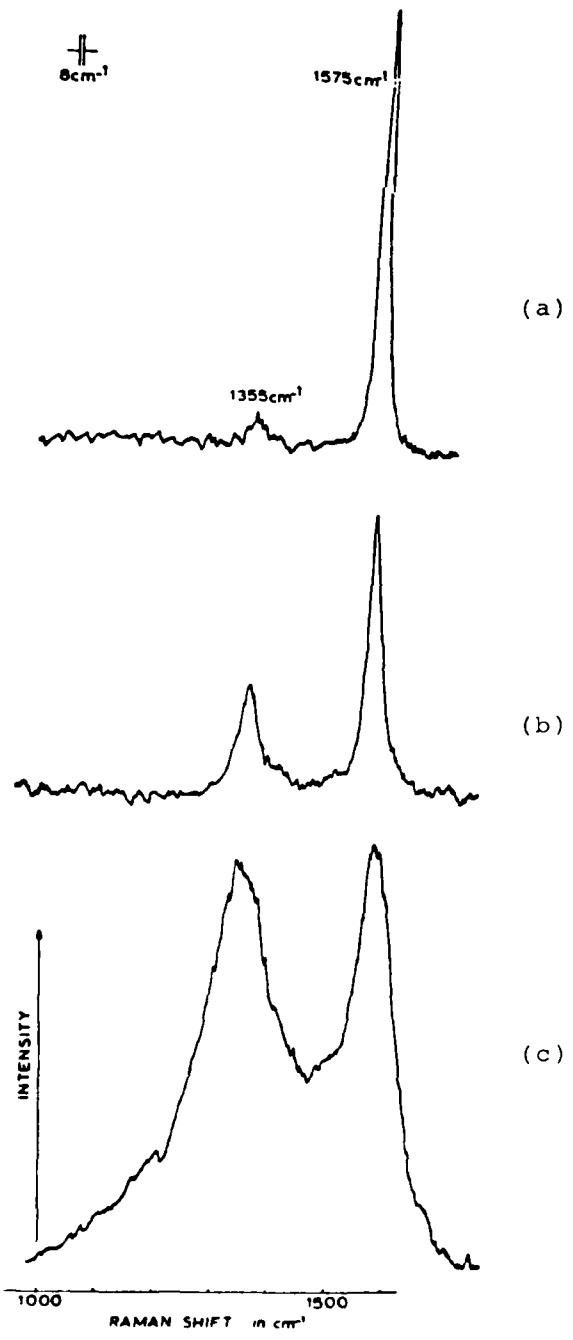

Fig. 14. Raman spectra for graphitic and nongraphitic carbons: (a) stress-annealed pyrolytic graphite, (b) commercial graphite, (c) activated charcoal. [From Tuinstra and Koenig (23)]

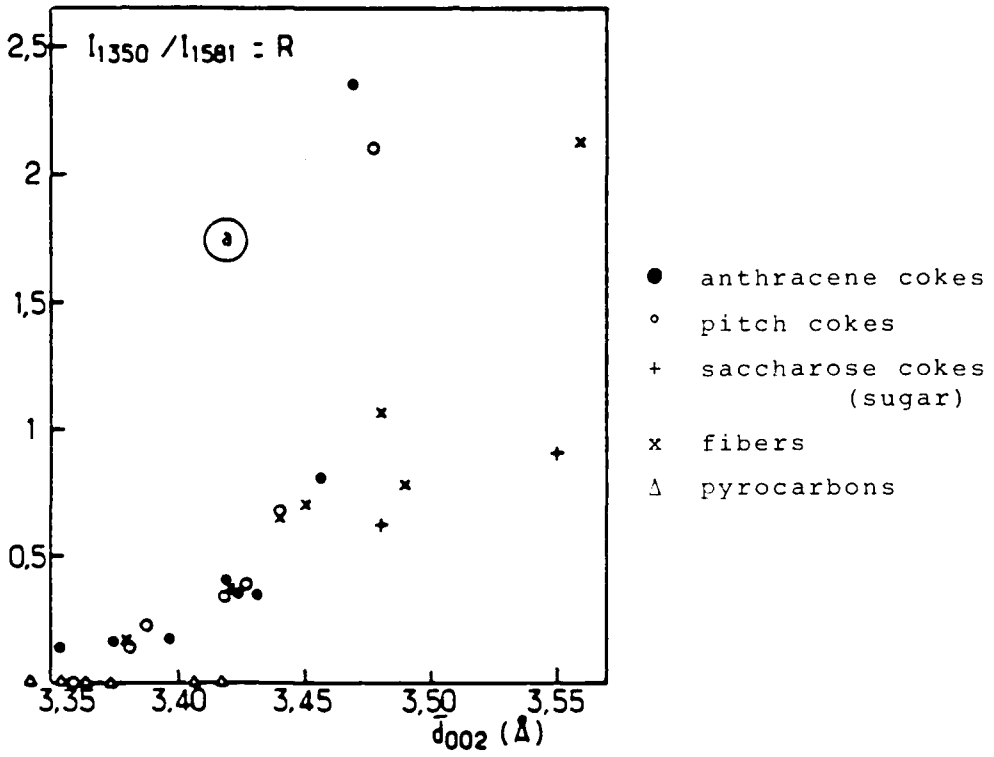

Fig. 15. R versus $\bar{d}_{002}$ for various graphitizing and nongraphitizing carbons. [From Lespade et al. (24)]

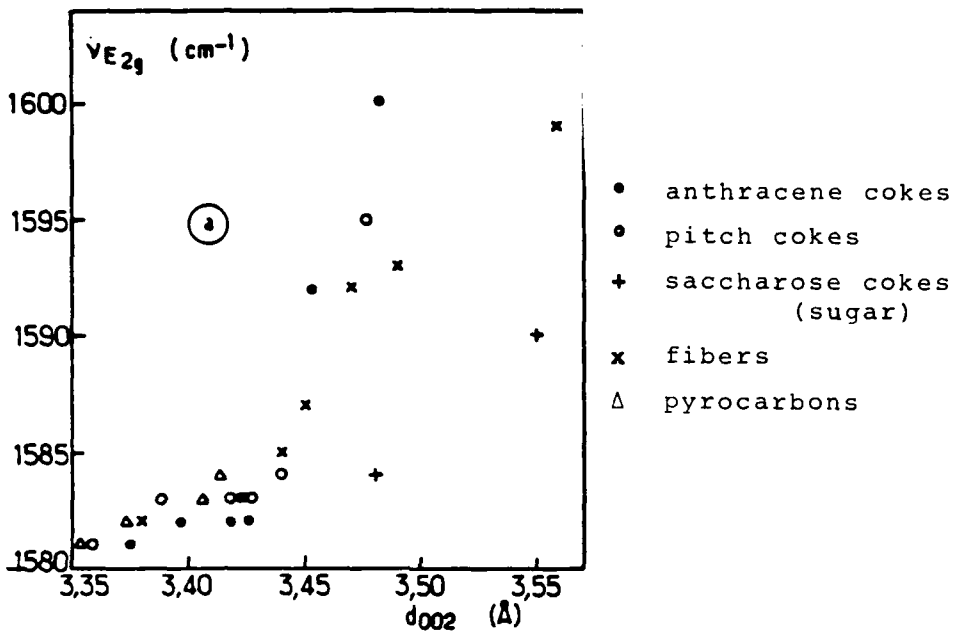

Fig. 16. $\nu_{E_{2g}}$ versus $\bar{d}_{002}$ for various graphitizing and nongraphitizing carbons. [From Lespade et al. (24)]

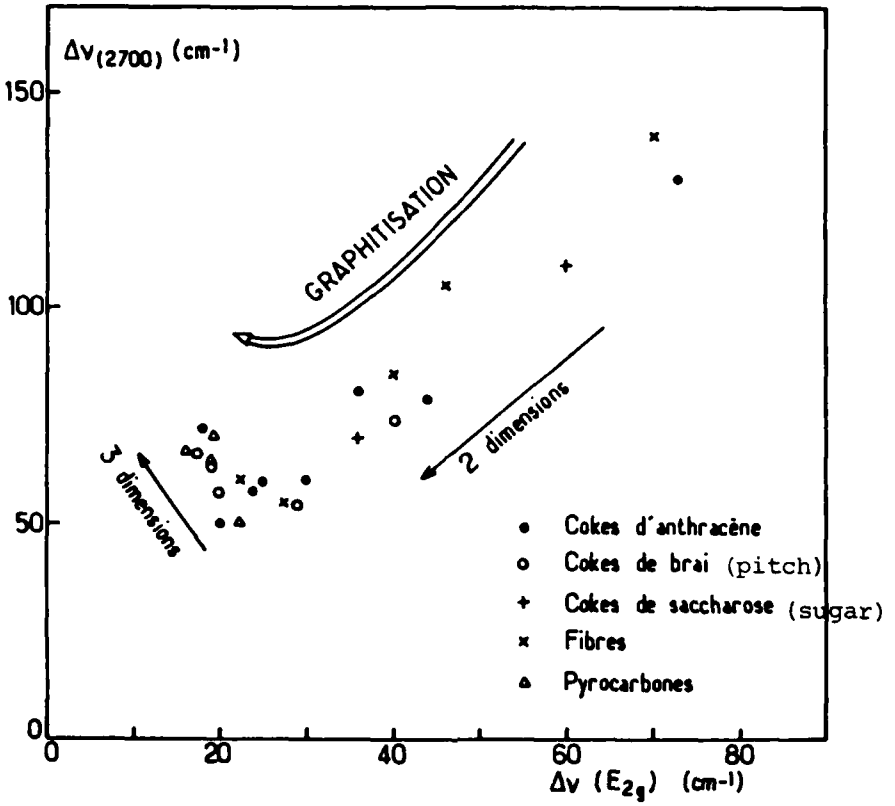

Fig. 17. $\Delta\nu(E_{2g})$ versus $\Delta\nu(2700)$ indicating the path of graphitization. [From Lespade et al. (24)]

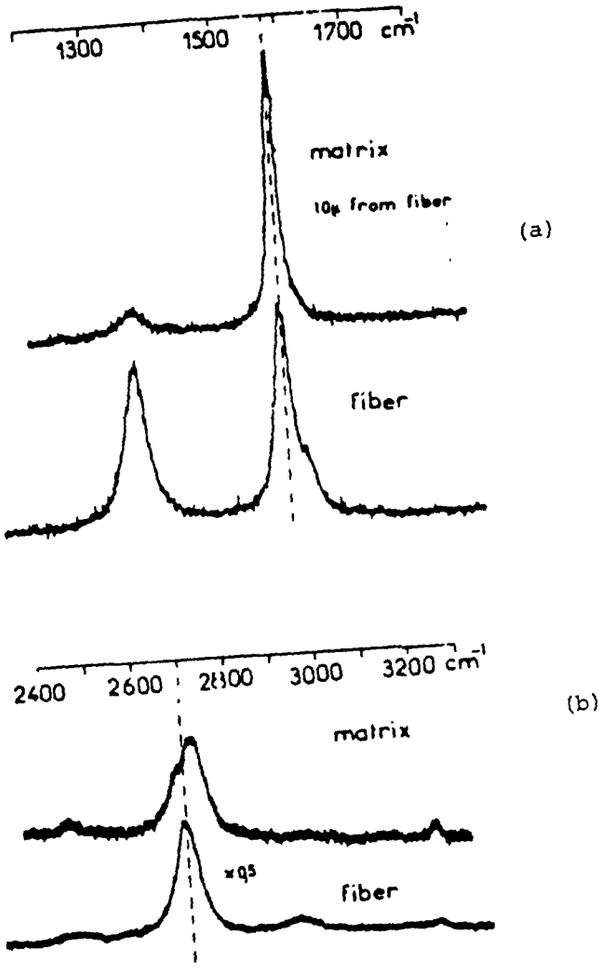

Fig. 18. Raman spectrum of a carbon/carbon composite: (a) first-order, (b) second-order. [From Lespade et al. (24)]

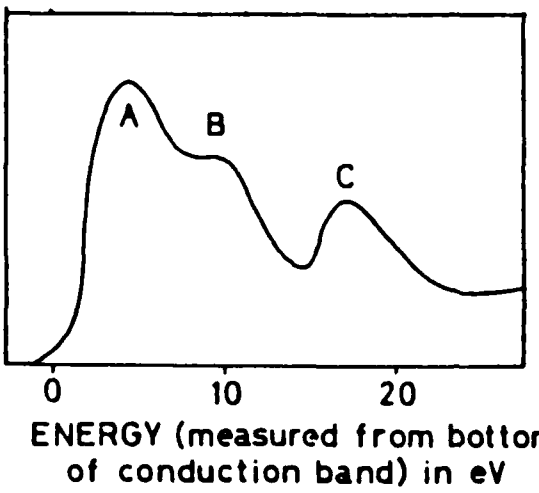

Diamond

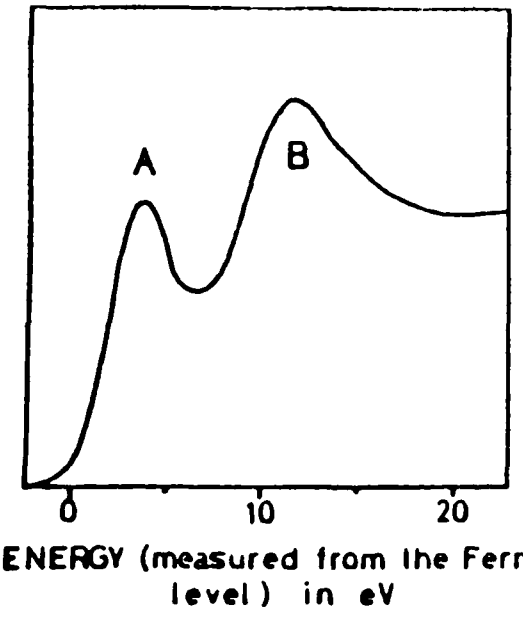

Graphite

Fig. 19. EELS spectrum for diamond and graphite.

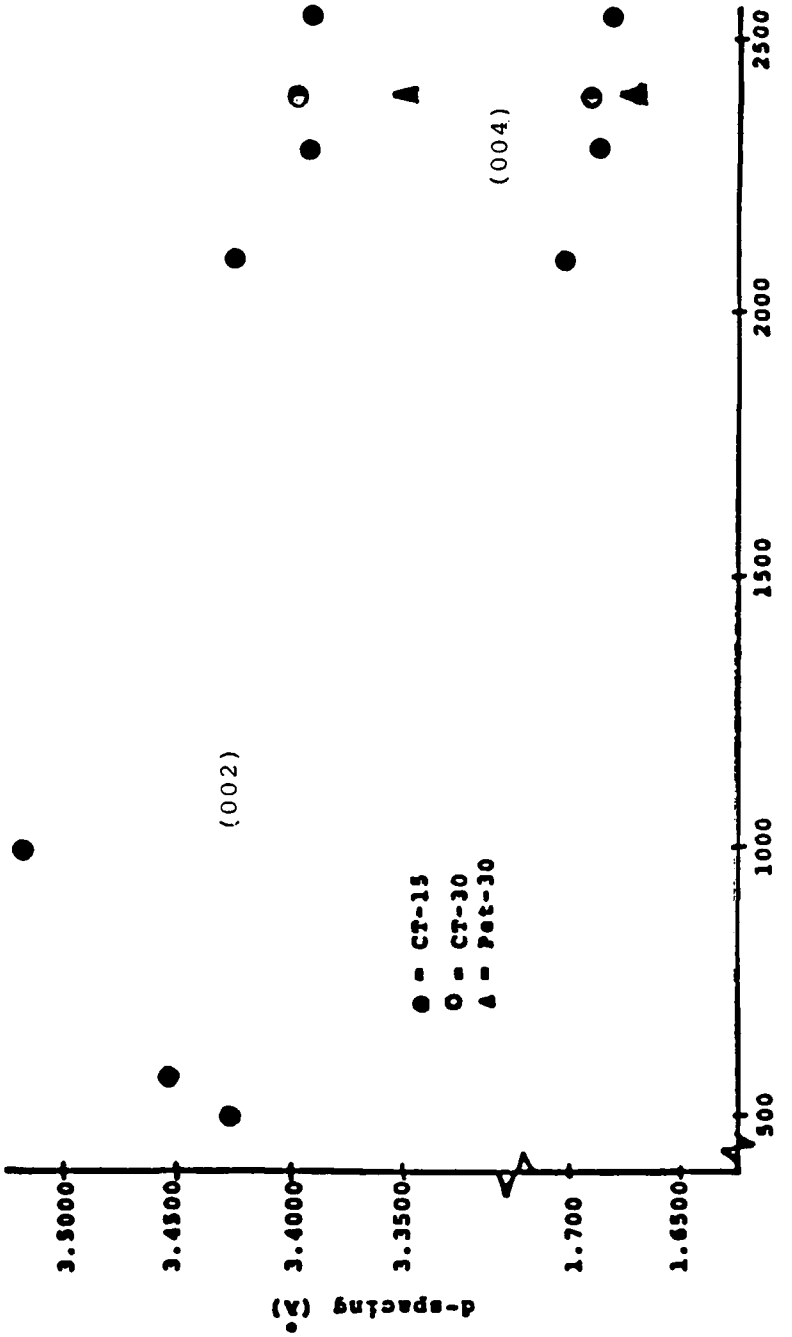

Fig. 20. d-spacing versus heat-treatment temperature. [From Table IV)

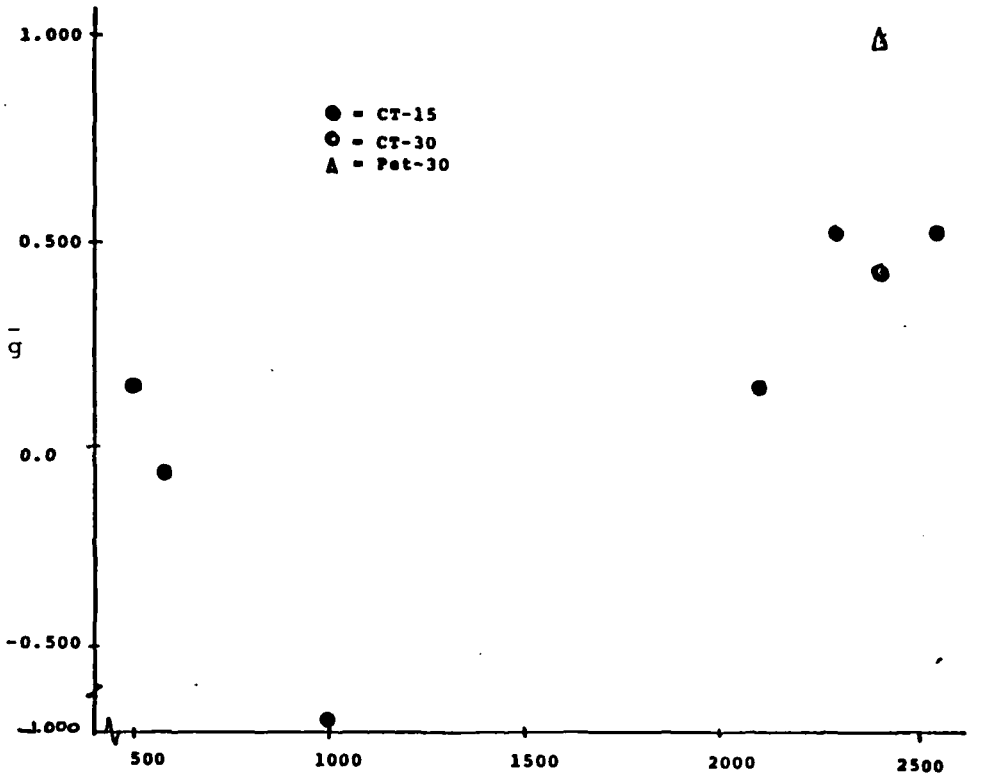

Fig. 21. Graphitization index versus heat-treatment temperature.

[From Table IV)

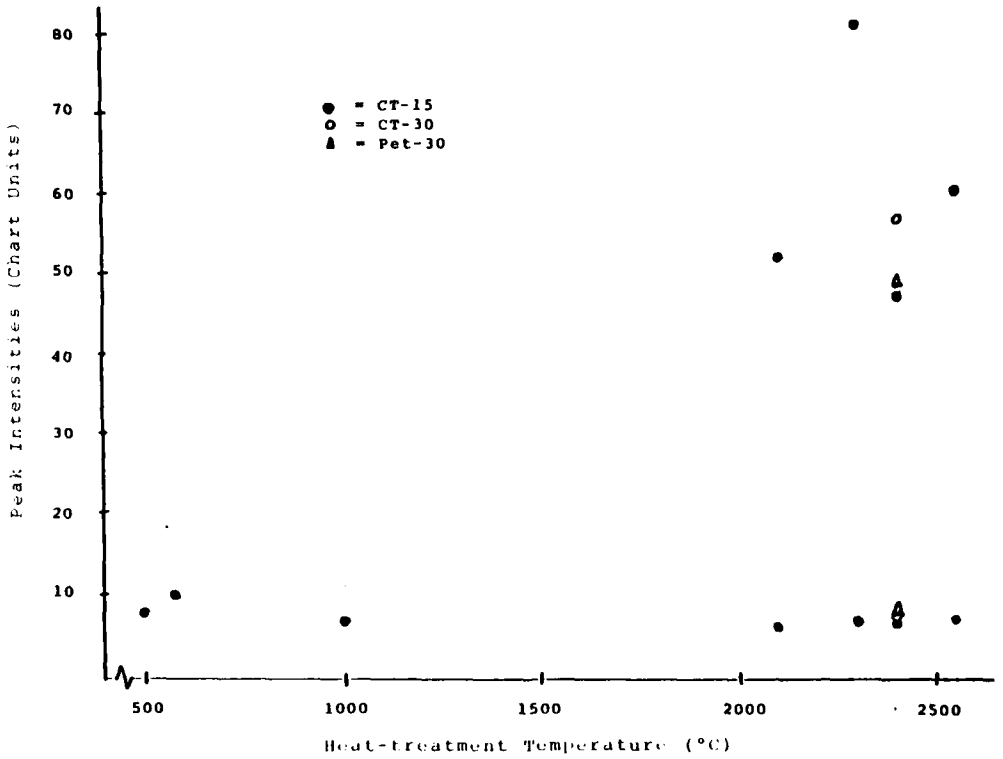

Fig. 22. X-ray diffraction peak intensities versus heat-treatment temperature. [From Table V]

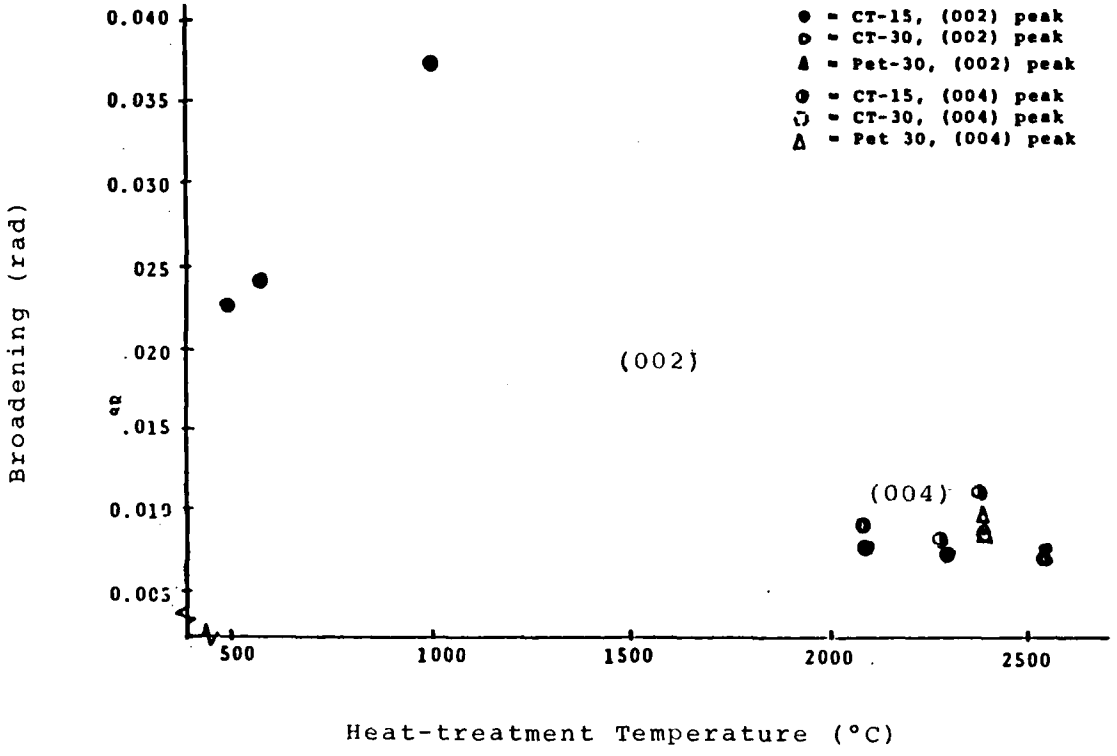

Fig. 23. X-ray diffraction peak broadening versus heat-treatment temperature.

[From Table VI]

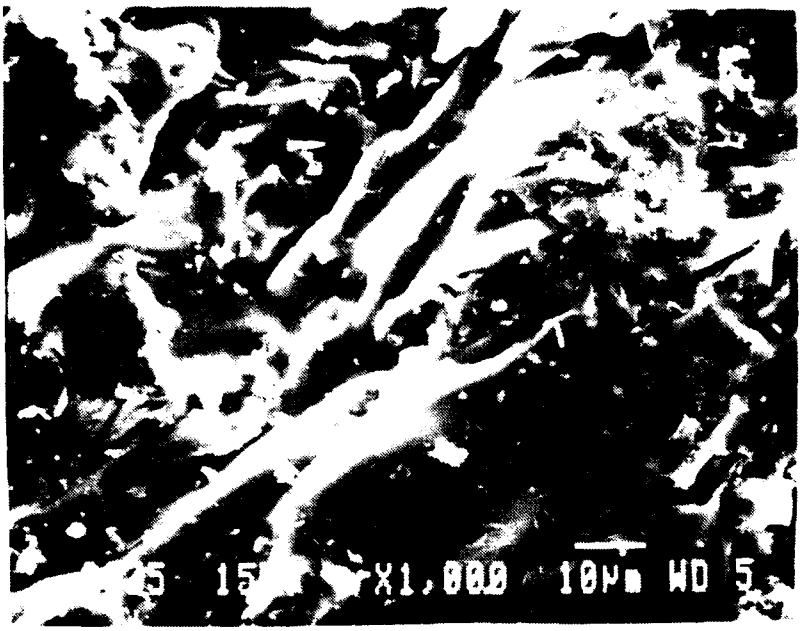

Fig. 24. SEM micrograph (1000x) of coal-tar pitch heat-treated to 585°C for 15 minutes.

Fig. 25. SEM micrograph (500x) of coal-tar pitch heat-treated to 1000°C for 15 minutes.

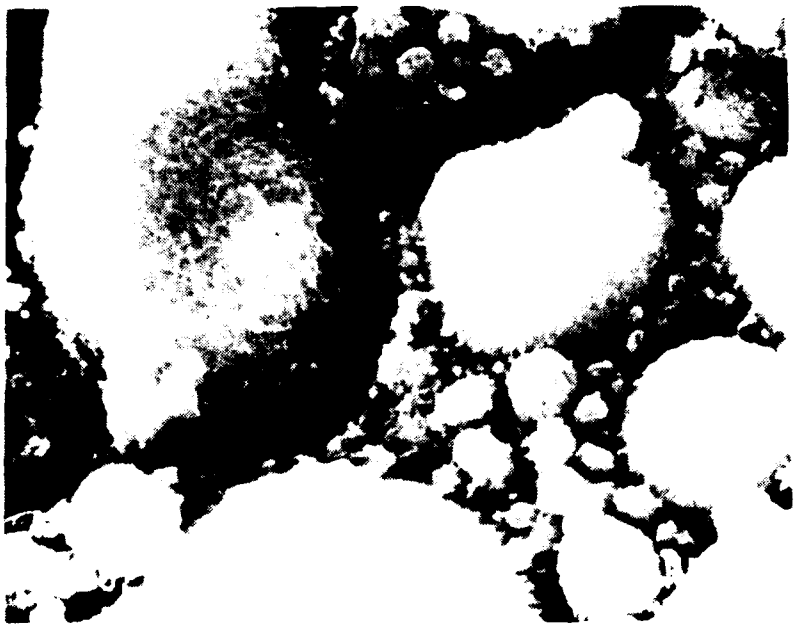

Fig. 26. SEM micrograph (10,000x) of coal-tar pitch heat-treated to 1000°C for 15 minutes.

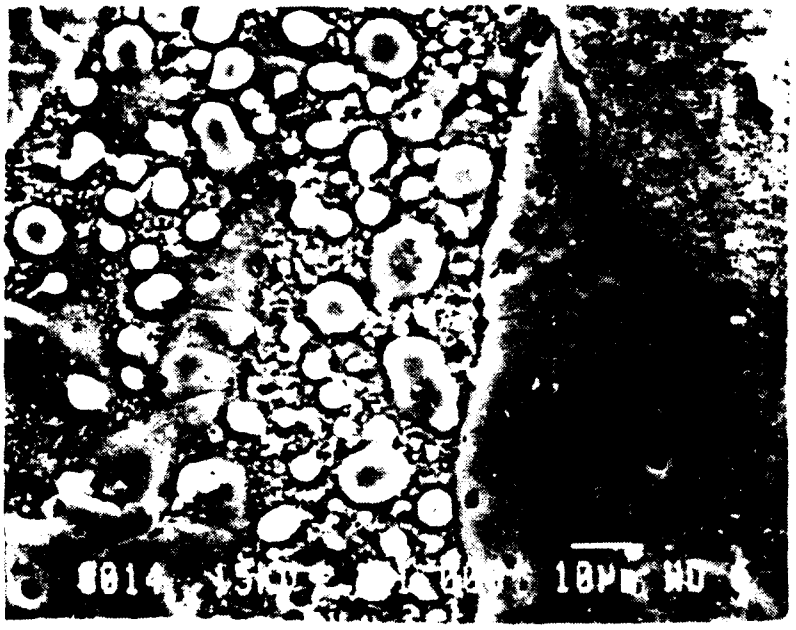

Fig. 27. SEM micrograph (1000x) of coal-tar pitch heat-treated to 1000°C for 15 minutes.

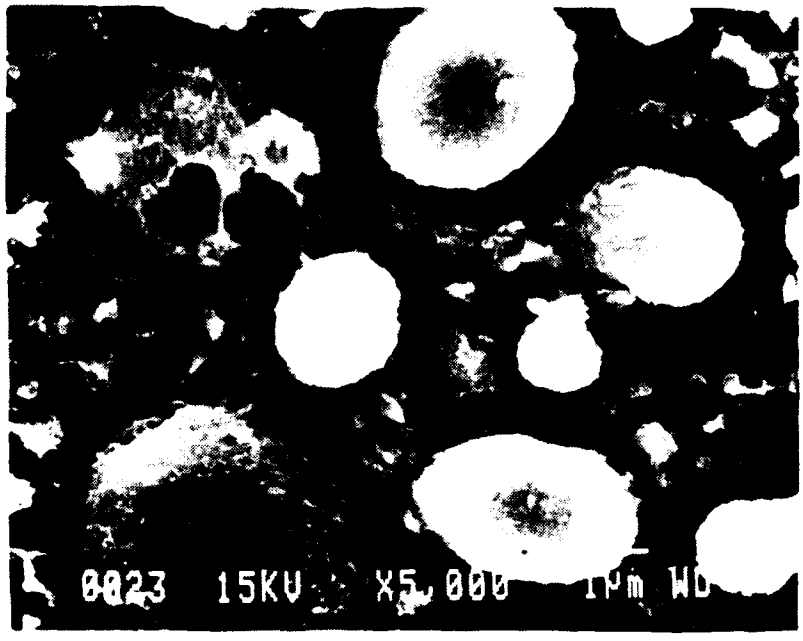

Fig. 28. SEM micrograph (5000x) of coal-tar pitch heat-treated to 1000°C for 15 minutes.

Fig. 29. SEM micrograph (500x) of coal-tar pitch heat-treated to 2100°C for 15 minutes.

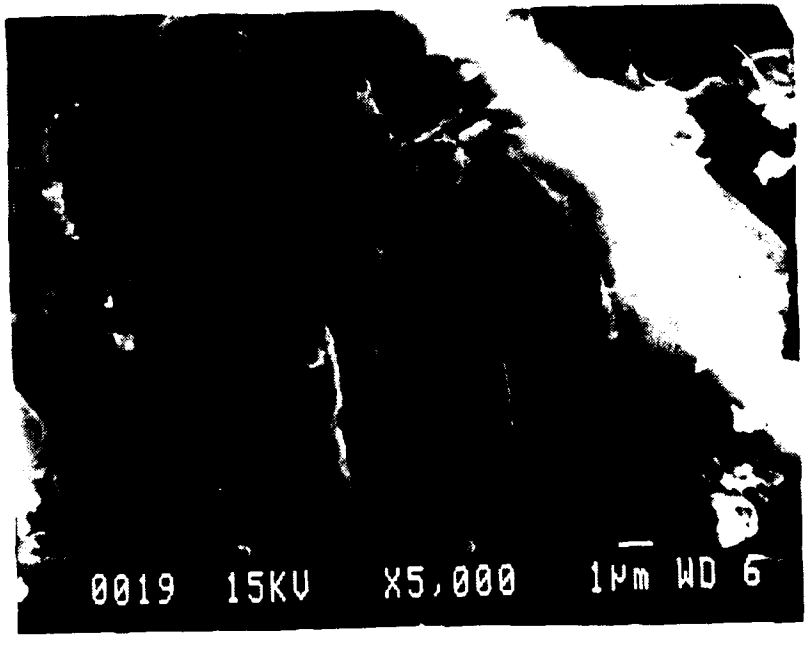

Fig. 30. SEM micrograph (5000x) of shrinkage cracks in coal-tar pitch heat-treated to 2100°C for 15 minutes.

Fig. 31. SEM micrograph (100x) of coal-tar pitch heat-treated to 2300°C for 15 minutes.

Fig. 32. SEM micrograph (1000x) of coal-tar pitch heat-treated to 2300°C for 15 minutes.

Fig. 33. SEM micrograph (1000x) of crack interior in coal-tar pitch heat-treated to 2400°C for 30 minutes.

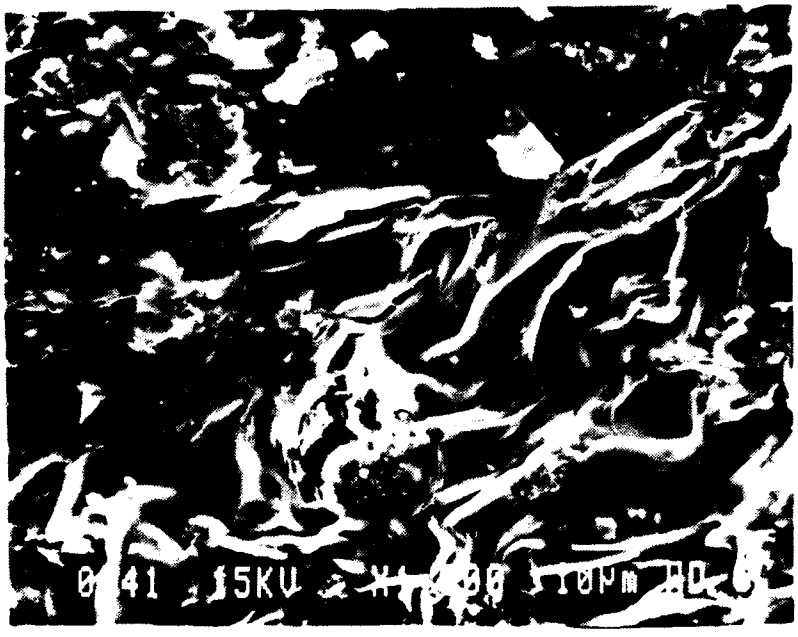

Fig. 34. SEM micrograph (1000x) of coal-tar pitch heat-treated to 2400°C for 30 minutes.

Fig. 35. SEM micrograph (10,000x) of crack interior in coal-tar pitch heat-treated to 2400°C for 30 minutes.

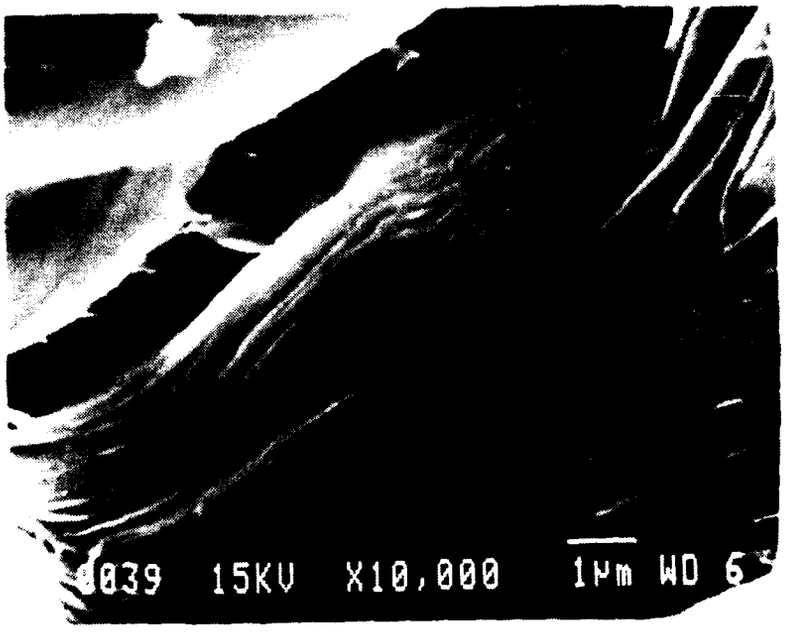

Fig. 36. SEM micrograph (10,000x) of coal-tar pitch heat-treated to 2400°C for 30 minutes.

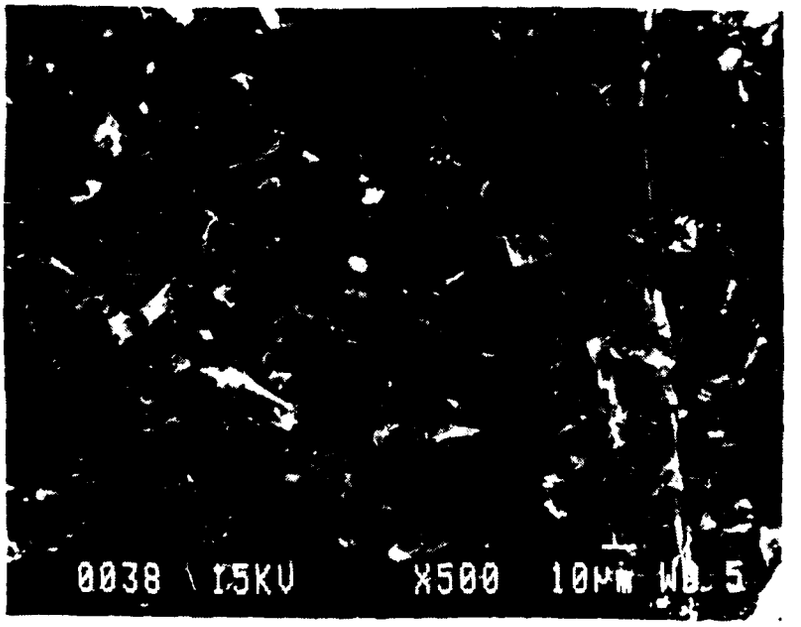

Fig. 37. SEM micrograph (500x) of coal-tar pitch heat-treated to 2400°C for 30 minutes.

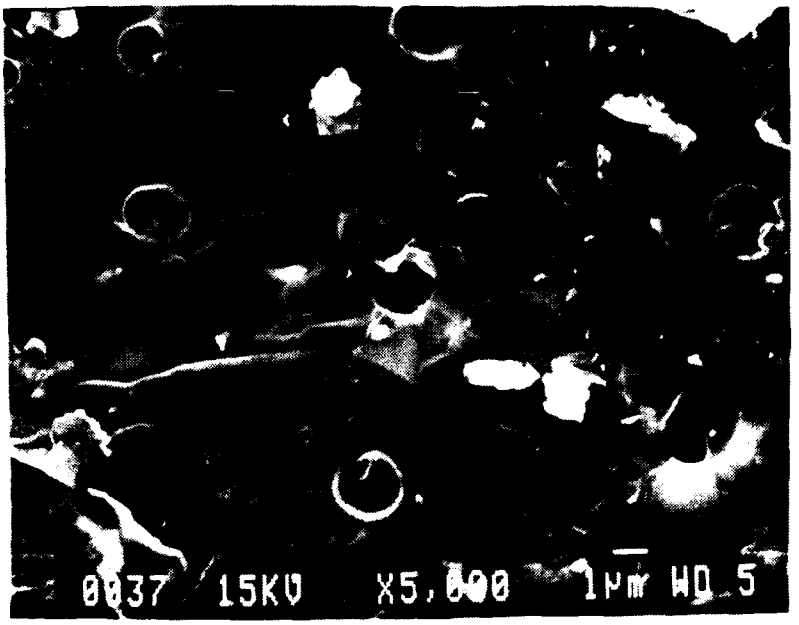

Fig. 38. SEM micrograph (5000x) of coal-tar pitch heat-treated to 2400°C for 30 minutes.

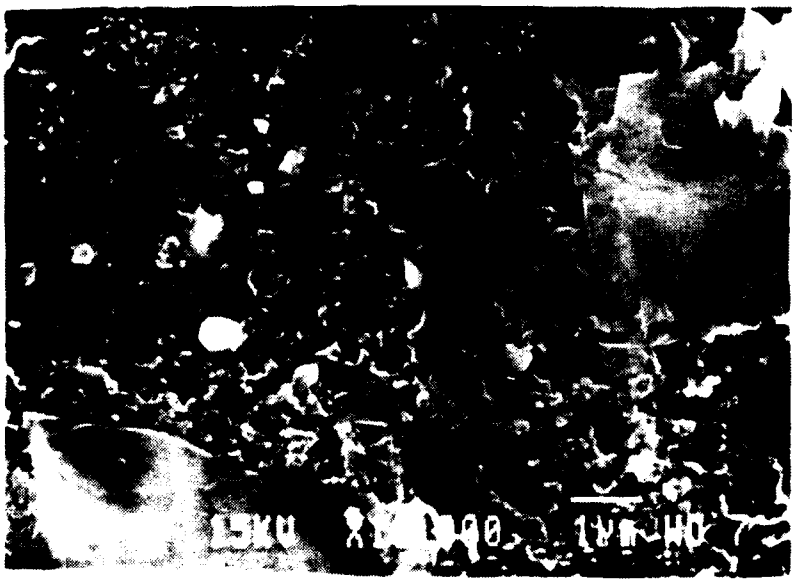

Fig. 39. SEM micrograph (10,000x) of "fish scale" surface in petroleum pitch heat-treated to 2400°C for 30 minutes.

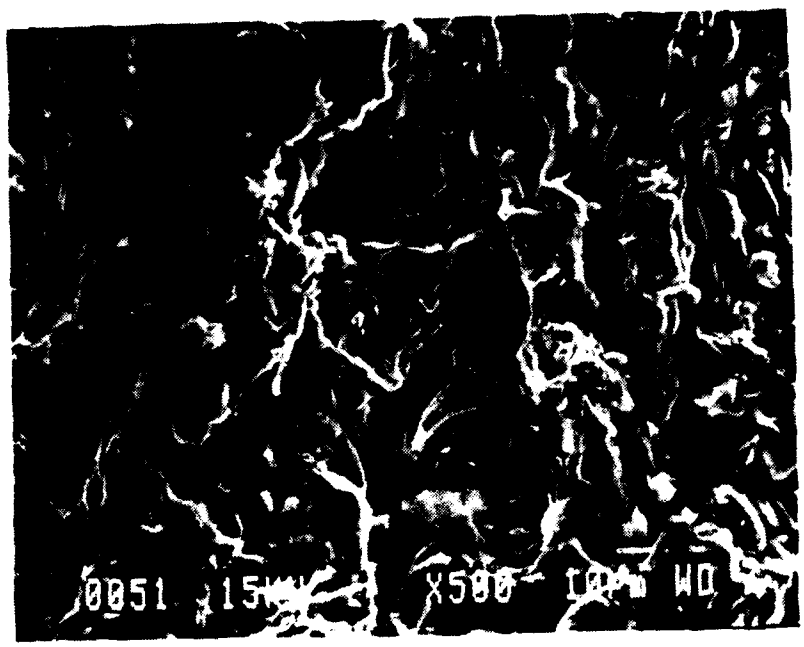

Fig. 40. SEM micrograph (500x) of petroleum pitch heat-treated to 2400°C for 30 minutes.

Fig. 41. SEM micrograph (10,000x) of delamination in petroleum pitch heat-treated to 2400°C for 30 minutes.

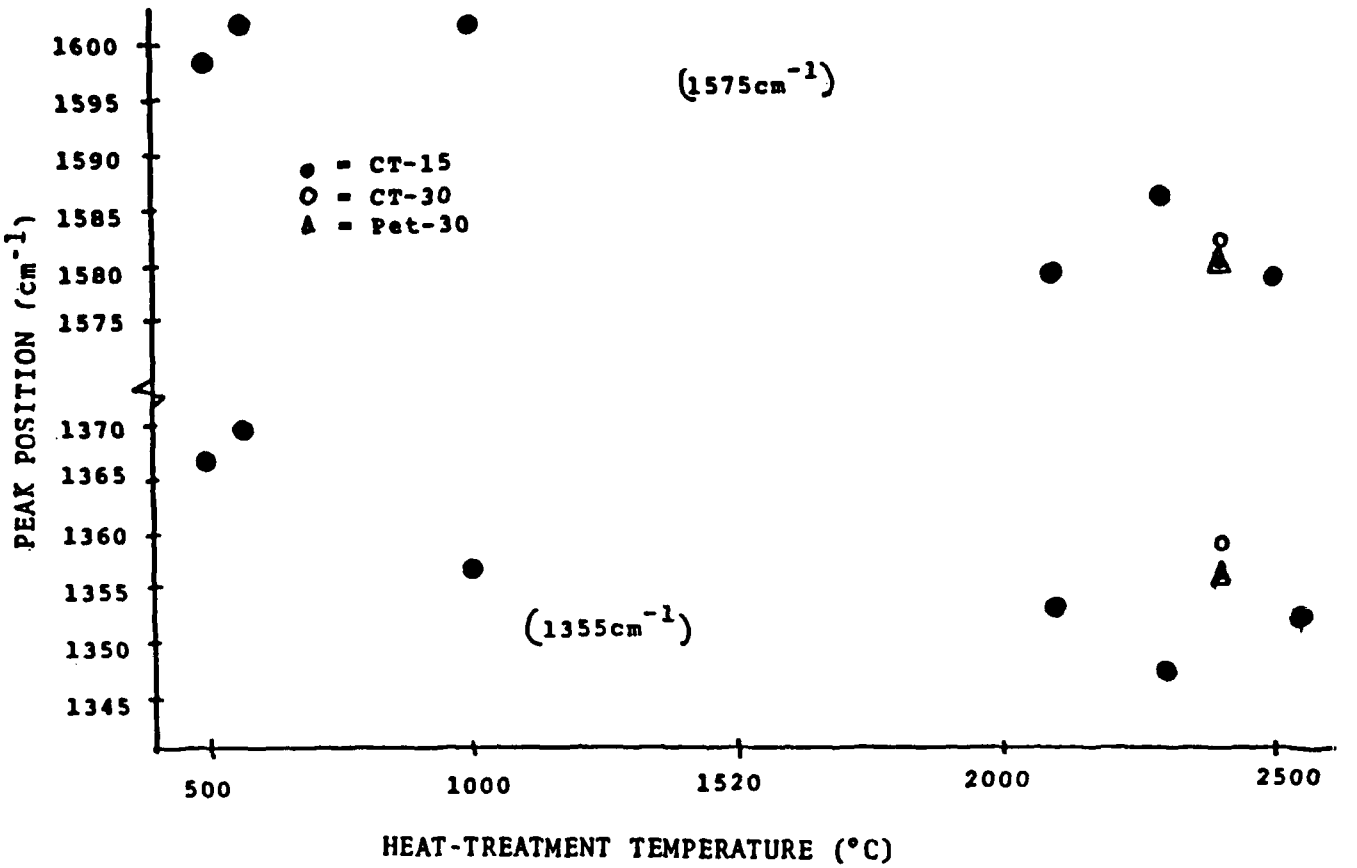

Fig. 42. Raman spectra peak position versus heat-treatment temperature.

[From Table VII]

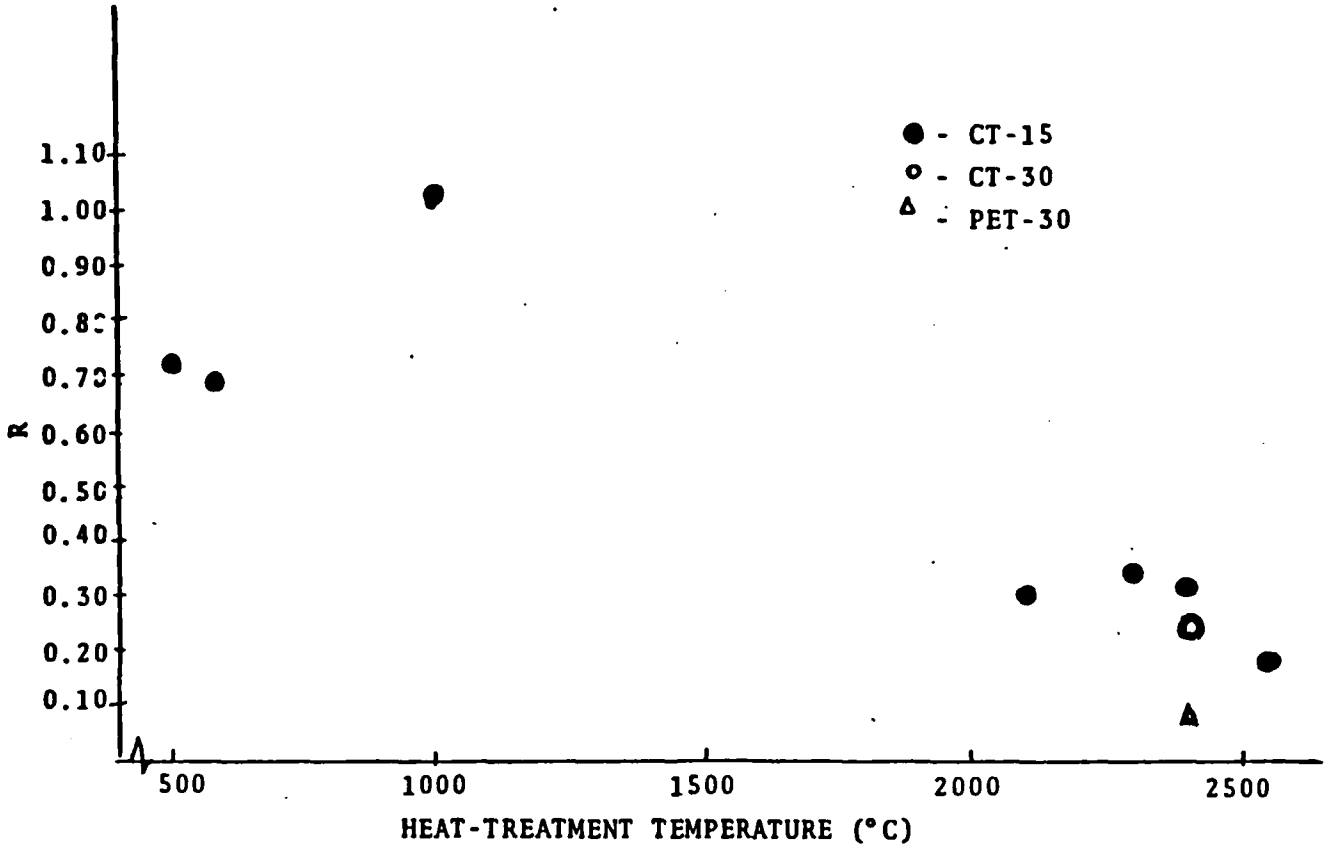

Fig. 43. Ratio of peak intensity versus heat-treatment temperature.

[From Table VIII]

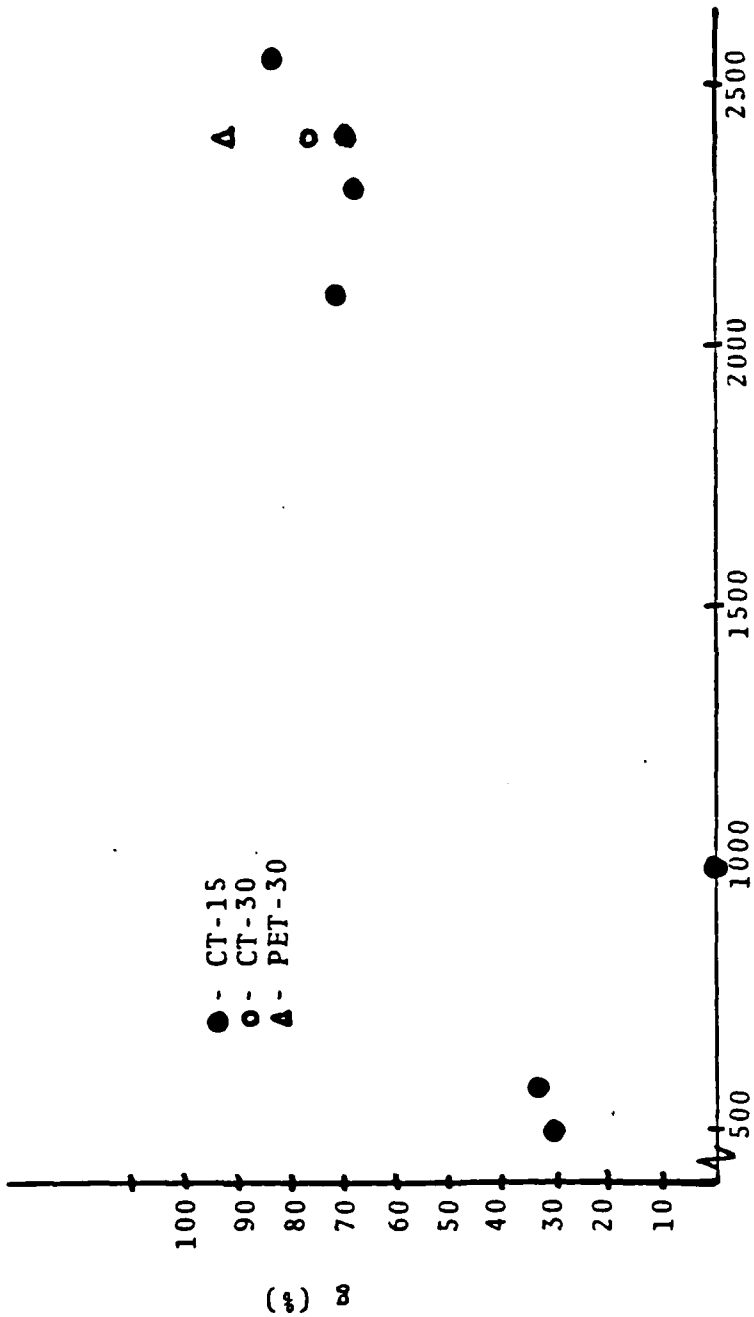

Fig. 44. Degree of graphitization versus heat-treatment temperature.

[From Table VIII]

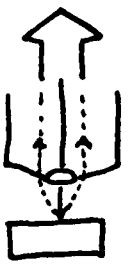

Raman scattering: to spectrometer

laser beam

microscope objective

sample

SAMPLE (top view)

⊕ laser beam spots (≈1 μm)

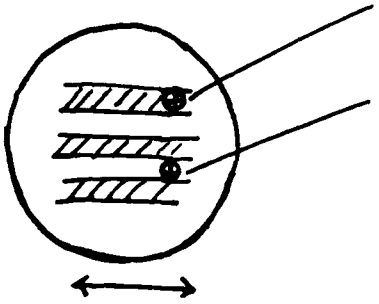

fibers: micro-Raman spot run

coal-tar pitch

$\tilde{E}$ (electric vector of laser beam)

Fig. 45. Unidirectional composite, pyrolyzed at 550°C, then heat-treated at 2400°C for 30 minutes. Thornel P-55 fiber with a coal-tar pitch matrix.

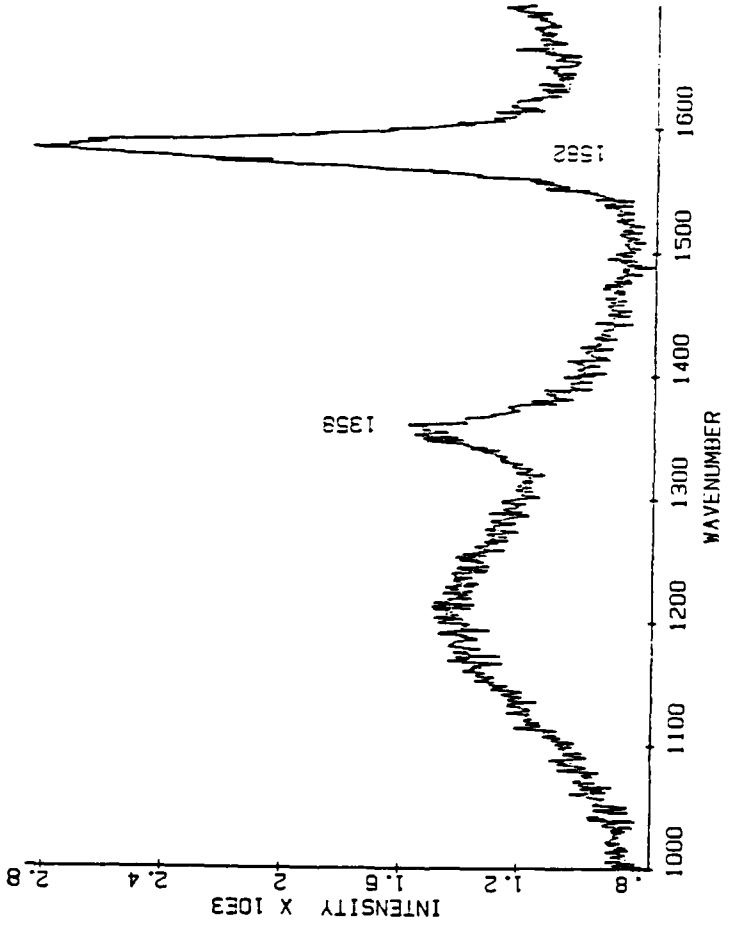

Fig. 46. Unidirectional carbon/carbon composite Raman spectrum on the fiber.

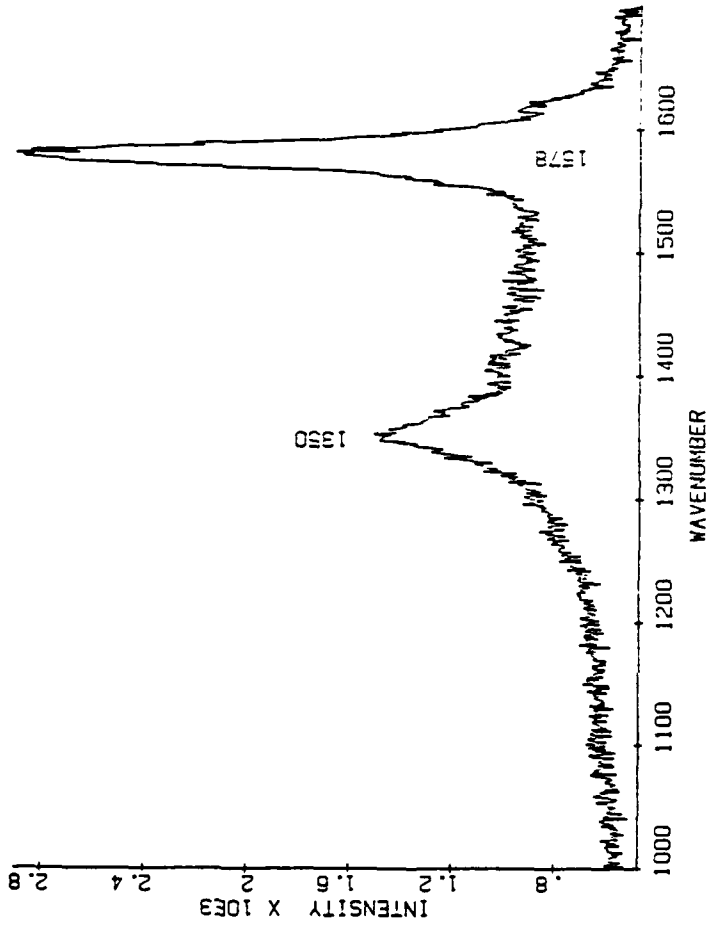

Fig. 47. Unidirectional carbon/carbon composite Raman spectrum on the matrix.

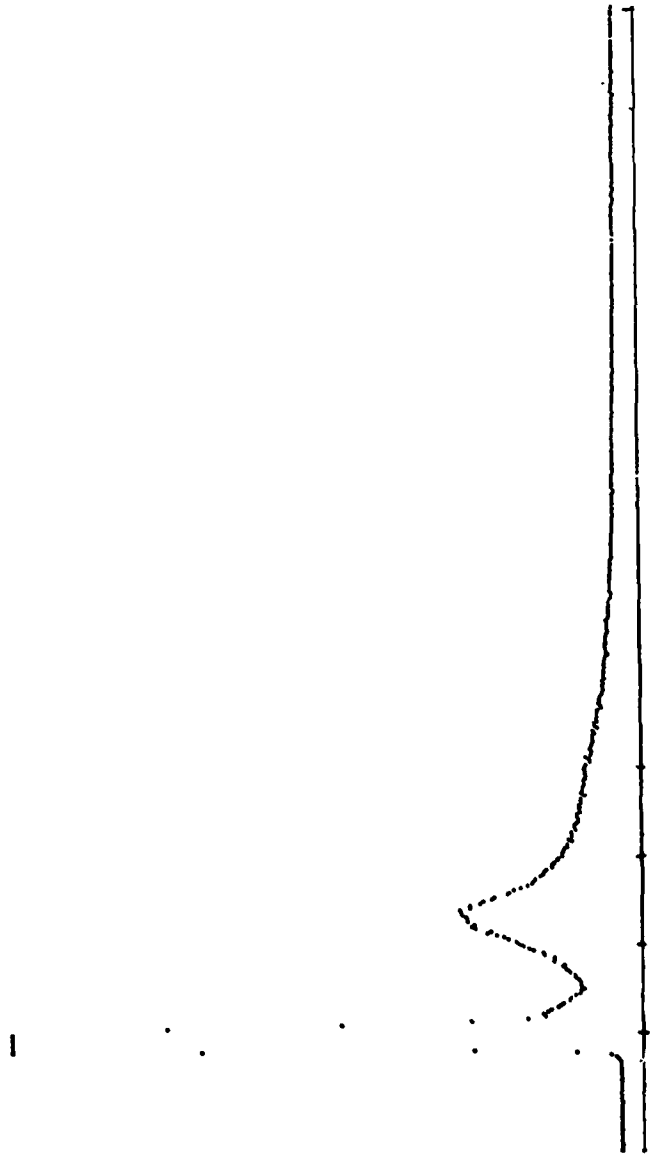

Fig. 48. EELS spectrum of a holey carbon grid.

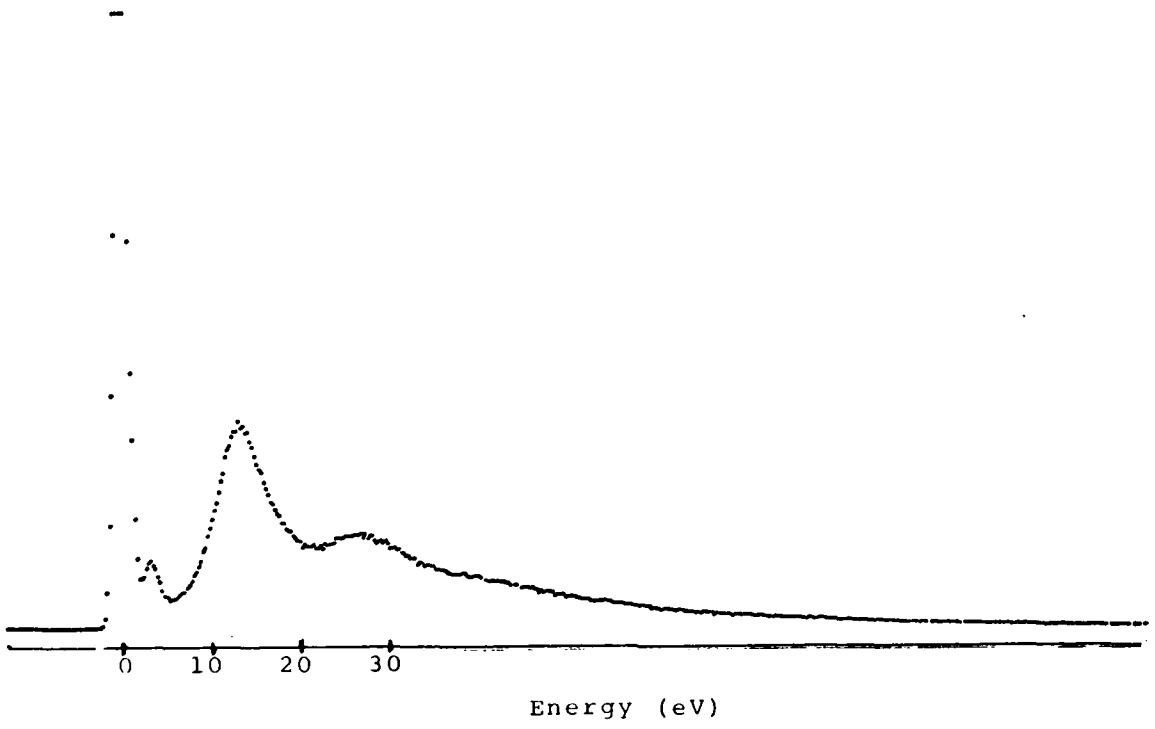

Fig. 49. EELS spectrum of coal-tar pitch heat treated to 1000°C for 15 minutes.

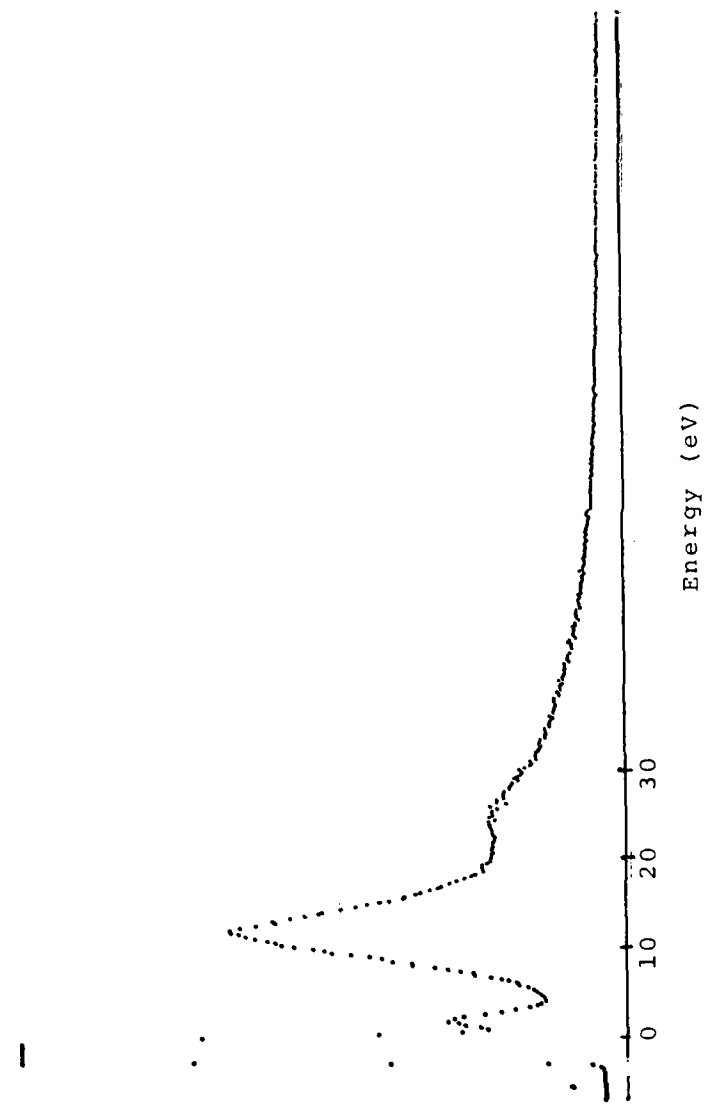

Fig. 50. EELS spectrum of coal-tar pitch heat treated to 2400°C for 15 minutes.

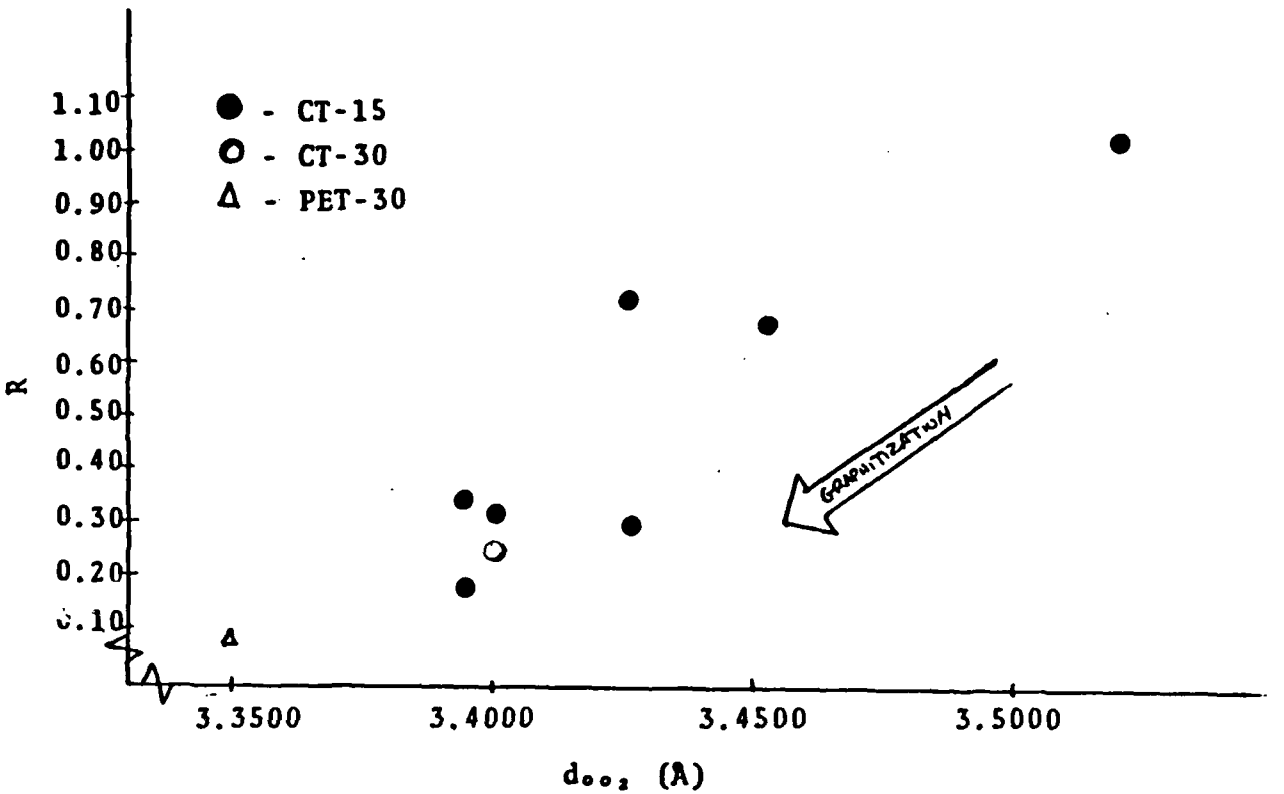

Fig. 51. d-spacing versus Raman peak intensity.

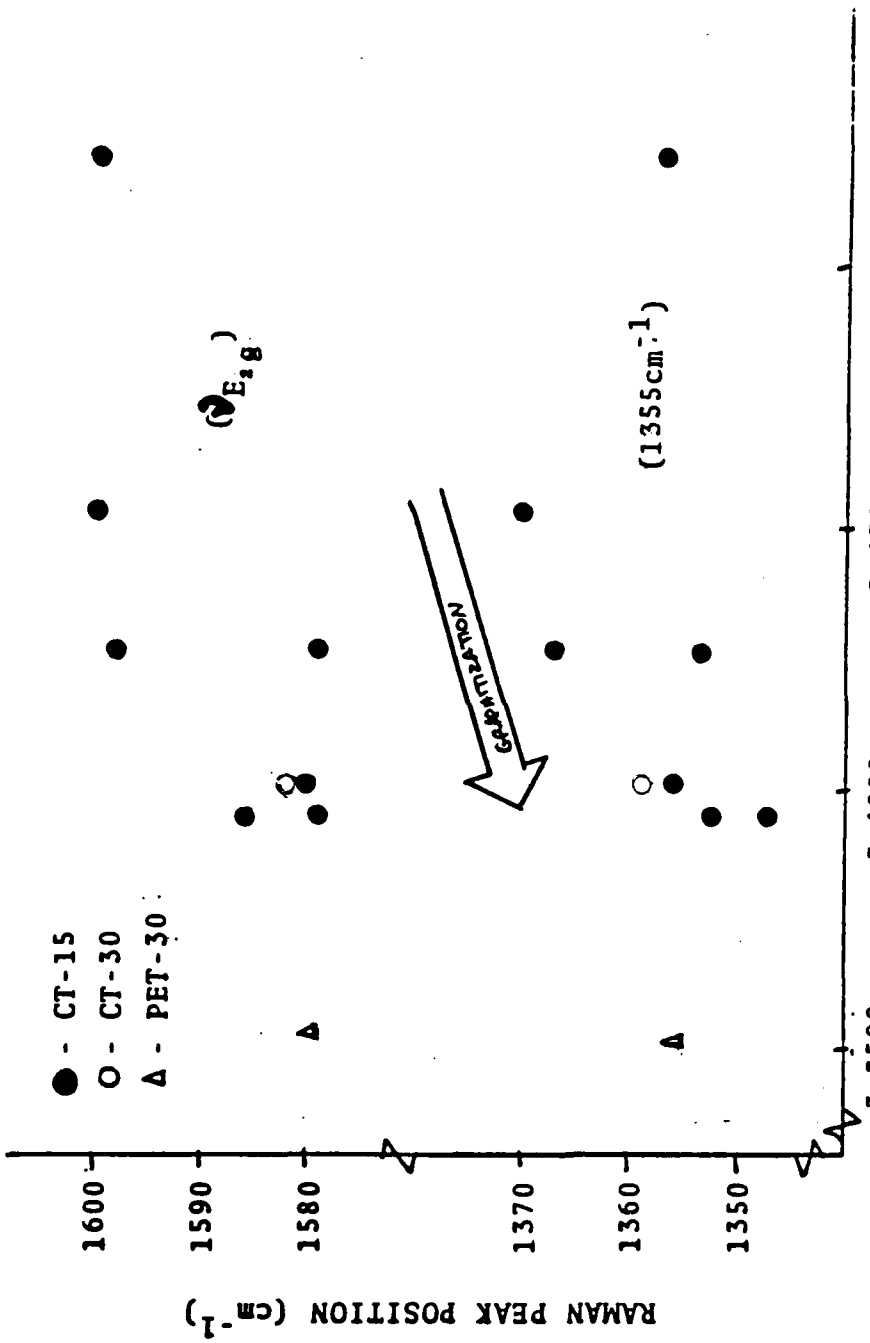

Fig. 52. d-spacing versus Raman peak position.

REFERENCES

1. L. S. Singer, *Fuel* 60, 839(1981).
2. I. Asimov, *The World of Carbon*, (1962).
3. D. McNeil, *Bituminous Materials, Asphalts, Tars, and Pitches* 3, 139(1966).
4. J. L. White, *Progress in Solid State Chemistry* 9, 59(1975).
5. J. H. Cranmer, I. G. Plotzker, L. H. Peebles, Jr., and D. R. Uhlman, *Carbon* 21, 201(1983).
6. K. Miyazawa, T. Yokono and Y. Sanada, *Carbon* 17, 223(1979).
7. P. M. Sheaffer, *A240 Analysis Report*, Unpublished study.
8. J. D. Brooks and G. H. Taylor, *Chemistry and Physics of Carbon* 4, 243(1968).
9. H. Marsh and P. L. Walker, Jr., *Chemistry and Physics of Carbon* 15, 229(1979).
10. K. J. Hüttinger and U. Rosenblatt, *Carbon* 15, 69(1977).
11. M. Ihnatowicz, P. Chiche, J. Deduit, S. Pregermain and R. Tournant, *Carbon* 4, 41(1966).
12. H. Honda, H. Kimura, Y. Sonada, S. Sugawara and T. Furata, *Carbon* 8, 181(1970).

13. J. S. Evangelides, *Extended Abstracts, 14th Biennial Conference on Carbon,* American Carbon Society, 249(1979).

14. J. Jortner, *Proceedings of the Symposium on Solid Mechanics,* 81(1976).

15. K. H. Kochling, B. McEnaney, F. Rozploch and E. Fitzer, *Carbon* 21, 517(1983).

16. Ibid., *Carbon* 20, 445(1982).

17. G. Pietzka, H. Pauls and W. Ulsancer, *Carbon* 72, 397(1972).

18. J. D. Bernal, *Proceedings of the Royal Society in London* A106, 749(1924).

19. D. B. Fischbach, *Chemistry and Physics of Carbon* 7, 1(1971).

20. B. E. Warren, *The Physical Review* 59, 693(1941).

21. W. Ruland, *Chemistry and Physics of Carbon* 4, 1(1968).

22. R. J. Nemanich and S. A. Solin, *Physical Review B* 20, 3192(1979).

23. F. Tuinstra and J. L. Koenig, *The Journal of Chemical Physics* 53, 1126(1970).

24. P. Lespade, A. Marchand, M. Couzi and F. Cruege, *Carbon* 22, 375(1984).

25. R. F. Egerton and M. J. Whelan, *Journal of Electron*

Spectroscopy and Related Phenomena 3, 232(1974).

26. S. C. Thakur and L. F. Brown, *Carbon* 20, 17(1982).

27. B. D. Cullity, *Elements of X-ray Diffraction*, (1978).

28. *Joint Committee on Powder Diffraction Standards*, 23-64(1975).

29. Ibid., 25-284(1975).

APPENDIX A

X-ray Diffraction Patterns

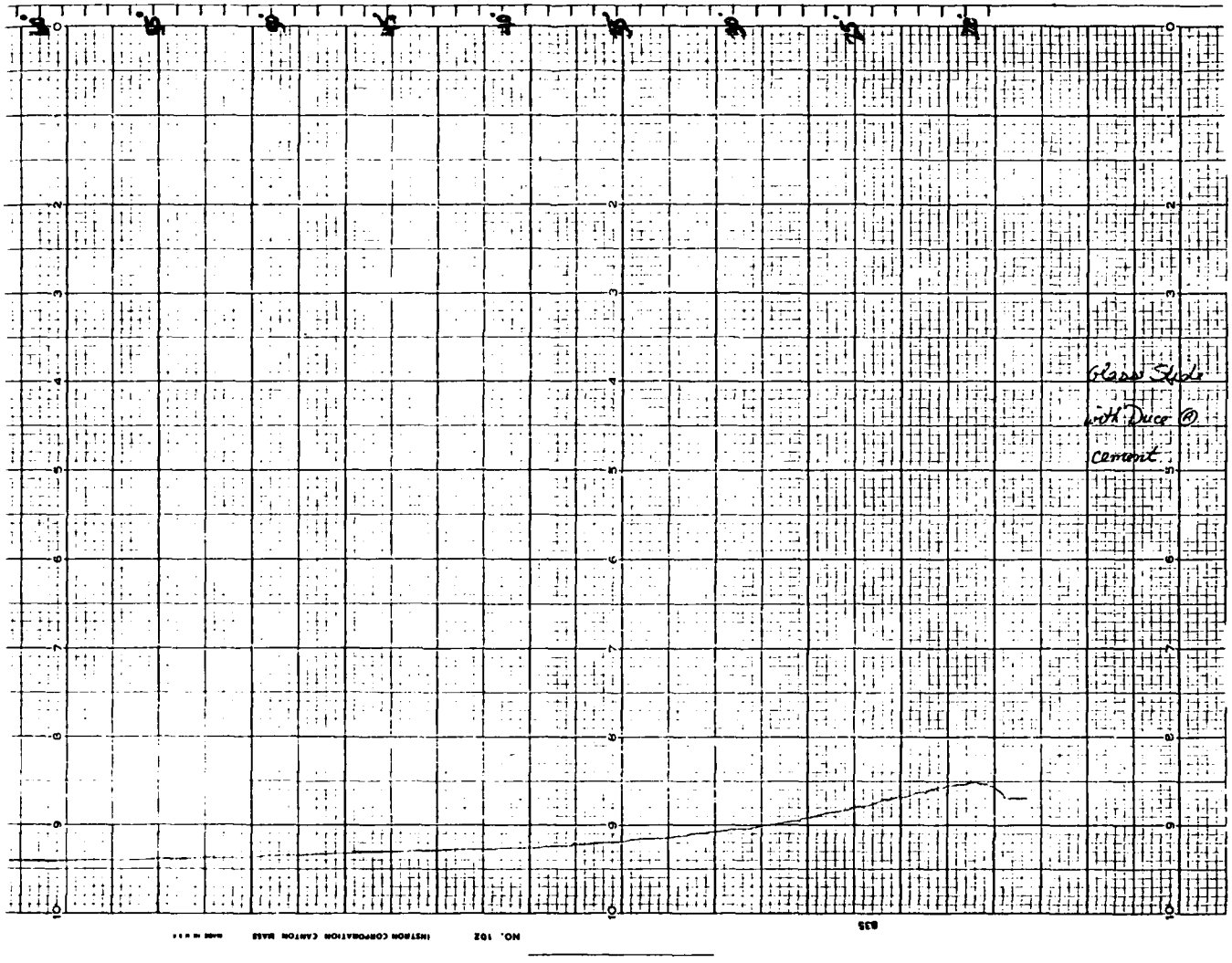

X-ray diffraction pattern of glass slide with Duco cement.

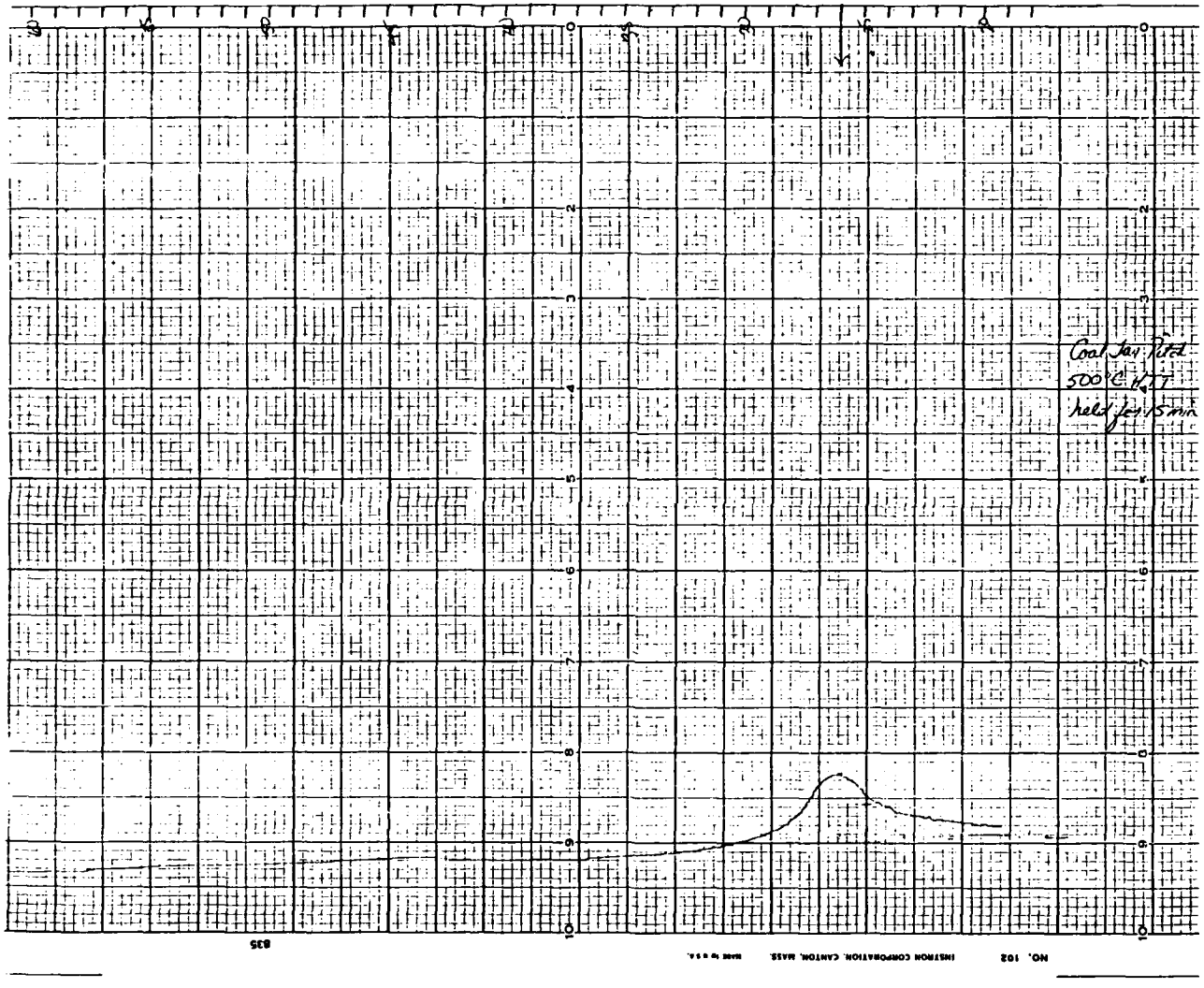

X-ray diffraction pattern of coal-tar pitch, HTT 500°C-15 min

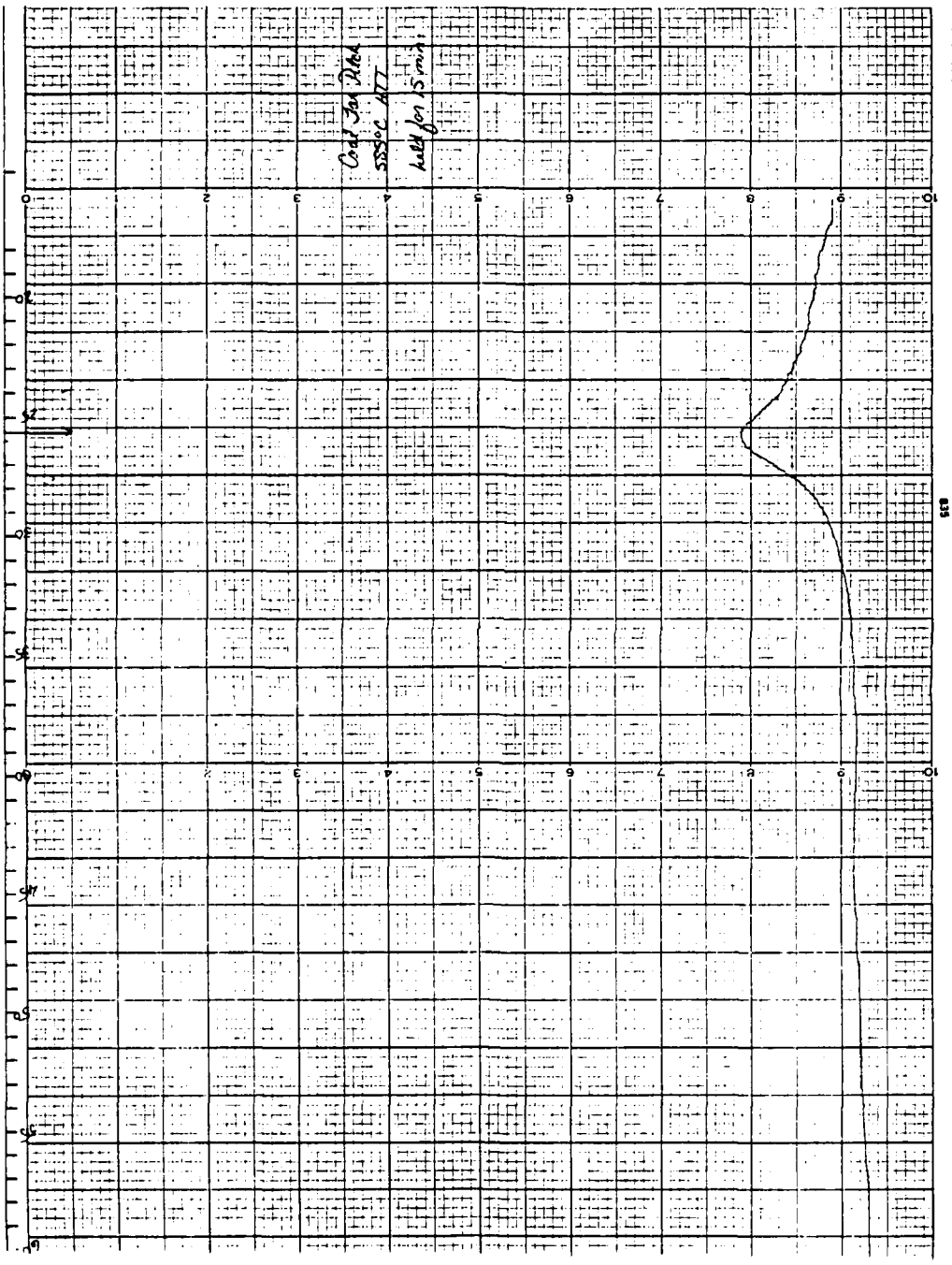

X-ray diffraction pattern of coal-tar pitch, HTT 585°C-15 min

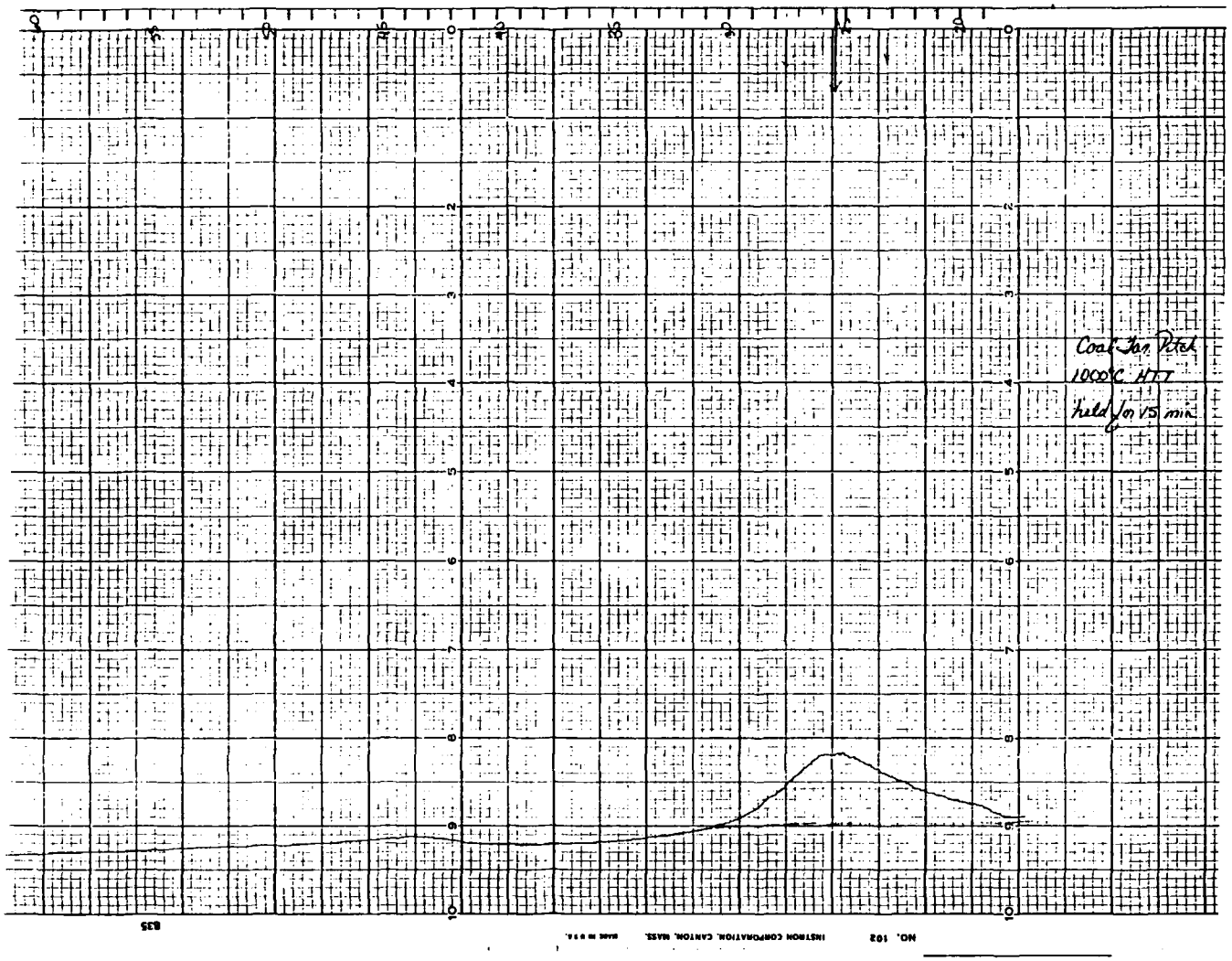

X-ray diffraction pattern of coal-tar pitch, HTT 1000°C-15 min

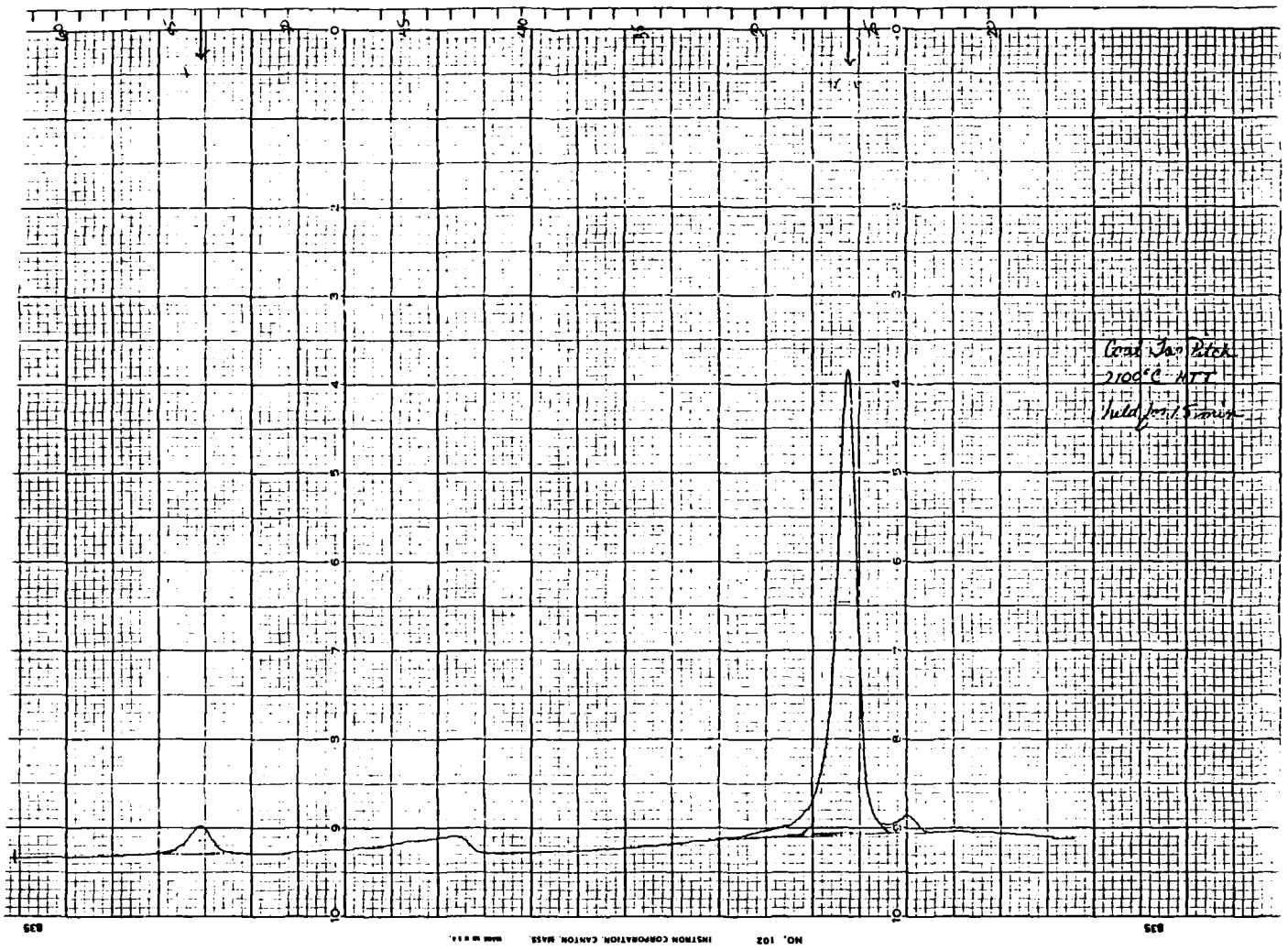

X-ray diffraction pattern of coal-tar pitch, HTT 2100°C-15 min

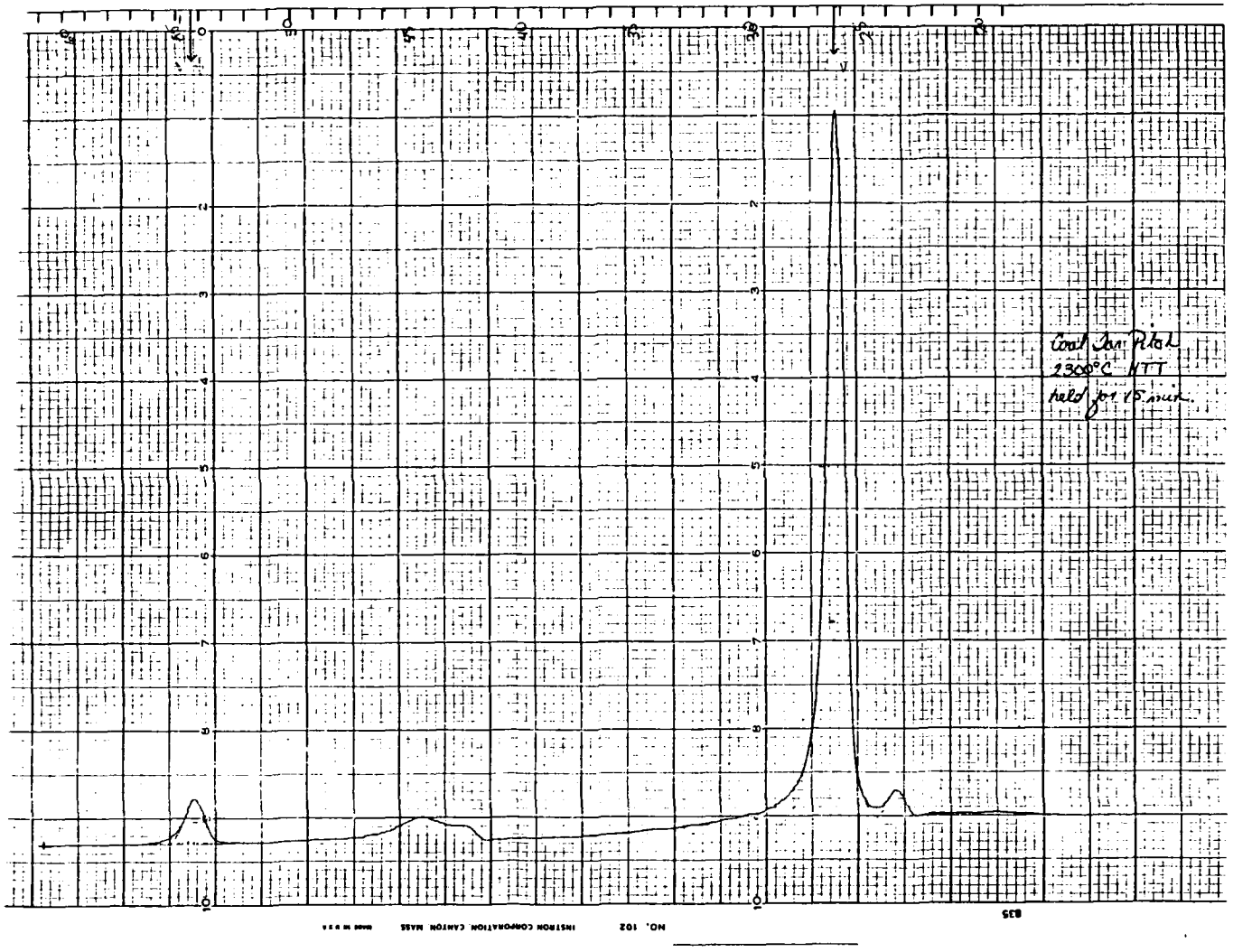

X-ray diffraction pattern of coal-tar pitch, HTT 2300°C-15 min

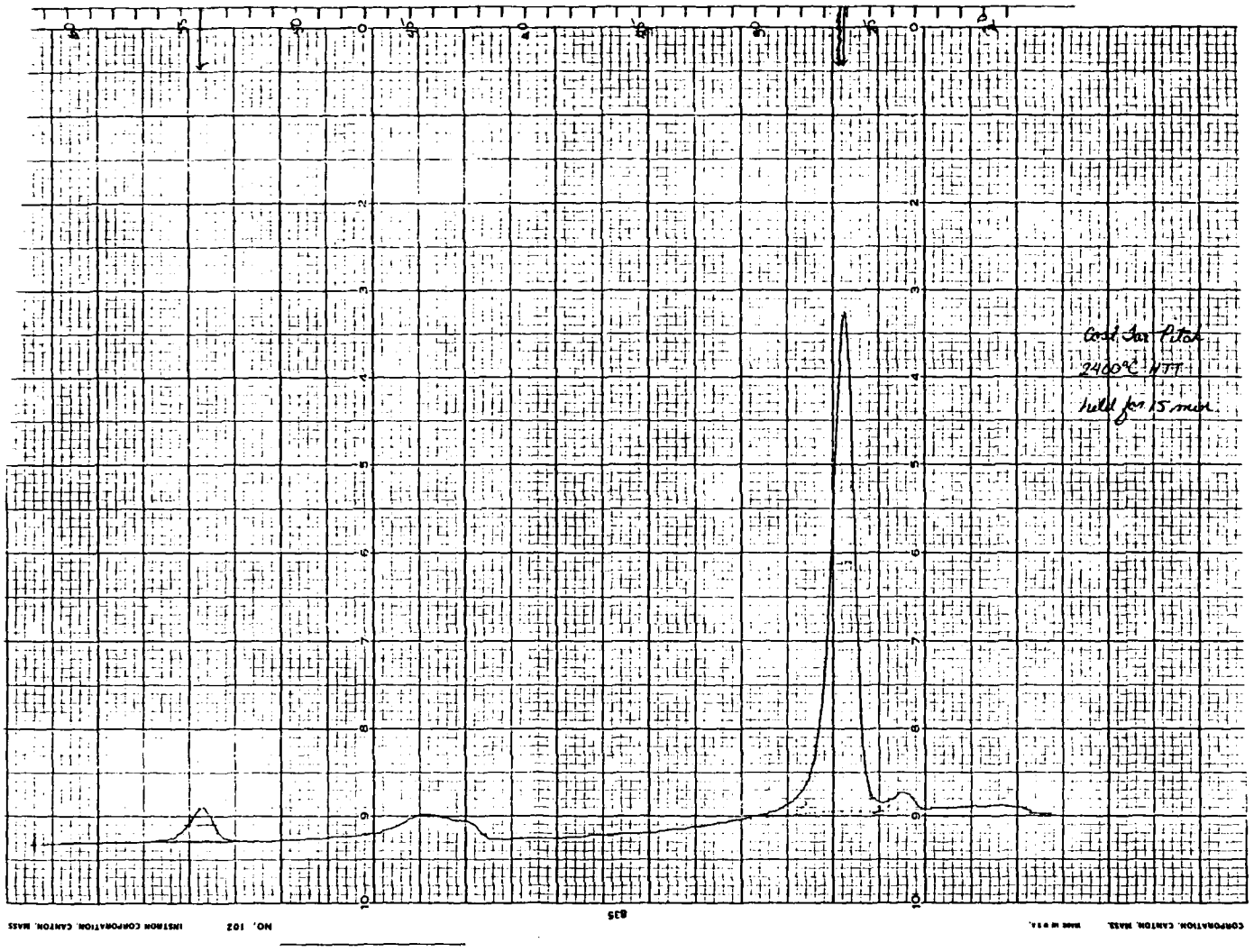

X-ray diffraction pattern of coal-tar pitch, HTT 2400°C-15 min

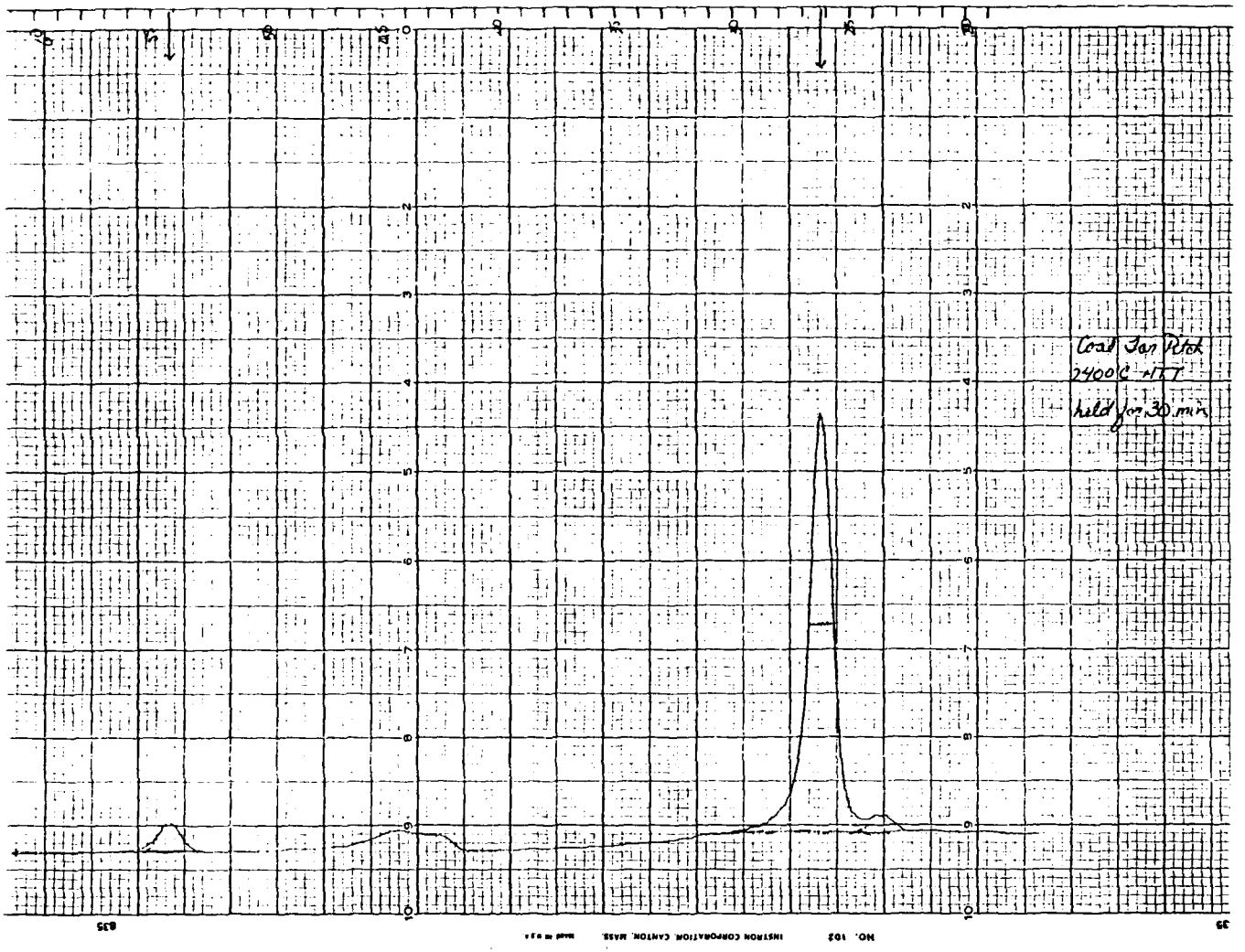

X-ray diffraction pattern of coal-tar pitch, HTT 2400°C-30 min

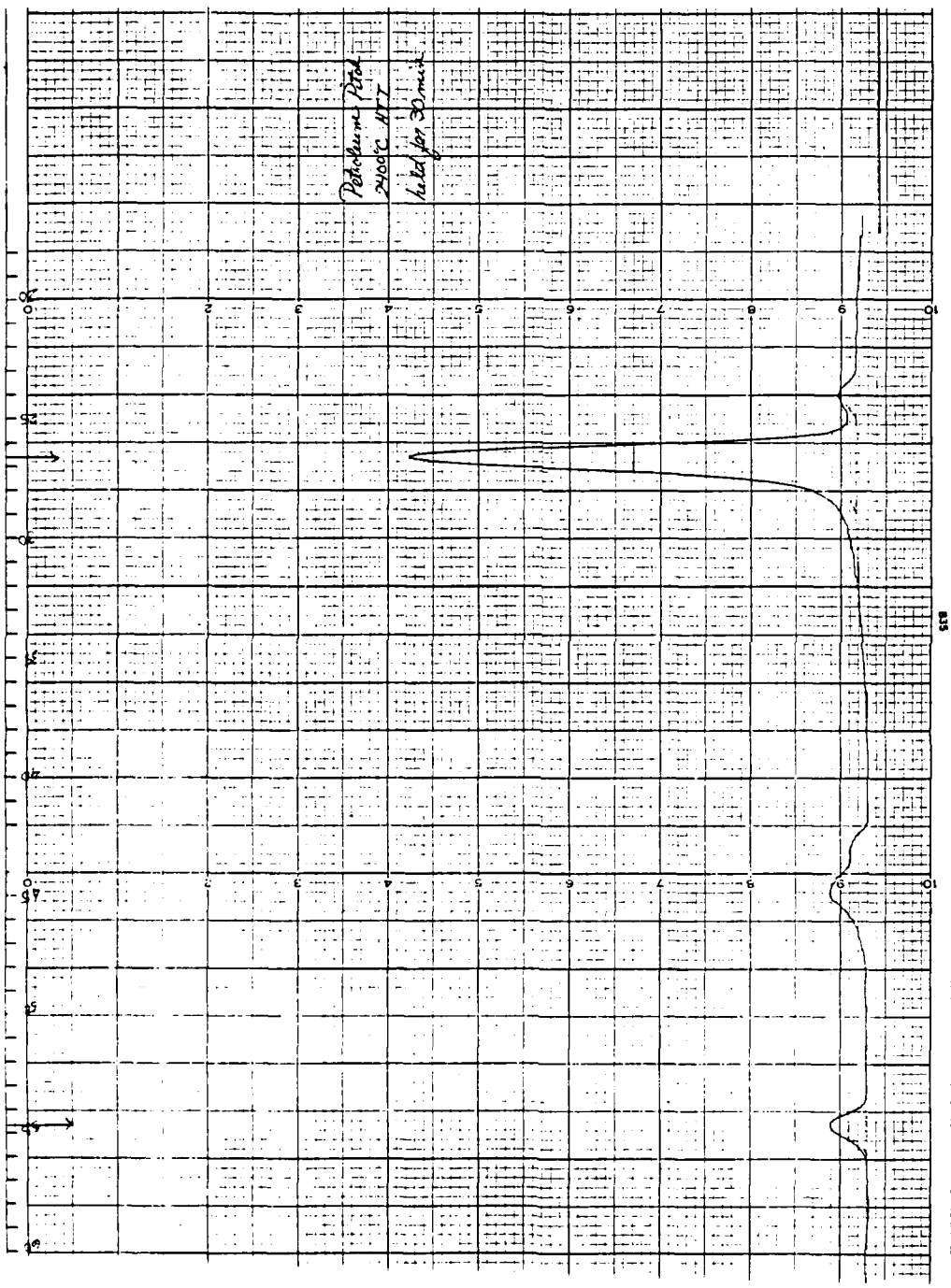

X-ray diffraction pattern of petroleum pitch, HTT 2400°C-30 min

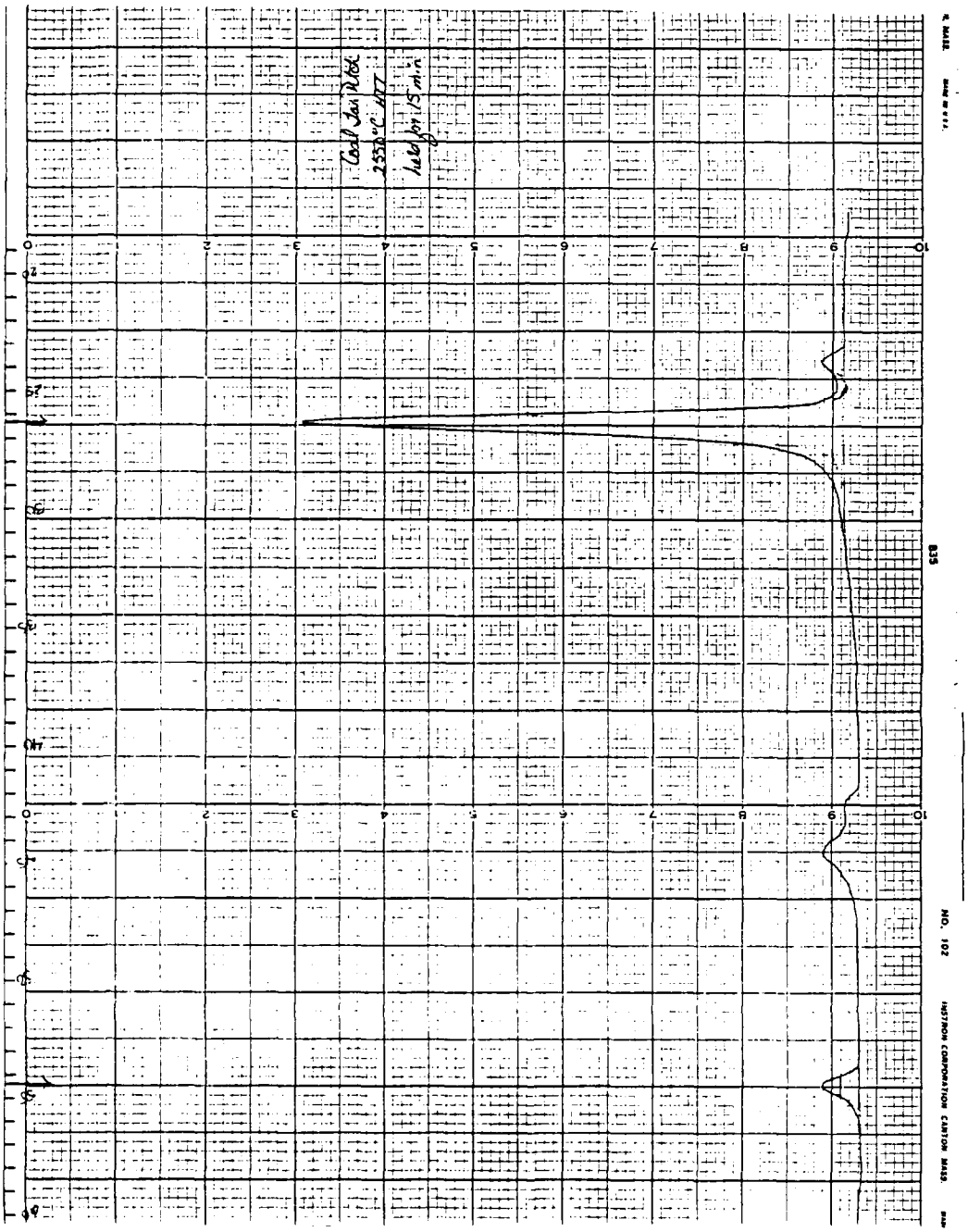

X-ray diffraction pattern of coal-tar pitch, HTT 2550°C-15 min

APPENDIX B

Laser Raman Microprobe Spectra

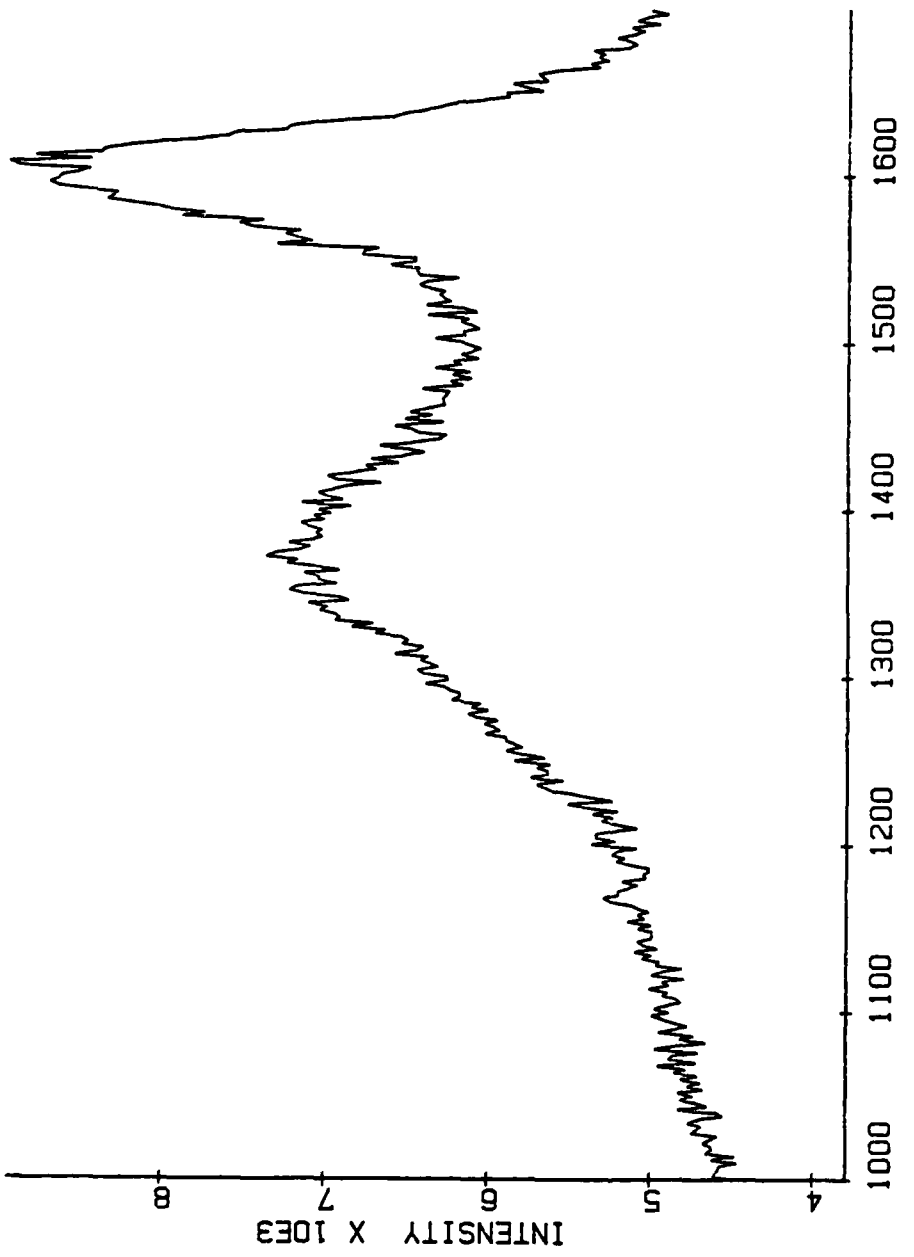

Raman spectrum for coal-tar pitch, HTT 500°C-15 min

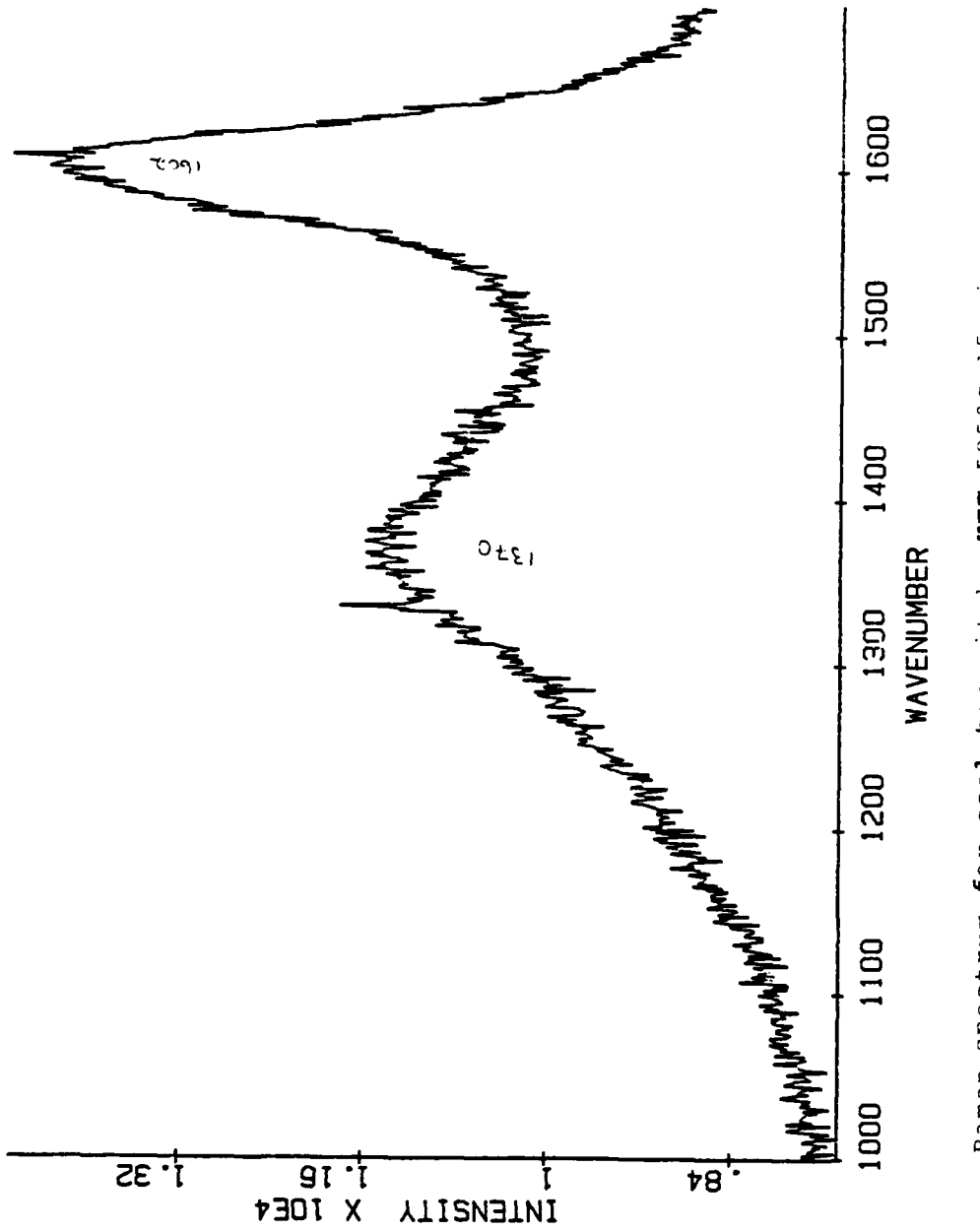

Raman spectrum for coal-tar pitch, HTT 585°C-15 min

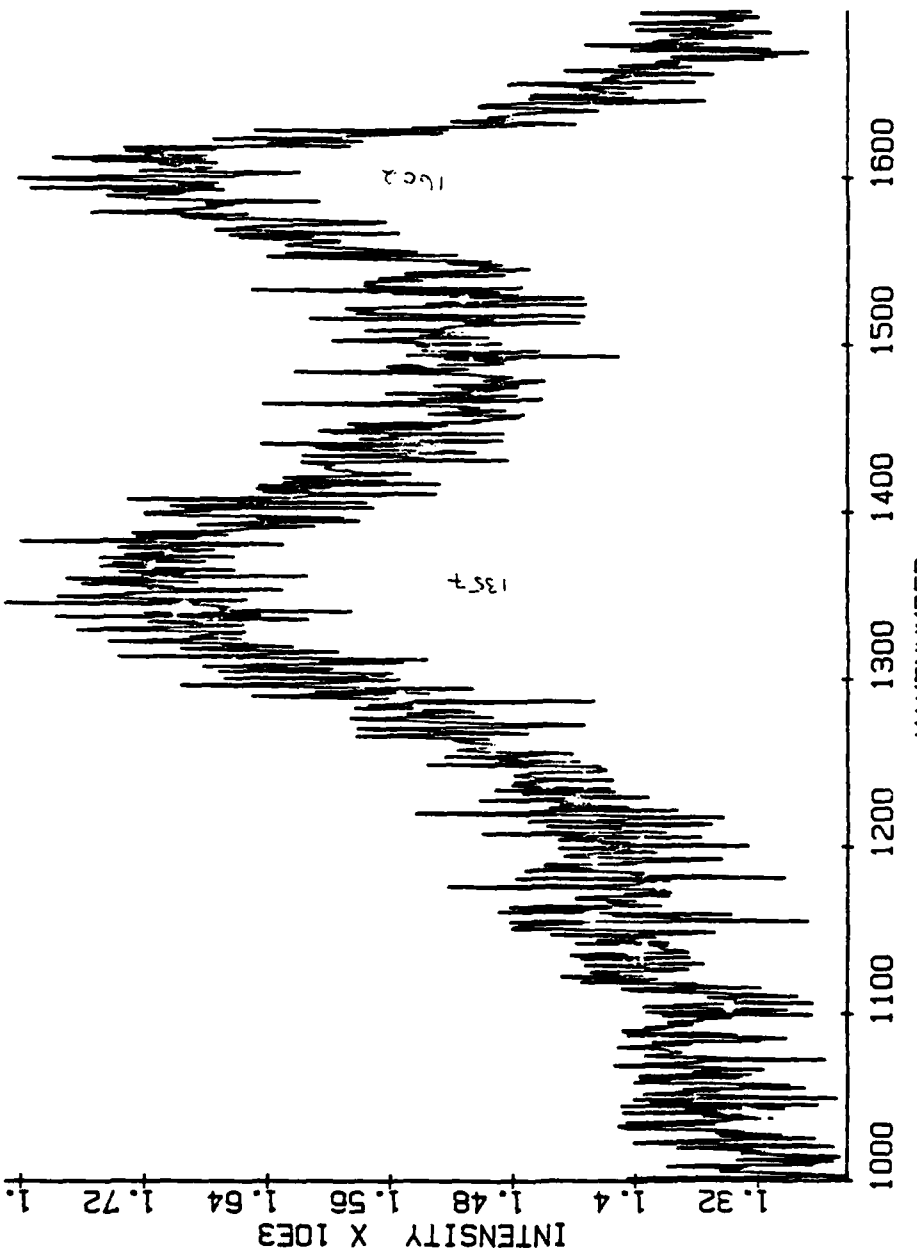

Raman spectrum for coal-tar pitch, HTT 1000°C-15 min

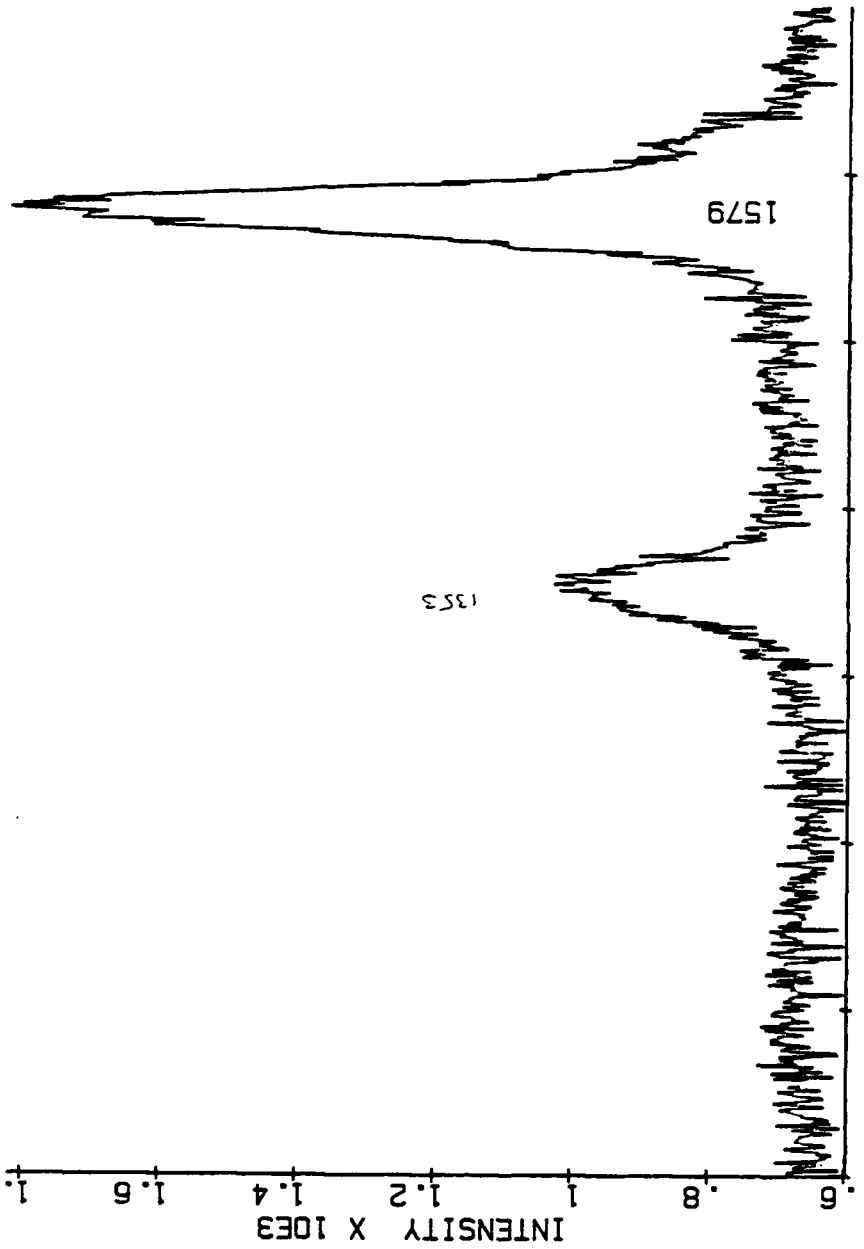

Raman spectrum for coal-tar pitch, HTT 2100°C-15 min

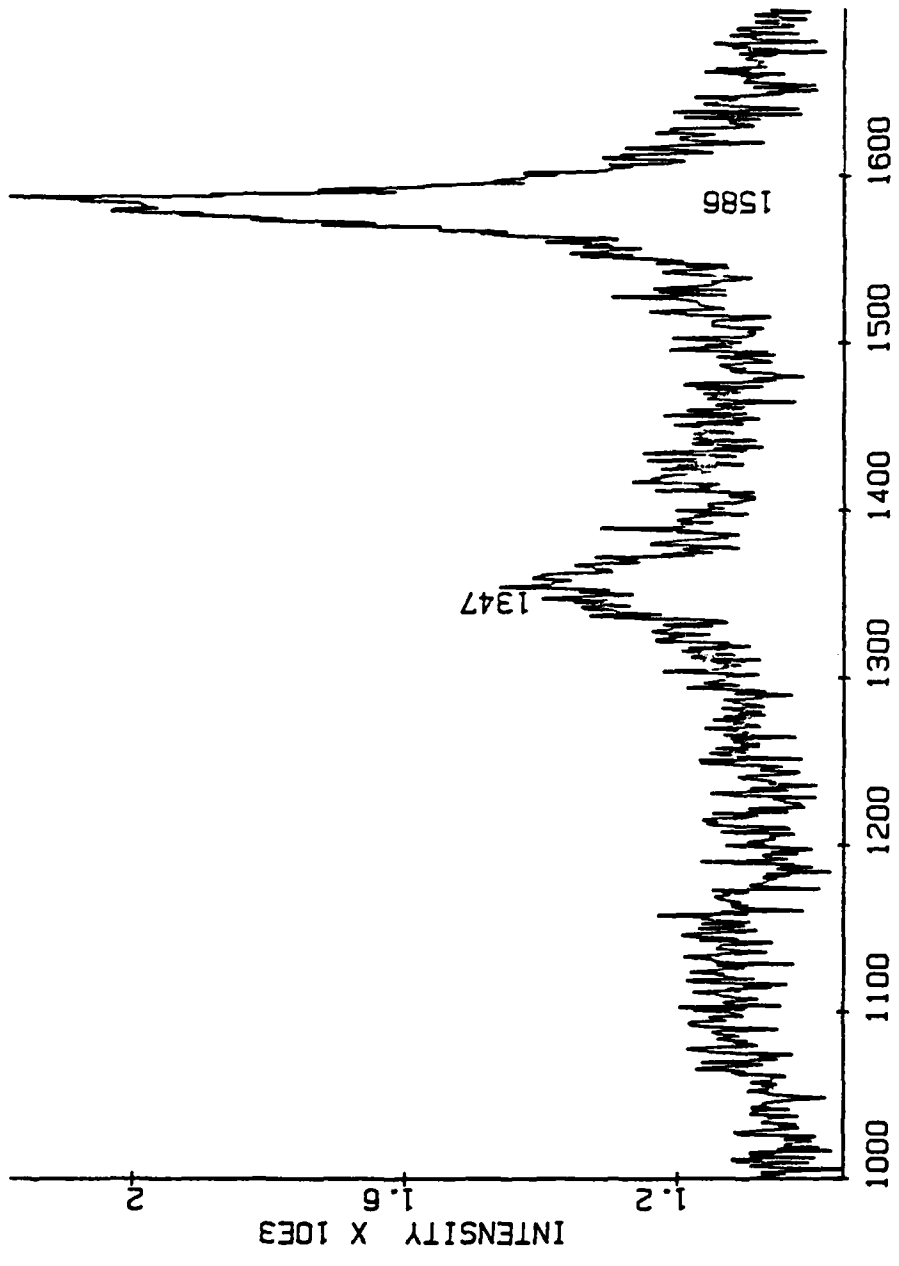

Raman spectrum for coal-tar pitch, HTT 2300°C-15 min

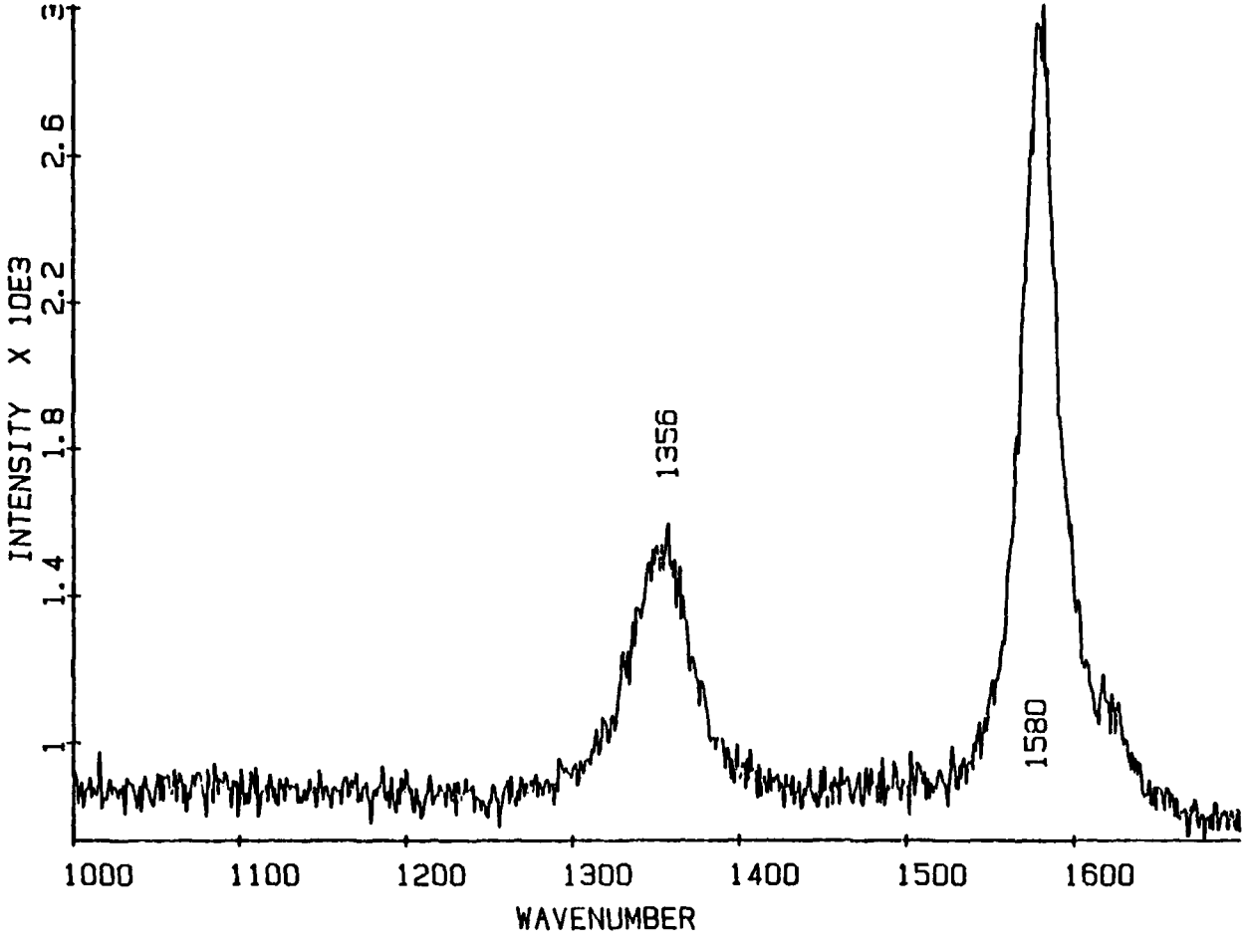

Raman spectrum for coal-tar pitch, HTT 2400°C-15 min

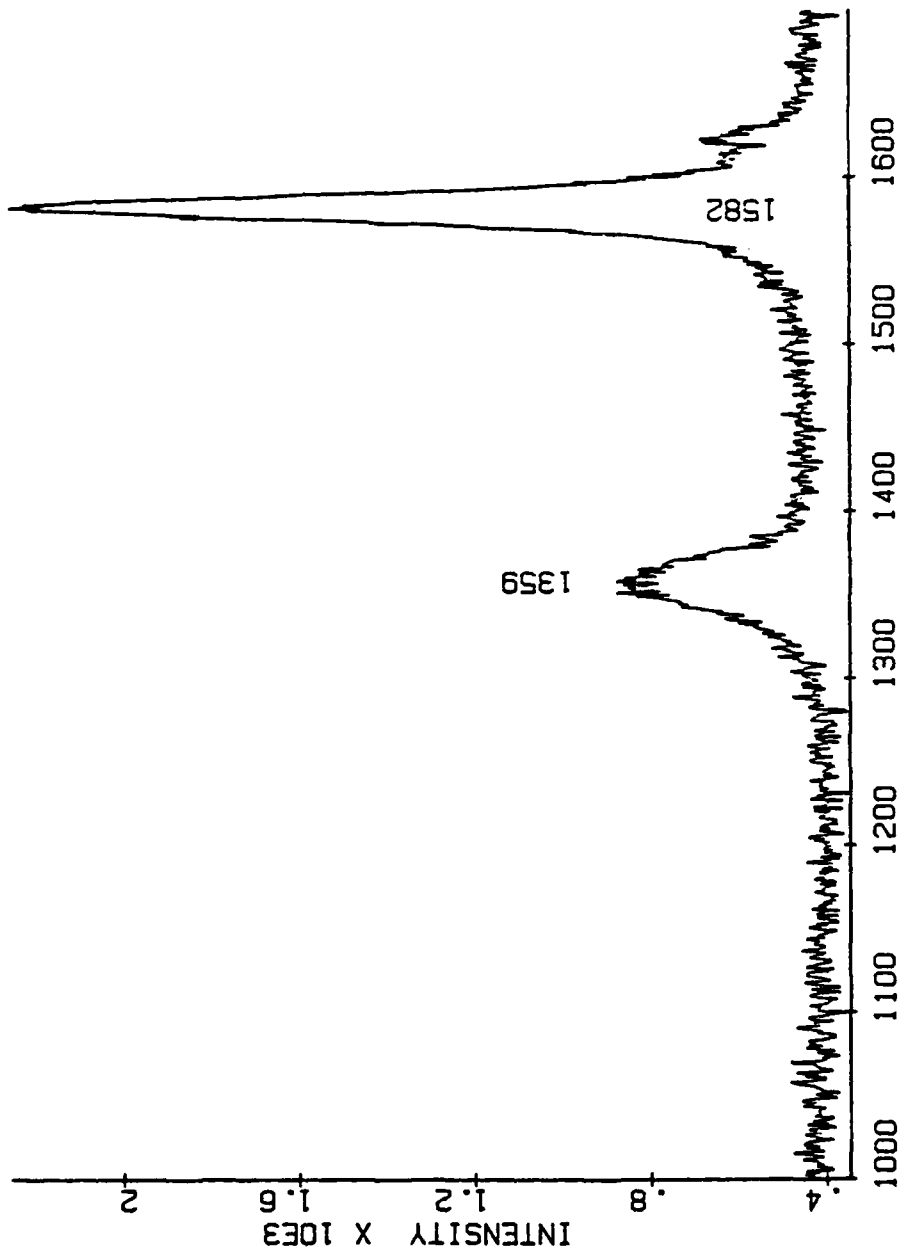

Raman spectrum for coal-tar pitch, HTT 2400°C-30 min

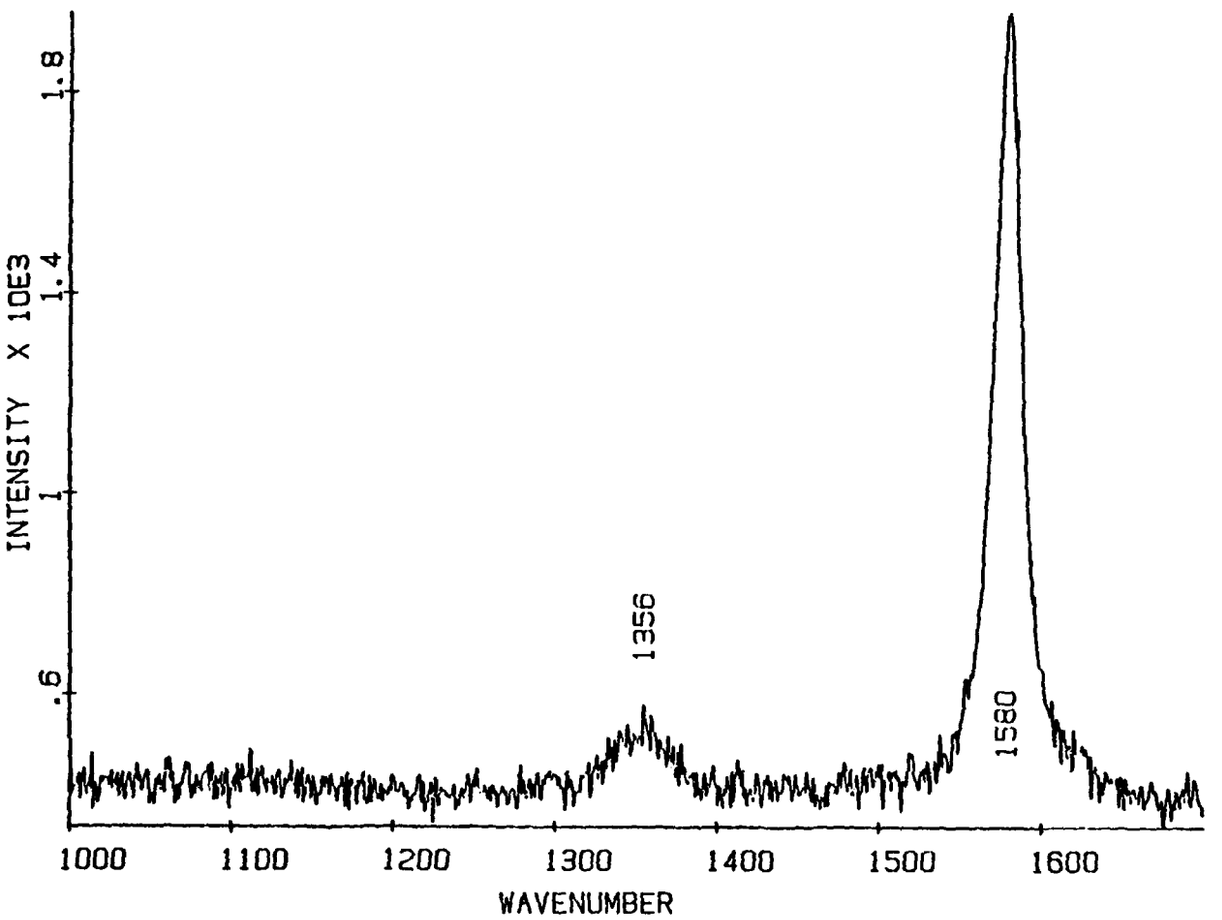

Raman spectrum for petroleum pitch, HTT 2400°C-30 min

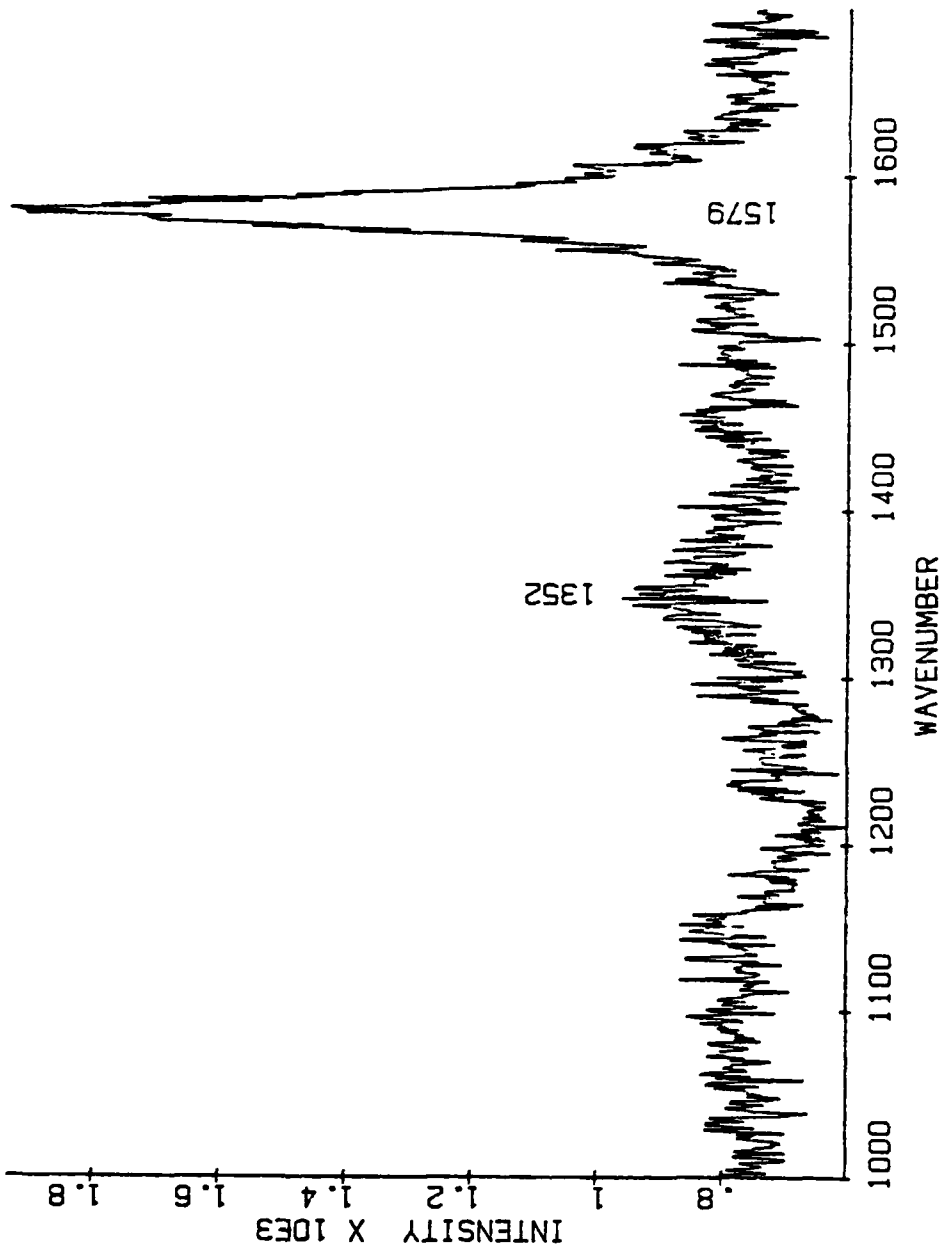

Raman spectrum for coal-tar pitch, HTT 2550°C-15 min

BIOGRAPHICAL SKETCH

Janet Claire Karika, nee Pfeiffer, is currently a Captain in the United States Air Force. She received her Bachelor of Science degree at the University of Central Florida, formerly Florida Technological University, studying Mechanical Engineering. She was a four-year Air Force ROTC student and received her B.S. degree and commission as a Second Lieutenant on June 13, 1980. Upon graduation she was assigned to Space Division/Medium Launch Vehicles and there worked with carbon/carbon composites used as exit cones and throat materials for small solid propellant rocket motors. She was assigned to Arizona State University after three years at Space Division to obtain her Master of Science degree in Mechanical Engineering. Captain Karika is married to Thomas Karika, an Air Force pilot, assigned to March Air Force Base. She will be joining him upon completion of her M.S. degree, and will be working at Norton Air Force Base in the Ballistic Missile Office.

END

FILMED

5-86

DTIC